SECONDARY FLOWS IN RIVER BENDS

A Thesis submitted to the

University of London

(Imperial College of Science and Technology)

for the degree of

Doctor of Philosophy in the Faculty of Engineering

by

Ahmad Faisal Asfari B.Sc.(Eng.)

November 1968

ABSTRACT

In this study on secondary flows in river bends, experimental investigations were carried out in three 180° open channel bends of rectangular cross-sections, but of different curvatures, in order to examine the main features of the flow. The breadth : depth ratios, between 24 and 3, are thought to be larger than have previously been reported in laboratory experiments.

The characteristics of the secondary currents were measured, both by finding velocity distributions, and also by finding the bed shear stress distribution. The measured velocity distributions in turbulent flow are then compared with those calculated by solving the general equations of motion by the method of finite differences.

Velocities were determined in laminar flow by photographing particles of neutral density, and in turbulent flow by using a miniature current meter. The spiral motions in a cross-section were observed photographically. The distribution of shear stress in both the radial and tangential directions on the bed were mapped, and a correlation between velocity and bed shear is suggested.

The regions susceptible to the most serious effects

of the stream curvature are identified from the consideration of bed shear distribution, and these locations are related to channel curvature. These regions were further investigated by studying flows over loose beds, which were prepared by covering the rigid beds with an industrial sand.

The energy losses in curved flows, additional to the usual bed friction, are compared to the straight channel friction factors at the same Reynolds number.

ACKNOWLEDGEMENT

The research work presented in this thesis was carried out in the Hydraulics Laboratory of the Civil Engineering Department, Imperial College of Science and Technology, under the supervision of Professor J.R.D. Francis, M.Sc.,M.I.C.E., M.I.W.E. The author is very grateful to him for his invaluable suggestions and advice throughout the period of this work.

The author also wishes to thank Professor (Emeritus) C.M. White for suggesting the problem and for his guidance in the design of the apparatus.

Thanks are also due to the members of staff of the Hydraulics Section, the author's colleagues, and all those in the Department who offered assistance.

The author gratefully acknowledges the leave of absence granted by the University of Aleppo, Syrian Arab Republic, the generous scholarship awarded to him by the Ministry of Overseas Development, United Kingdom, and the hospitality extended through the British Council.

All gratitude is due to the author's wife for her care and patience throughout the course of this study.

CONTENTS

NOTATIONS

SYMBOL	MEANING
A	Turbulent or eddy viscosity of the fluid
C	Chezy coefficient, or a constant, according to the context
d	diameter of a circular pipe
x, y, z; r, θ, z	Cartesian coordinates
u, v, w; $\bar{u}, \bar{v}, \bar{w}$; u', v', w'	Cylindrical coordinates
~~v_r, v_θ, v_z~~ v_r, v_z, v_z	instantaneous, temporal mean and fluctuating components of velocity in x,y,z respectively, designated in the text as the temporal mean values of velocity in r, θ, z coordinates
X, Y, Z	components of body force (gravity) in x,y,z directions
r_i, r_c, r_o	inner side radius, centre-line radius and outer side radius of the channel bend
b	width of the cross-section
h	depth of the flow cross-section
μ	molecular viscosity of the fluid
ρ	density of the fluid
i/s, o/s	inner side and outer side respectively
$\bar{m}$	hydraulic radius
$\nu = \mu/\rho$, $\nu_T = A/\rho$	kinematic coefficient of molecular and eddy viscosity respectively
$v_{\theta m}$	mean forward velocity along the flow depth

SYMBOL	MEANING
$\bar{V}$	mean velocity over the cross-section
$Re = \frac{\bar{V}.\bar{m}}{\nu}$	Reynolds number
$F = \frac{\bar{V}}{\sqrt{g\bar{h}}}$	Froude number
$\bar{\tau}_o$	mean value of bed shear stress in straight uniform flow
τ_{or}, $\tau_{o\theta}$	radial and tangential components of bed shear stress
I_r, I_θ	radial and tangential slopes of water surface
z	height of a point above the channel bed
$\eta = z/h$	relative depth of a point in the cross-section
κ	Karman constant
$v_* = \sqrt{\tau_o/\rho}$	Friction velocity
S	slope of channel bed in uniform flow, or of energy line generally
K	roughness height, or a constant, according to the context
α_o	bed angles
α	flow angles
S_{rz}	strength of secondary currents
γ	specific weight of fluids
b/r_c	channel curvature
b/h	aspect ratio
g	acceleration due to gravity

CHAPTER I

REVIEW OF LITERATURE

The literature reviewed herein has been selected for its direct application to the present work.

It was as early as 1876 that the phenomenon of secondary flow was first observed by Thomson. From his experiments on curved ducts, Thomson noted that a stream flowing into a curve has an increased velocity along the inner side and a diminished velocity along the outer side; the water surface has, therefore, a transverse inclination rising towards the outer side. The movement of water near the surface is directed outward and that near the bottom is directed inward.

Subsequently, many other investigators have carried out analytical as well as experimental work on this problem.

I-1. Secondary currents around the bend

Shukry (1950) carried out experiments on a 180° open channel bend of 30 cm. width and $r_c/b = 1$. He stated that the superposition of the secondary flow on the main flow gives a kind of spiral (or helical) motion along the bend and even to some distance downstream of the bend. The strength (S_{rz}) of this spiral motion was defined by him as the percentage ratio of the mean kinetic energy of the lateral motion to the total kinetic energy of the flow :

$$S_{rz} = \frac{(v_{rz}^2/2g)m}{(\bar{v}^2/2g)m}$$

He also stated that the proportions of S_{rz} occurring in the first half of the bend is twice that in the second half, and that S_{rz} decreases with increasing Reynolds number and with the radius-breadth ratio.

Hawthorne (1951) concluded, from inviscid flow theory, that the secondary flow is not spiral but oscillatory lengthwise. His theoretical development showed that the secondary circulation remained unchanged when streamlines were geodesics on the surfaces of constant total pressure. His experiments were carried out on a 90° bend of circular pipe, as well as 90° and 180° bends of rectangular ducts (with $r_c/b = 3$).

In rivers with erodible boundaries, and in all flow passages with transported sediments, the helical motion is of great importance. Once a bend is formed in a natural stream, by some geological or other cause, the helical motion created there will continue downstream of the bend exit and consequently act as the disturbance at the entry into another region. Prus-Chacinski and Francis (1952) emphasized the importance of entry conditions in the meandering process and concluded from their experiments that it is possible to change the flow pattern in a bend, and downstream, by changing the conditions of motion at the bend entry.

In a later study, Einstein and Harder (1954) referred the circulation in bends to the unbalance between the centrifugal and the tranverse pressure forces. They also revealed the existence, near the outer side, of a small vortex rolling in the opposite direction to that of the main vortex; they attributed its existence to friction, and claimed that the early erosion in this region of the outer bank is due to this small vortex. Their experiments were carried out on a 180° bend of 0.4 m. width, 0.10 m. depth, with $r_c/b = 7.4$.

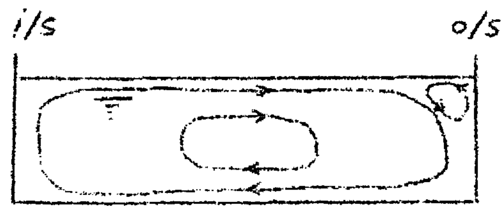

From experiments on a meandering channel of five opposite bends, Prus-Chacinski (1955) reaffirmed the importance of flow conditions at the entry and proved that by introducing a certain artificial secondary flow at the beginning of a natural stream bend, the pattern of secondary flow in the bend can be altered (as illustrated overleaf) and the phenomena of erosion and deposition can be governed.

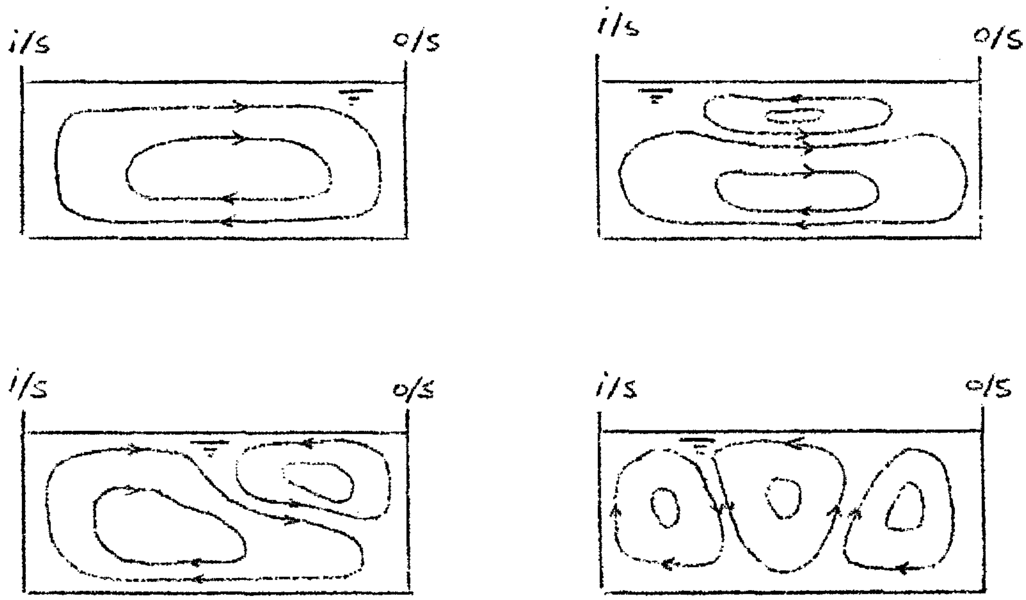

Patterns of spiral flow in

a rigid channel bend

The strength of secondary flow was defined by Malouf (1956) as the deviation (α_o) of the flow at the bed from the tangential direction. From his experiments on a 90° bend he developed the following equation :

$$\tan \alpha_o = 23.4 \, (h/r_c)^{\frac{1}{2}} \, Re^{-\frac{1}{4}}$$

where h is the depth of flow and r_c the central radius of the bend.

Wadekar (1956), from his experiments on a 180° bend of an open channel (b = 15 cm., r_c = 100 cm.), suggested the following equation for $\tan\alpha_o$:

$$\tan\alpha_o = 25.4(h/r_c)^{\frac{1}{2}} Re^{-\frac{1}{4}} - C$$

in which C is constant. He also confirmed the existence of the small vortex near the outer side as originally revealed by Einstein and Harder.

In Rozovskii's work (1957) on laboratory as well as river bends of different proportions, the following equation was suggested :

$$\tan\alpha_o = 11\ h/r$$

He also stated that helical motion depends only a little on the channel roughness, whereas water surface topography is greatly affected by the roughness of the boundaries. From his measurements on bends in the Desna river, he emphasized the existence of unilateral transverse circulation in the cross-section of a bend.

Regarding the transverse water surface profile, Leopold et al (1960) stated that, although the transverse profile varies in shape according to the different laws of radial distribution of tangential velocity, the overall bank-to-bank superelevation is remarkably independent of the law applied. They suggested that an equation for the total superelevation of the form

$$\Delta h = \frac{\bar{v}^2\ b}{g\ r_c}$$

in which $\bar{v}$ is the mean velocity of the flow, b is the width of the cross-section and Δh is the total superelevation, will give values near to those measured in rivers.

From measurements on a 60° trapezoidal channel bend of 0.6 m. bottom width and 1.52 m. central radius of curvature, Ippen et al (1962) concluded that superelevation is essentially independent of the frictional aspects and the velocity distribution of the flow, and is controlled primarily by the boundary geometry, in contradiction to Rozovskii's findings.

From his experiments on several trapezoidal bends of cross-section in natural canals (Horsetooth Feeder Canal and Poudre Supply Canal, Colorado) with curves ranging between 28° and 115°, and $2.78 < r_c/b < 23.93$, $3.4 < r_c/h < 7.7$, Ali (1964) concluded that in the middle section of the bends the maximum velocities are close to the centreline of the channel. He also concluded that the radial distribution of tangential velocities from the centreline towards the inner and outer sides can be represented as forced and free vortices respectively. Accordingly, the superelevation takes the value :

$$\Delta h = \frac{v_{max}^2}{2g}\left[2 - \left(\frac{r_i}{r_c}\right)^2 + \left(\frac{r_c}{r_o}\right)^2\right]$$

Through his recent studies, Prus-Chacinski (1967) demonstrated the advantage of secondary currents created by the construction of a series of short bends as a convenient means of separating the heavily polluted sewage in storm sewage overflows.

I-2. Velocity distribution around bends

In experiments on a 180° open channel bend, Shukry (1950) measured the magnitudes of the velocity components around the bend, using a pitot sphere to give the components of velocity simultaneously in three perpendicular directions. He concluded that the radial distribution of tangential velocity conforms to the free vortex law (vr = constant).

Later, Ananyan (1957) used the same device for velocity measurements, and stated that in long bends a shift of maximum tangential velocity from the inner side region takes place towards the outer side region of the bend as a result of transverse circulation.

In the same year, Rozovskii published his extensive study on curved open channel flow. He derived analytically the equations for velocity distributions around bends of different proportions of r_c/b, b/h, etc., and for different velocity profiles along the depth of flow at the entry: i.e., logarithmic, parabolic and elliptic profiles. He obtained good agreements between his calculations and measurements in the cases of both smooth and rough beds of long bends.

In a recent study by Fox and Ball (1968) on a 180°

open channel bend 30 cm. wide and $r_c/b = 3.5$, the behaviour of secondary currents in the bend was analysed, and its effects on the main flow explored, by calculating, in finite difference procedure, the distribution of foward velocity around the bend, taking into consideration the effect of the transversal flow. A comparison was then made between the calculated and the measured isovels and a good agreement between the two was obtained. This study also confirmed the shift of the high velocity region towards the outer side and below the water surface as a result of the secondary flow, and concluded a gradual development of a low velocity region near the inner side of the bend starting at about 30° from the bend entry.

I-3. Bed shear stress distribution

Owing to the secondary currents, the flow velocity and hence the shear stress very near the channel bed are directed inward at an angle α_o. Wadekar (1956) stated that $\tan\alpha_o$, which represents the ratio of the radial to the circumferential velocity very near the bed, is also equal to the ratio of the shear stress components in these two directions,

$$\tan\alpha_o = \frac{v_r}{v_\theta} = \frac{\tau_{or}}{\tau_o}$$

To measure the local bed shear stress around the bend of a trapezoidal channel (Paragraph I-1), Ippen et al (1960) used a round surface pitot tube, similar to that originally developed by Preston (1954). They plotted the local shear stress around the bend non-dimensionally, considering only the tangential components of bed shear stress, and estimated that the error due to the neglect of the radial component of shear was proportional to $(1 - \cos\alpha_o)$. From their experiments they concluded that localized shear stresses in curved flow exceed in intensity the normal mean shear for uniform flow, as measured before the bend entry, by as much as 100 % depending only on the stream geometry.

I-4. Flow over erodible beds.

The most important effects of secondary currents, and the resulting helical motion, are exhibited in natural streams with erodible boundaries. Many studies have been carried out in both straight and curved open channels. Both the movement of sediments and the configuration of beds of rivers are intimately interrelated to the secondary currents in the flow. Even in straight channels of non-circular cross-sections, the secondary currents due to turbulence in the flow have a dominant role in the configuration of the channel cross-sections; it is believed that these secondary currents are the cause of keeping sediments in suspension. One of the most systematic studies carried out in this field was that of

Vanoni (1946).

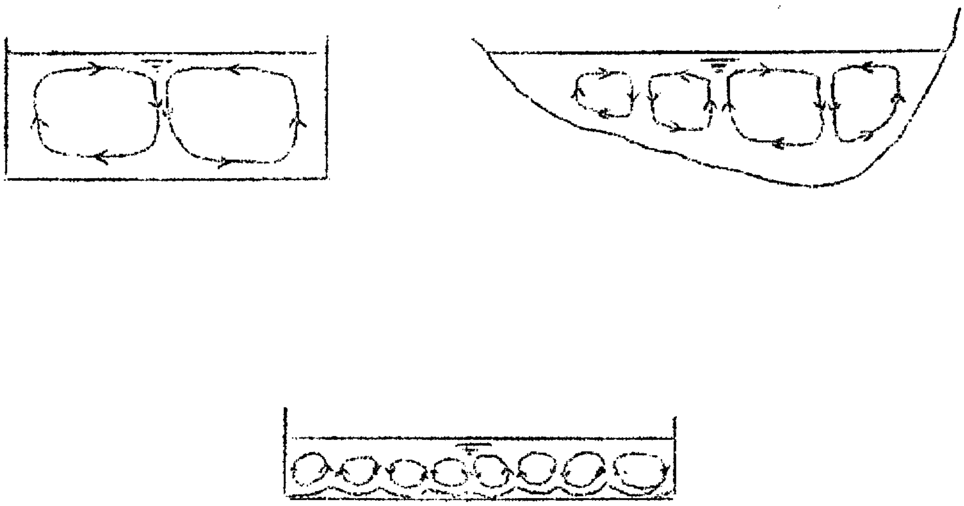

Flow patterns in straight channels
(from Vanoni)

In a study on flow about struts and airfoils of different shapes, Hawthorne (1954) measured the configuration of sand surrounding different struts under flowing water. He

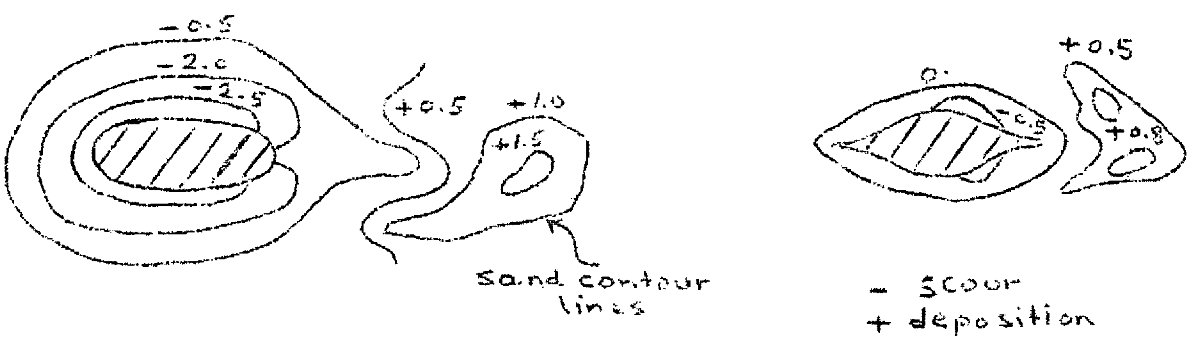

concluded that the sand around a bicusped strut is markedly less disturbed than that around an elliptical strut, due to the more gradual change in curvature in flow lines in the former case than in the latter.

Rozovskii (1957) suggested that the non-erosive velocity at the exit from the bend is about 78 % of that in a straight uniform channel of the same rate of flow.

I-5. Resistance factor in curved flow

One of the characteristics of flow around bends is the additional losses of energy due to helical motion. In experiments carried out by White (1929) on resistance to flow in coiled pipes of circular cross-section, the value of critical Reynolds number was found to increase with increasing curvature, i.e., decrease with the mean radius of coil; for curvature of 1/50, $Re_{cr}(= \bar{v}.d/\nu)$ was equal to 9000. The ratio of resistance coefficient in a curved pipe to that in a straight one, in which R_e is the same, was found to increase when the criterion $R_e(d/D)^{\frac{1}{2}}$, in which d is the pipe diameter and D is the mean radius of coil, increases.

Raju (1937) found that the coefficient of energy dissipation in a bend of an open channel $\Gamma = \dfrac{H_b}{v_n^2/2g}$, in which v_n is the average velocity for normal flow and H_b is the head loss due to curvature only, decreases nearly asymptotically to the value $\frac{2}{3}$ as h/b increases.

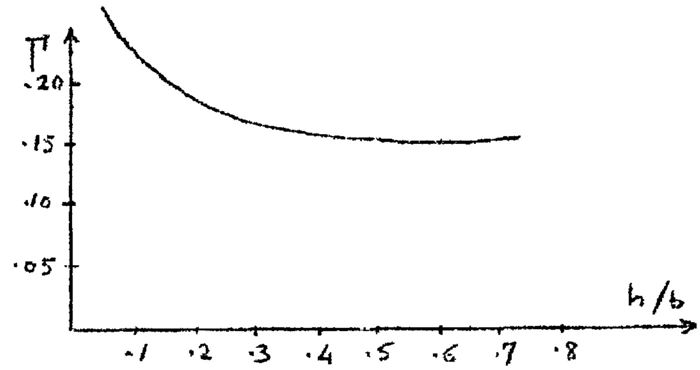

The coefficient λ_c of bend resistance, as given by Wadekar (1956), is a function of the following dimensionless parameters :

$$(Re\ ,\ \theta\ ,\ h/r_c\ ,\ b/h\ ,\ K/h)$$

in which θ is the angle of turn, h is the depth of flow and K is the height of roughness. He also stated that the energy loss which arises from the transition regions between the straight approaches and the bend is more than that arising from direct actions of the curved walls.

According to a statement by Allen and Shahwan (1954), the excess in energy loss in bends may be greater than that of the normal loss due to friction; from their experiments they concluded that bends and changes of channel geometry, as distinct from textural roughness, account for 47-76 % of the total resistance.

A brief study has been carried out in this field and can be seen in Appendix A.

CHAPTER II

THEORETICAL CONSIDERATIONS

The equations of motion of a continuous incompressible medium have often been written as (Schlichting) :

$$\left.\begin{aligned} \rho \frac{Du}{Dt} &= X + \left(\frac{\partial \sigma_x}{\partial x} + \frac{\partial \tau_{xy}}{\partial y} + \frac{\partial \tau_{xz}}{\partial z}\right) \\ \rho \frac{Dv}{Dt} &= Y + \left(\frac{\partial \tau_{xy}}{\partial x} + \frac{\partial \sigma_y}{\partial y} + \frac{\partial \tau_{yz}}{\partial z}\right) \\ \rho \frac{Dw}{Dt} &= Z + \left(\frac{\partial \tau_{xz}}{\partial x} + \frac{\partial \tau_{yz}}{\partial y} + \frac{\partial \sigma_z}{\partial z}\right) \end{aligned}\right\} \qquad \text{(II-1)}$$

where u, v and w are the instantaneous velocity components in the x, y and z directions respectively;

X, Y and Z are the respective components of the body force, i.e., gravity;

σ_x, σ_y and σ_z are the respective components of the normal stresses, or pressure, caused by the surface forces;

τ_{xy}, τ_{yz} and τ_{xz} are the respective components of the shearing stresses, or friction, caused by the surface forces.

Applying Stokes' law of friction in the case of fluid flow, where the stresses σ and τ are proportional to the time rate of change of strain, with proportionality factor μ the molecular viscosity of the fluid, and considering the continuity of flow, the above equations (II-1) become the Navier-Stokes equations.

On the other hand, the instantaneous components of velocity and stresses, u, v, w, σ and τ can be substituted by the sum of their temporal mean values and fluctuating ones :

$$\left.\begin{aligned} & u = \bar{u} + u' \;; \qquad v = \bar{v} + v' \;; \qquad w = \bar{w} + w' \\ & \sigma_x = -\bar{p} + 2\mu \frac{\partial \bar{u}}{\partial x} - \rho \overline{u'^2} \;; \quad \sigma_y = \cdots \;; \quad \sigma_z = \cdots \\ & \tau_{xy} = \mu\left(\frac{\partial \bar{u}}{\partial y} + \frac{\partial \bar{v}}{\partial x}\right) - \rho \overline{u'v'} \;; \quad \tau_{yz} = \cdots \;; \quad \tau_{xz} = \cdots \end{aligned}\right\} \qquad \text{(II-2)}$$

in which $\overline{u'^2}$, $\overline{u'v'}$, ... are the turbulent or apparent stresses of the flow.

Substituting these values into Eqs.(II-1), the Reynolds' equations are obtained.

Again, it is assumed that there exists a linear relationship between the turbulent stresses and the rate of change of strain of the fluid, with proportionality factor A. The stresses in Eq.(II-2) then become :

$$\left.\begin{aligned} & \sigma_x = -\bar{p} + 2\mu \frac{\partial \bar{u}}{\partial x} + 2A \frac{\partial \bar{u}}{\partial x} \;; \quad \sigma_y = \cdots \;; \quad \sigma_z = \cdots \\ & \tau_{xy} = \mu\left(\frac{\partial \bar{u}}{\partial y} + \frac{\partial \bar{v}}{\partial x}\right) + A\left(\frac{\partial \bar{u}}{\partial y} + \frac{\partial \bar{v}}{\partial x}\right) \;; \quad \tau_{yz} = \cdots \;; \quad \tau_{xz} = \cdots \end{aligned}\right\} \text{(II-3)}$$

The factor A, often called the coefficient of turbulent, or eddy, viscosity, is, unlike μ , dependent on the point coordinates in the flow.

In what follows, the derivation of the equations of motion in curved open channels is mainly quoted from Rozovskii (1957).

II - 1. Basic equations of fluid motion through a curved passage

In the study of flow in curved passages, particularly in circular bends, it is more convenient to write the equations of motion in cylindrical coordinates r, θ, z.

By introducing the set of equations (II-3) into Eqs.(II-1), and after transforming from Cartesian into cylindrical coordinates, the basic general equations of steady motion of a heavy incompressible fluid become (Schlichting and Rozovskii) :

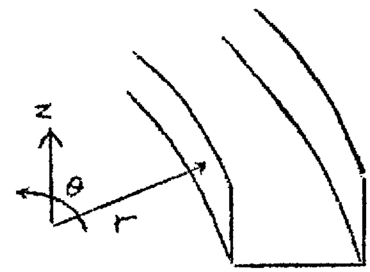

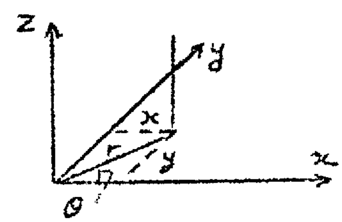

$$
\left.
\begin{aligned}
&\overline{v}_r \frac{\partial \overline{v}_r}{\partial r} + \frac{\overline{v}_\theta}{r}\frac{\partial \overline{v}_r}{\partial \theta} + \overline{v}_z \frac{\partial \overline{v}_r}{\partial z} - \frac{\overline{v}_\theta^{\,2}}{r} = -\frac{1}{\rho}\frac{\partial \overline{p}}{\partial r} + \\
&+\left(\frac{\mu - A}{\rho}\right)\left(\frac{\partial^2 \overline{v}_r}{\partial r^2} + \frac{1}{r}\frac{\partial \overline{v}_r}{\partial r} - \frac{\overline{v}_r}{r^2} + \frac{1}{r^2}\frac{\partial^2 \overline{v}_r}{\partial \theta^2} - \frac{2}{r^2}\frac{\partial \overline{v}_\theta}{\partial \theta} + \frac{\partial^2 \overline{v}_r}{\partial z^2}\right) + \\
&+ 2\frac{\partial (A/\rho)}{\partial r}\frac{\partial \overline{v}_r}{\partial r} + \frac{\partial (A/\rho)}{r\,\partial \theta}\left(\frac{1}{r}\frac{\partial \overline{v}_r}{\partial \theta} + \frac{\partial \overline{v}_\theta}{\partial r} - \frac{\overline{v}_\theta}{r}\right) + \frac{\partial (A/\rho)}{\partial z}\left(\frac{\partial \overline{v}_z}{\partial r} + \frac{\partial \overline{v}_r}{\partial z}\right) \\
&\overline{v}_r \frac{\partial \overline{v}_\theta}{\partial r} + \frac{\overline{v}_\theta}{r}\frac{\partial \overline{v}_\theta}{\partial \theta} + \overline{v}_z \frac{\partial \overline{v}_\theta}{\partial z} + \frac{\overline{v}_r \overline{v}_\theta}{r} = -\frac{1}{\rho}\frac{\partial \overline{p}}{r\,\partial \theta} + \\
&+\left(\frac{\mu + A}{\rho}\right)\left(\frac{\partial^2 \overline{v}_\theta}{\partial r^2} + \frac{1}{r^2}\frac{\partial^2 \overline{v}_\theta}{\partial \theta^2} + \frac{\partial^2 \overline{v}_\theta}{\partial z^2} + \frac{1}{r}\frac{\partial \overline{v}_\theta}{\partial r} + \frac{2}{r^2}\frac{\partial \overline{v}_r}{\partial \theta} - \frac{\overline{v}_\theta}{r^2}\right) + \\
&+ \frac{\partial (A/\rho)}{\partial r}\left(\frac{1}{r}\frac{\partial \overline{v}_r}{\partial \theta} + \frac{\partial \overline{v}_\theta}{\partial r} - \frac{\overline{v}_\theta}{r}\right) + \frac{2\,\partial (A/\rho)}{r\,\partial \theta}\left(\frac{\partial \overline{v}_\theta}{r\,\partial \theta} + \frac{\overline{v}_r}{r}\right) + \frac{\partial (A/\rho)}{\partial z}\left(\frac{\partial \overline{v}_\theta}{\partial z} + \frac{1}{r}\frac{\partial \overline{v}_z}{\partial \theta}\right) \\
&\overline{v}_r \frac{\partial \overline{v}_z}{\partial r} + \frac{\overline{v}_\theta}{r}\frac{\partial \overline{v}_z}{\partial \theta} + \overline{v}_z \frac{\partial \overline{v}_z}{\partial z} = -g - \frac{1}{\rho}\frac{\partial \overline{p}}{\partial z} + \\
&+\left(\frac{\mu + A}{\rho}\right)\left(\frac{\partial^2 \overline{v}_z}{\partial r^2} + \frac{1}{r^2}\frac{\partial^2 \overline{v}_z}{\partial \theta^2} + \frac{\partial^2 \overline{v}_z}{\partial z^2} + \frac{1}{r}\frac{\partial \overline{v}_z}{\partial r}\right) + \\
&+ \frac{\partial (A/\rho)}{\partial r}\left(\frac{\partial \overline{v}_z}{\partial r} + \frac{\partial \overline{v}_r}{\partial z}\right) + \frac{\partial (A/\rho)}{r\,\partial \theta}\left(\frac{\partial \overline{v}_\theta}{\partial z} + \frac{\partial \overline{v}_z}{r\,\partial \theta}\right) + 2\frac{\partial (A/\rho)}{\partial z}\frac{\partial \overline{v}_z}{\partial z}
\end{aligned}
\right\} \quad \text{(II-4)}
$$

The continuity equation is :

$$\frac{\partial \bar{v}_r}{\partial r} + \frac{\bar{v}_r}{r} + \frac{\partial \bar{v}_\theta}{r \partial \theta} + \frac{\partial \bar{v}_z}{\partial z} = 0 \qquad \text{(II-5)}$$

By solving the above equations for particular boundary conditions, the relations between $\bar{v}_r$, $\bar{v}_\theta$ and $\bar{v}_z$ can be obtained.

In laminar flow, and in the laminar sub-layer of turbulent flow, all the terms containing the factor A can be dropped from Eqs.(II-4), and the Navier-Stokes equations are then obtained.

In turbulent flow away from the boundaries, on the other hand, all the terms containing μ , being of relatively very small magnitude compared to A, can be dropped from Eqs.(II-4).

Henceforth, the bars over velocities and pressures in the basic equations (II-4) and (II-5) will be omitted for the sake of simplicity.

II - 2. Simplification of the general equations in the case of two-dimensional flow in a long circular bend of a wide stream away from the side walls

The following investigation is limited to turbulent flow.

In a long bend (gentle curvature where $b/r_c \ll 1$, where b is the width of the stream and r_c is the central radius of curvature), the flow at some distance from the bend entry reaches a fully developed state in which the flow pattern and the velocity distribution do not change from section to section, and all the derivatives with respect to θ , except that of the pressure where $\frac{\partial p}{r\,\partial\theta}$ = constant, become equal to zero.

Moreover, it was found from experimental observations, Ben-Chie Yen (1965), that in a wide stream in which $h/b \ll 1$ and $h/r \ll 1$, where h is the depth of the flow, the order of magnitude of the ratio $\frac{v_r}{v_\theta}$ is of the order of h/r, and that of $\frac{v_z}{v_\theta}$ is of the order of (h/r)(h/b) except at regions near the side walls, where the order of magnitude of v_z approaches that of v_r.

As regards the turbulent stresses, Eqs.(II-2), it is also assumed that the pressure fluctuations $\rho\overline{u'^2}$, $\rho\overline{v'^2}$ and $\rho\overline{w'^2}$ are all of the same order of magnitude and found, from experimental observations, to be of the order of magnitude of $(h/r)(\frac{v_r}{v_\theta})$, or $(h/r)^2$. The Reynolds shear stresses $\rho\overline{u'v'}$, $\rho\overline{v'w'}$ and $\rho\overline{u'w'}$ are also found to be of the order of magnitude of $(h/r)^2$, (Ben-Chie Yen).

With the aforesaid orders of magnitudes of the different terms in Eqs.(II-4), and considering a first approximation (with an accuracy of h/r), the third equation of this set reduces, in the case of a long bend $(\frac{\partial v}{\partial\theta} = 0)$, to :

$$g + \frac{1}{\rho}\frac{\partial p}{\partial z} = 0 \qquad \text{(II-6)}$$

meaning a hydrostatic pressure distribution along the flow depth.

Integrating Eq.(II-6), and then differentiating the result with respect to r and θ respectively, one obtains :

$$\frac{\partial p}{\partial r} = \rho g \frac{\partial z}{\partial r} = \rho g I_r \qquad \text{(II-7)}$$

$$\frac{\partial p}{\partial \theta} = \rho g \, r \frac{\partial z_o}{r \partial \theta} = -\rho g I_\theta r \qquad \text{(II-8)}$$

in which I_r and I_θ are the radial and tangential slopes of the free surface respectively.

Substituting Eqs.(II-7) and (II-8) into the first and second equations of (II-4), and considering the orders of magnitudes mentioned above, the first and second equations for turbulent flow in a long bend $(v_r^2 \cong 0)$ of a wide stream reduce to :

$$-\frac{v_\theta^2}{r} = -g I_r + \frac{\partial}{\partial z}\left(\frac{A}{\rho}\frac{\partial v_r}{\partial z}\right) \qquad \text{(II-9)}$$

$$v_r \frac{\partial v_\theta}{\partial r} + v_z \frac{\partial v_\theta}{\partial z} + \frac{v_r v_\theta}{r} = g I_\theta + \frac{\partial}{\partial z}\left(\frac{A}{\rho}\frac{\partial v_\theta}{\partial z}\right) \qquad \text{(II-10)}$$

and the continuity equation to :

$$\frac{\partial v_r}{\partial r} + \frac{v_r}{r} + \frac{\partial v_z}{\partial z} = 0 \qquad \text{(II-11)}$$

As the coefficient of eddy viscosity $A = \nu_T \rho$ (in which ν_T is called the kinematic coefficient of eddy viscosity) changes from point to point in the flow, its distribution should be determined, and the distribution of v_θ should be known in order to solve v_r and v_z in Eqs.(II-9) and (II-10).

Regarding the distribution of the forward velocity v_θ for the present work, the logarithmic distribution, as suggested by Prandtl and Von Karman, is found to be very close to the experimental distribution at the bend entry (see Chapter IV). It was also concluded, by Rozovskii, that the logarithmic distribution (assumed to hold true in both the straight and curved sections) gives values of v_r and v_z in the bend close to their measured values. Referring by η = z/h (when z is the height of the considered point from the channel bed) to the relative depth of a point from the channel bed, and $v_* = \sqrt{\tau_o/\rho}$ to the friction velocity in which τ_o is the shearing stress at the bed, the logarithmic profile is written as :

$$v_\theta = v_{\theta max} + \frac{1}{\chi} v_* \ln \eta \qquad \text{(II-12)}$$

in which χ is the Karman constant and $v_{\theta\, max}$ is at the water surface.

Alternatively, Equation (II-12) can be written in terms of the average velocity over the depth of the flow $v_{\theta m}$ as :

$$v_\theta = v_{\theta m} \left[1 + \frac{\sqrt{g}}{\chi C} \left(1 + \ln \eta \right) \right] \qquad \text{(II-13)}$$

in which C is the Chezy coefficient.

On the assumption of a logarithmic velocity profile and linear distribution of frictional stresses (τ_o at bottom, zero at the free surface), the analysis of turbulent flow over a flat plate ($v_r = v_z = 0$) produces the following distribution, along the depth, of the kinematic coefficient of eddy viscosity ν_T :

$$\nu_T = \chi\, h\, v_{\theta m} \frac{\sqrt{g}}{C} \eta \left(1 - \eta \right) \qquad \text{(II-14)}$$

in which h is the depth of flow, $v_{\theta m}$ is the average velocity over the flow depth and $\eta = z/h$.

Equation (II-9) can be written, in terms of ($\eta = z/h$), as :

$$-\frac{v_\theta^2}{r} + g\,I_r = \frac{1}{h^2}\frac{\partial}{\partial \eta}\left(\nu_T \frac{\partial v_r}{\partial \eta}\right) \qquad \text{(II-15)}$$

To determine v_r from this last equation, the first term on the left-hand side can be known from Eq.(II-13), ν_T can be known from Eq.(II-14); the radial slope I_r of the free surface can be calculated in a first approximation solution from:

$$I_r \simeq \alpha_0 \frac{v_{\theta m}^2}{g\,r_c} \qquad \text{(II-16)}$$

with $\alpha_0 \simeq 1$

Equation (II-15), with only v_r unknown, was integrated by Rozovskii, and the following formula resulted :

$$v_r = \frac{1}{\chi^2} v_{\theta m} \frac{h}{r}\left[F_1(\eta) - \frac{\sqrt{g}}{\chi C} F_2(\eta)\right] \qquad \text{(II-17)}$$

with

$$\left.\begin{aligned} F_1(\eta) &= \int \frac{2\ln \eta}{\eta - 1}\,d\eta \\ F_2(\eta) &= \int \frac{\ln^2 \eta\,d\eta}{\eta - 1} \end{aligned}\right\} \qquad \text{(II-18)}$$

The functions $F_1(\eta)$ and $F_2(\eta)$ are given graphically in the following figure.

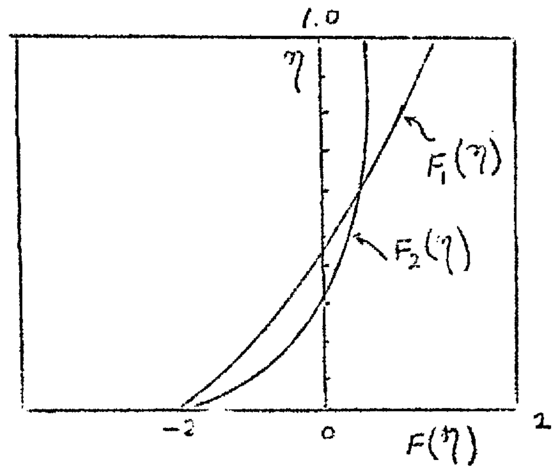

II - 3. Influence of inertia forces due to secondary currents

In deriving Eq.(II-17), no account was given to the inertia terms of the form $v_r \frac{\partial v_r}{\partial r} + v_z \frac{\partial v_r}{\partial z}$, and the argument was based on the assumption that flow in a bend follows circular trajectories of constant radii along the depth of the flow. In actual fact, however, the curvature of flow lines changes continuously around the bend and also along the flow depth. Due to velocity changes from bottom to top, the bottom trajectories are of higher curvature (1/r) than that of the bend, whereas the top trajectories are of smaller curvature than that of the bend. Consideration of this is particularly important in a bend of sharp curvature where b/r_c is not much less than one, as in the case of Channel I. However, Equation (II-9) has been re-integrated by Rozovskii after considering these inertia terms, and Eq.(II-17) is modified to the following form:

$$v_r = \frac{1}{X^2} v_{\theta m} \frac{h}{r}\left[F_1(\eta) - \frac{\sqrt{g}}{Xc} F_2(\eta) + \frac{2.25}{X^3}\frac{c}{\sqrt{g}}\left(\frac{h}{r}\right)^i\left(\eta^2 - \eta + \frac{1}{6}\right)\right] \quad \text{(II-17-a)}$$

The additional term (the last on the right-hand side) in Eq.(II-17-a) exhibits its effect when h/r is not much less than one, and its effect diminishes rapidly otherwise.

II - 4. Side walls effects

As mentioned above, Eq.(II-17) was derived by assuming the flow to be unaffected by the side walls, due to the large width of the cross-section compared with the flow depth. The effect of the side walls, in these cases, is suggested by Rozovskii to extend over a narrow strip of about twice the depth of the flow from each bank. However, near the side walls of a wide stream and in a flow in a narrow channel, $b/h \leqslant 4$, the turbulent stresses $\rho\overline{u'^2}$,...., and $\rho\overline{u'v'}$,...., neglected in the previous derivation, are no longer negligible. Corresponding terms, considering the changes of v_r and v_z along r and z must, therefore, be introduced back into the simplified equations (II-6) and (II-9), bringing them to the forms :

$$g + \frac{1}{\rho}\frac{\partial p}{\partial z} = \nu_T\left(\frac{\partial^2 v_z}{\partial r^2} + \frac{\partial^2 v_z}{\partial z^2}\right) \quad \text{(II-6-a)}$$

$$-\frac{v_\theta^2}{r} = -\frac{1}{\rho}\frac{\partial p}{\partial r} + \nu_T\left(\frac{\partial^2 v_r}{\partial r^2} + \frac{\partial^2 v_r}{\partial z^2}\right) \quad \text{(II-9-a)}$$

These two equations have been solved by Ananyan (1957), and a distribution of v_r across the width of the channel was obtained for various aspect ratios b/h, as shown in the figure overleaf.

In Chapter IV, the radial velocity components were calculated on the basis of Eq.(II-17-a), and corrections in the regions under the effect of the side walls were introduced by interpolation from the figure alongside for the two channels, I (b/h = 8) and III (b/h = 3.3).

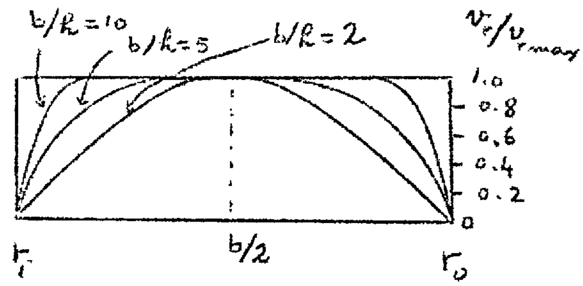

The corresponding vertical component v_z was then calculated from continuity.

II - 5. Approximate solution in the case of three-dimensional flow. - Modification of forward velocity around the bend due to secondary flow

Due to the secondary components of velocity mentioned in the above investigation, the fluid particles travelling along the bend suffer vertical as well as radial displacements. Owing to these displacements, an exchange of momentum between the separate currents takes place, and this alters the distribution of forward velocity around the bend. Unless the bend is very long, which is rarely the case in practice, no stable state of flow in curved channels, where it is justifiable to put $\frac{\partial v}{\partial \theta} = 0$, is maintained anywhere around the bend.

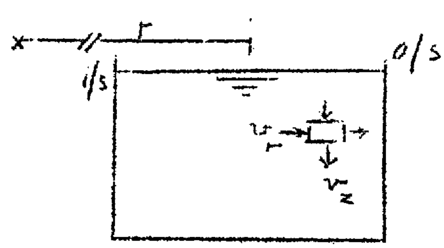

Such an assumption is only used as a first step in an approximate solution.

The modified value of v_θ, at any cross-section in the bend, can be calculated by adding the momentums in the main flow direction, due to the transversal flow, to the momentum due to the original forward velocity v_θ. The resultant value of momentum so calculated gives the new modified value of forward velocity. The solution {in the case of a wide stream under no effect of side walls} can be obtained by considering Eq.(II-10), adding back into it the term $\frac{v_\theta}{r}\frac{\partial v_\theta}{\partial \theta}$ and substituting τ_θ for $\left(A\frac{\partial v_\theta}{\partial z}\right)$, so that it becomes :

$$v_r \frac{\partial v_\theta}{\partial r} + \frac{v_\theta}{r}\frac{\partial v_\theta}{\partial \theta} + v_z \frac{\partial v_\theta}{\partial z} + \frac{v_r v_\theta}{r} = g I_\theta + \frac{1}{\rho}\frac{\partial \tau_\theta}{\partial z} \qquad \text{(II-19)}$$

This last equation was integrated by Rozovskii over the flow depth with the boundary conditions

$$(v_z)_{z=0} = (v_z)_{z=h} = (\tau_\theta)_{z=h} = 0$$

for logarithmic distribution of v_θ, Eq.(II-13), and v_r as taken from Eq.(II-17). The integration of Eq.(II-19) yields for these conditions :

$$0.75\frac{\sqrt{g}}{\chi^3 C}\,\frac{1}{r}\frac{\partial}{\partial r}\left(r h v_{\theta m}^2\right) + \frac{\partial}{\partial \theta}\left(v_{\theta m}^2 h\right) = -\frac{g}{C^2} r v_{\theta m}^2 + g r I_\theta h \qquad \text{(II-20)}$$

Equation (II-20) gives the solution for the change around the bend of the average velocity over the depth of the flow. It is applied in Chapter IV after transforming it into a finite difference equation, and solved by a digital computer. The solution was based on the measured averages of v_θ at the bend entry, and a comparison between the measured and calculated values at several cross-sections around the bend is performed.

However, to solve the distribution of forward velocity around the bend, at several points along the depth and across the width of the cross-sections (not only the average values over the depth), the second equation of motion (Eq.II-19), together with continuity considerations, was applied at 65 points in Channel I and 30 points in Channel III, at cross-sections every 15°. The results were computed by the method of finite differences on the basis of Eq.(II-17-a) at regions away from the side walls. In the side-wall regions, corrections were introduced to the values of v_r and v_z. A comparison between the calculated values of velocity v_θ with the measured values at these cross-sections was then made. A detailed investigation of this solution, and of the approximations adopted for it, is given in Chapter IV.

CHAPTER III

THE EXPERIMENTAL APPARATUS AND FLOW MEASUREMENT TECHNIQUES

III.A - The Apparatus

To identify and investigate the features of water flow in bends, an open channel of rectangular cross-section, consisting of a 180° semicircular bend and two straight approach sections, was built of reinforced concrete.

The dimensions of this channel were :-

Width of the cross-section	0.61 m.
Depth of the cross-section	0.28 m.
Length of upstream straight portion	3.36 m.
Radius on central line of semicircular bend	1.83 m.
Length of downstream straight portion	4.48 m.
Slope of the channel bed	horizontal

The aim of constructing such a big apparatus of heavy material was :

(i) To adapt to natural river proportions of width to depth ratios : it is possible to study, in this model, a 2 cm. flow-depth (and even less), making the aspect ratio, width to depth, equal to $\frac{61}{2} \cong 30$. A simplified solution of the equations of motion in such cases can be adopted.

(ii) To avoid possible twist and distortion which may occur in time to wide cross-sections of thin steel or perspex sheets; creep in concrete is very small and can be significant only after a very long period of time.

(iii) To reduce to a minimum the effect of vibration due to working pumps and mechanical appliances in the laboratory, an advantage particularly useful for research in low-speed flows.

(iv) To enable heavy additional equipment to be fitted safely on to the apparatus, or the experimentation with dense materials (sand, etc.)

After finishing the experiments on the full width of the channel, it was divided into two smaller channels, each 0.255 m. wide, by fitting a wooden barrier 10 cm. wide along the centre line of the original channel.

When experimenting on one of these two small channels, the other one was tightly blocked at each end. To avoid possible leakage through the barrier during the flow, the blocked channel was filled with water so that, when the flow was steady, a balance in static pressures of the moving and still water in the two channels took place, and leakage effects could no longer occur.

The three channels studied were of the following dimensions :-

Channel	Width of the cross-section (b), (m)	Central radius of bend (r_c), (m)	b/r_c
I	0.61	1.83	0.333
II	0.255	1.65	0.154
III	0.255	2.02	0.127

Figure (III-1) represents a general layout of the apparatus, and Plates (III-1) and (III-2) show the model after construction.

The most practical way of constructing the reinforced concrete channel (Channel I) was to pre-cast eleven small sections, seven of which were straight and 1.12 m. in length; the remaining four were 45° curved sections. These pre-cast sections were finally assembled in their permanent locations on reinforced concrete frames fixed to the laboratory floor; 0.63 cm. steel sheets were interposed on top of these frames to distribute the channel load uniformly. Three of the seven straight sections were fitted upstream of the bend, and the other four were fitted downstream of it.

For the purposes of flow visualization and measurements, transparent glass windows, 10 cm. wide, were provided every 1.12 m. in each side of the straight portions; in the curved section of the channel the windows were enlarged in width to 30 cm. to facilitate the photographing

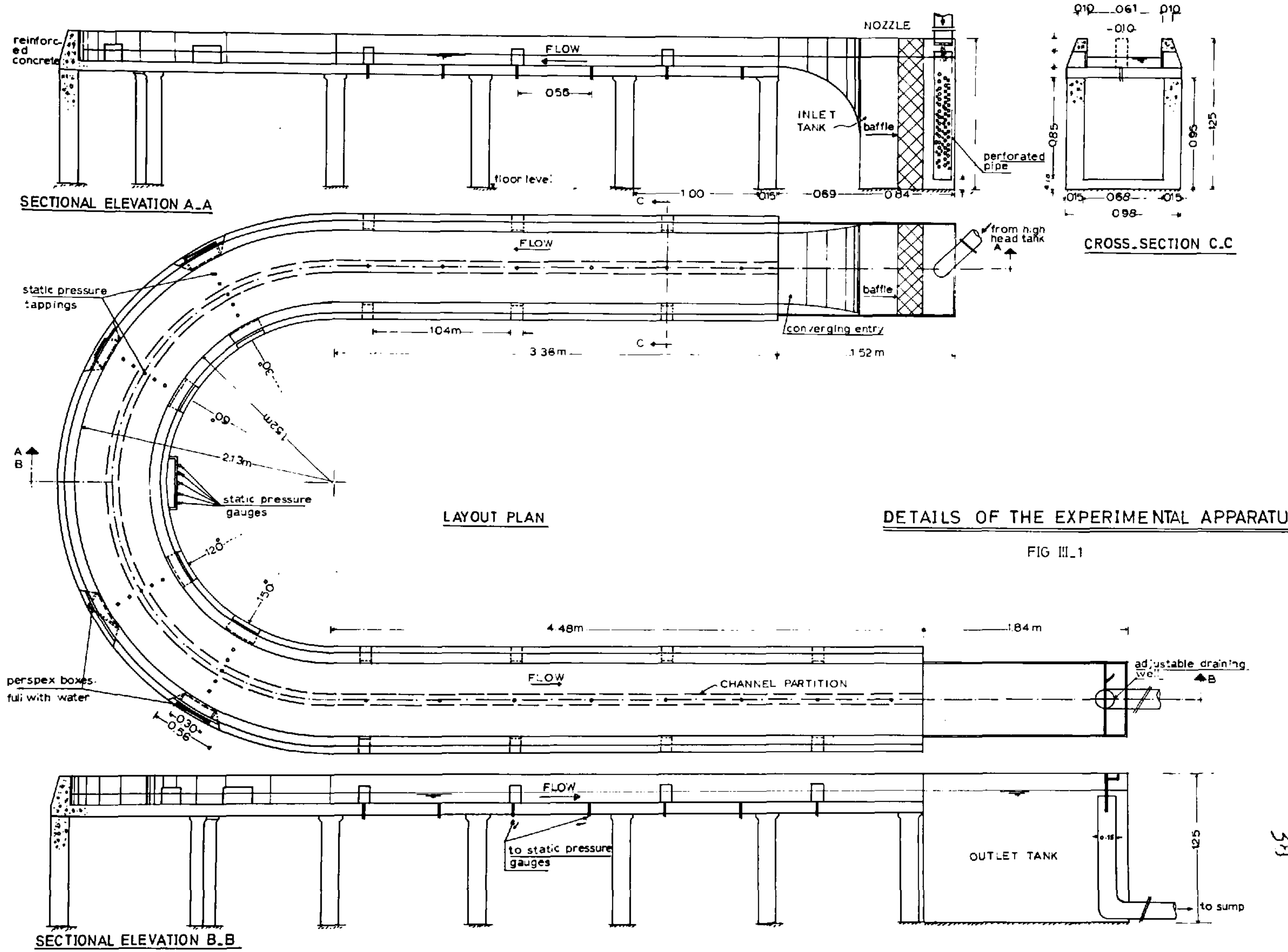

DETAILS OF THE EXPERIMENTAL APPARATUS

FIG III_1

Plate III-1, General view of Channel I, with photographic arrangements

Plate III-2, General view of Channels II and III of secondary currents. These windows were situated at both sides of cross-sections $\theta = 30^\circ$, 60°, 120° and 150° along the bend of Channel I.

For levelling the channel bed, the constituent sections were raised a little above the supporting frames by means of adjustable steel jacks over which they temporarily rested. Using a sensitive surveying level, the bed was made horizontal, and the pre-cast sections were then assembled together by steel bolts passing through holes designed for this purpose in the channel sides. The joints between the sections and the gaps between the channel and the supporting frames were then sealed by injecting SBD Certite, a compound prepared into a workable paste which hardened very rigidly and watertight within 40 minutes.

The heaviness of the structure (approximately 300 kg. for each pre-cast section), and the procedure of its assembly, called for a step-by-step technique for its levelling, since any levelled section would subsequently be affected by the neighbouring sections. In spite of the careful procedure of levelling, there was, after assembly, about 2.5 mm. of drop towards one of the downstream straight sections, and this was corrected by using thin steel sheets underneath the channel bottom for shimming up.

The final maximum random differences in the bed level over the whole channel were within $\pm$ 0.6 mm.

The practical and easy procedure of correcting the bed level at any time anywhere in the channel, and the possibility of re-forming the bend into different shapes (90°, S-shape, etc.), is a great advantage of using pre-cast sections in the construction of the present apparatus.

All the joints between the constituent sections were made as flush with the channel bed as possible, and, in the final stage of preparation, the channel was painted with a white, chlorinated rubber undercoat paint, EVODYNE, supplied by EVODE LIMITED; three coats of this paint over the finished concrete channel, bed and sides, gave it a smooth surface and effectively served as a sealing agent, so that, out of 32 different bed and side joints, no leakage of water was noticed throughout the time the experiments took place.

III.B - Flow Control and Flow Measurement Techniques

III.B.1 - Flow control. The water supply from an overhead tank discharged freely through a well-rounded circular nozzle at the end of a 15 cm. pipe. Two nozzles, of diameters 1.75 and 3.75cm. respectively, were used interchangeably to give a wide range of discharges. The flow in the 15 cm. supply pipe was controlled through a 5.1 cm. by-pass and a small valve for small changes in discharges. The pump which supplied the overhead tank was kept running throughout the experiments to maintain constant head. Water was freely discharged out of the nozzle into an entry tank 1.52 m. long by 0.9 m. wide, which, together with a 15 cm. thickness of hairlock and gentle elliptical convergences, provided efficient stilling and smooth flow before entry into the flume. After leaving the channel, the water was directed into a 1.84 x 0.9 m. exit tank from which it was drained over an adjustable 15 cm. diameter vertical tail well to the laboratory sump.

III.B.2 - Discharge measurements. For small discharges ($0.14 \times 10^{-3} \rightarrow 1 \times 10^{-3}$ m^3/sec.), the 1.75 nozzle was used. It was calibrated by weighing the issuing water on a scale with a capacity of 500 kg. Readings of corresponding heads were taken from a vertical, open-top water manometer connected to the pressure tapping of the nozzle and resting on a millimetric scale supplied with verniers. By the use of a 1/10 sec. stop-watch, a calibration curve between head on the manometer and corresponding discharge was obtained, Fig.(III-2). In the present range of small discharges, the head in the manometer was steady enough

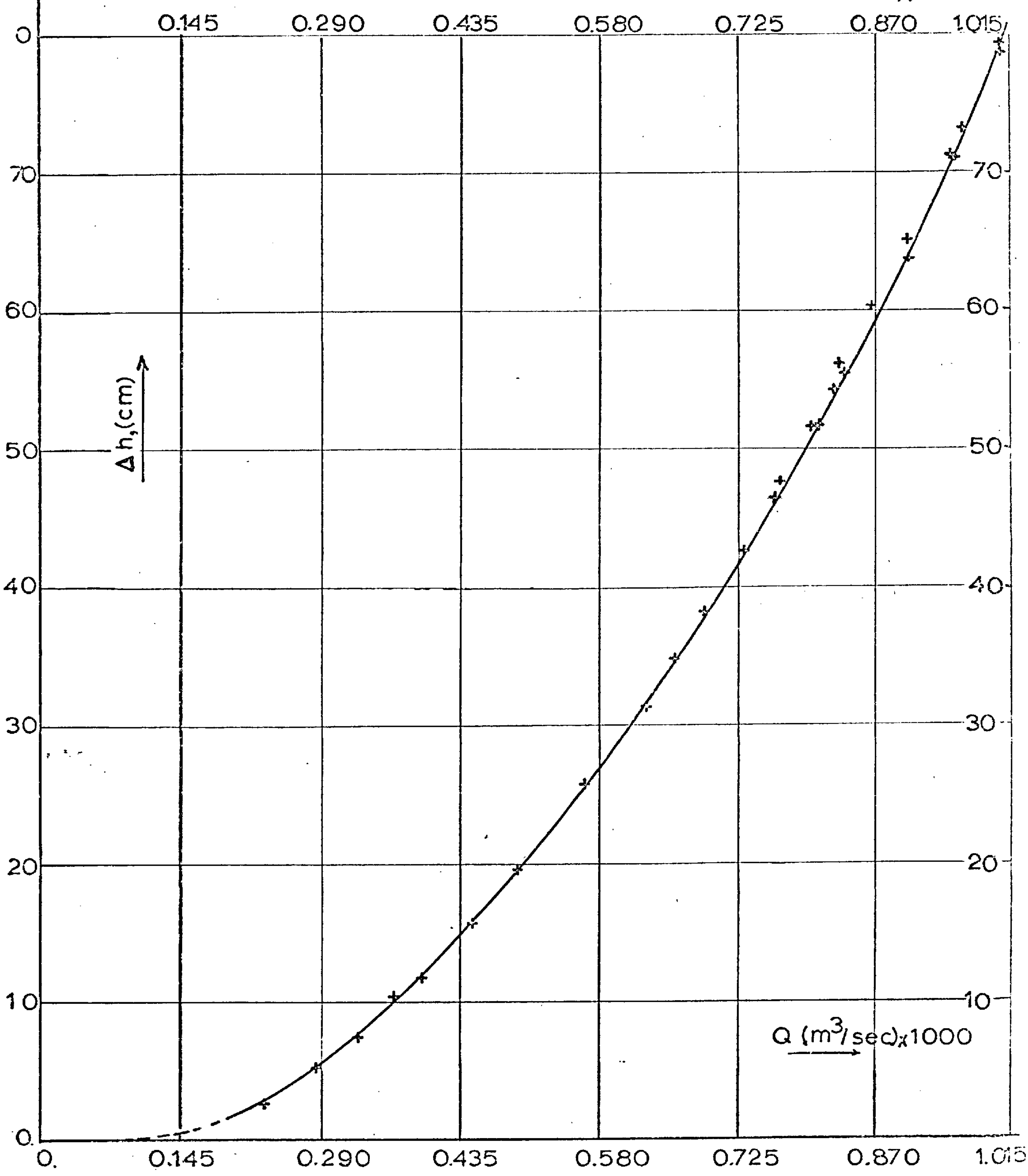

FIG III_2

CALIBRATION CURVE FOR THE SMALL NOZZLE D =1.75 cm.

to give an accuracy of readings of 1 mm.

For the high discharges ($0.86 \times 10^{-3} \rightarrow 5 \times 10^{-3}$ m^3/sec.), the larger nozzle, 3.75cm. diameter, replaced the small one, and, for calibration, the water discharged from the exit tank was diverted, temporarily, through a 15 cm. rubber hose to an underground measuring tank of plan area 10.85 m^2. A depth gauge, fitted on an inch scale with verniers, and read by an electrically-connected magic eye, enabled the reading of the water depths in the measuring tank; timing was of an accuracy of 1/10 second, and depth accuracy, on the gauge, was 0.01 inch (0.25 mm.). A calibration curve, between head and discharge, for this nozzle, was also drawn, Fig.(III-3). In this range of discharges, the readings on the manometer occasionally fluctuated to within a range of 1 cm., and the averages were considered.

III.B.3 - Depth measurements. The vertical adjustable tail well, 15 cm. in diameter, towards the end of the exit tank, over which the water discharged (referred to in III.B.1), provided an easy and efficient way of depth control, possible of exact depth resetting, whenever needed, to within 0.1 mm. of depth.

Because the flow in bends is substantially non-uniform, it was necessary to measure the depths of water at several locations in the bend and in the straight channels. Due to

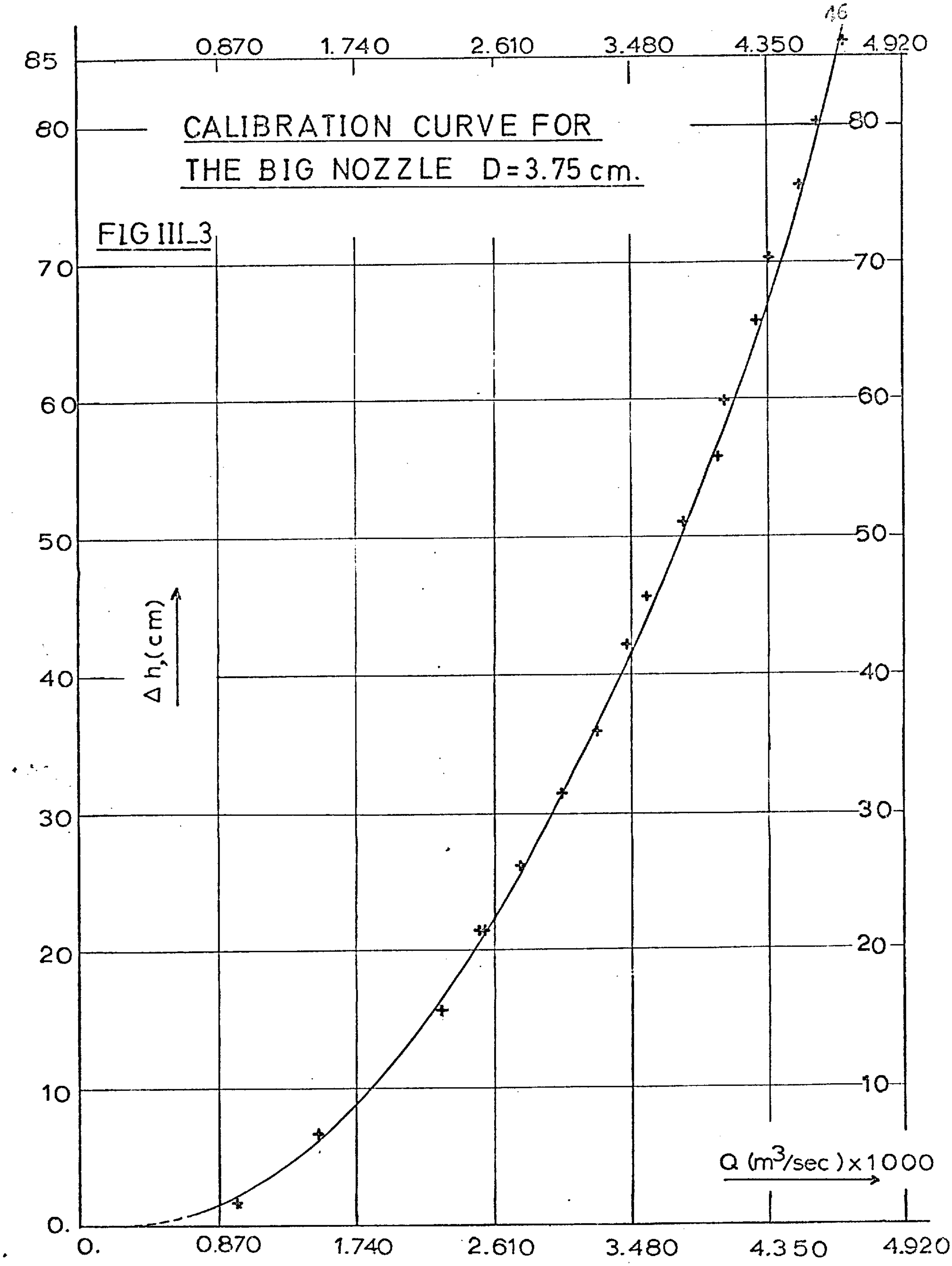
CALIBRATION CURVE FOR
THE BIG NOZZLE D=3.75 cm.
FIG III_3
Δ h,(cm)
Q (m3/sec) x 1000
0.
0.870
1.740
2.610
3.480
4.350
4.920
10
20
30
40
50
60
70
80
85
46

the curvature, it was difficult to construct the conventional depth gauge device which moves on rails fixed on top of the channel; static pressure holes, therefore, of 0.6 cm. diameter were provided along the centre line of the channel bed. The distances between these tappings along the straight portions were 56 cm. In the bend, on the other hand, five tapping points were provided equidistantly, about every 10 cm., at each of the cross-sections $\theta = 30^{o}$, 60^{o}, 120^{o} and 150^{o}, for measuring transversal water surface profiles. Readings of depths were obtained by connecting these tapping points through 0.6 cm. polythene tubes to a battery of six independent depth gauges supplied with verniers and supported on a vertical board at the middle of the bend, (Fig.III-1)

The connections between the tapping points and the depth gauges were in the following order :-

upstream straight channel .... connected to depth gauge 1
(6 tappings)

cross-section $\theta = 30^{o}$ .... connected to depth gauge 2
(5 tappings, designated from inner side to outer side as I,II,III,IV,V)

cross-section $\theta = 60^{o}$ .... connected to depth gauge 3
(5 tappings, as in $\theta = 30^{o}$)

cross-section $\theta = 120^{o}$ .... connected to depth gauge 4
(5 tappings, as in $\theta = 30^{o}$)

cross-section $\theta = 150^{o}$ .... connected to depth gauge 5
(5 tappings, as in $\theta = 30^{o}$)

downstream straight channel....... connected to depth gauge 6
(8 tappings)

All these depth gauges could read water depths to 0.025 mm. When reading at a particular point, the other tappings connected to that particular depth gauge were disconnected by means of locking clips.

In calculating mean velocities, Reynolds numbers and hydraulic mean radii, the depths of flow were calculated by taking the difference on the depth gauge between the corresponding readings of water surface and channel bed. For water surface configuration and energy gradient measurements (i.e., relative drop in water surface), on the other hand, all the depth gauges were referred to a still-water-level in the channel, and any flow surface was then defined, through these gauges, by the drop, or rise, from that still-water-level. This procedure was adopted since the small random differences in the channel bed, $\pm$ 0.6 mm., would only negligibly affect $\overline{V}$, Re, m, but would considerably affect i (the slope of the energy line) and the water surface configuration, particularly in low-speed flow, where i has but a small value. This will be numerically illustrated in Chapter V and Appendix A.

<u>III.B.4 - Velocity measurements.</u> The range of local velocities measured in this work extends from about 0.0025 m/sec. in laminar flow near the bed to about 0.177 m/sec. in turbulent flow at high velocity regions. This range necessitated two different techniques according to the speed of the flow :-

(i) Only Channel I was experimented upon for low-speed flow (laminar flow state), and a photographic technique was adopted for velocity measurements; the principle was to track and record the pathlines of well-distributed tiny neutrally-buoyant reflective tracer particles fed into the flow near the channel entry.

Under the steady laminar flow state, photographing a particular section at a time would give the distribution of local velocities at that section. To ensure identical pathlines between the tracer particles and the flow without introducing these particles, they should be of small size and neutral density.

The tracer agent used in these studies was a plastic powder, called Telcon, of specific gravity of 0.95 with mean particle size 0.1 - 0.2 mm.

The camera used was a Praktica VF reflex, for 24 x 36 mm. pictures. It is fitted with extension rings to take close photographs; the aperture ratio was 5.6 with exposure time depending on the speed of the flow.

Due to existing secondary currents in the bend, the particles' pathlines deviated radially, with different

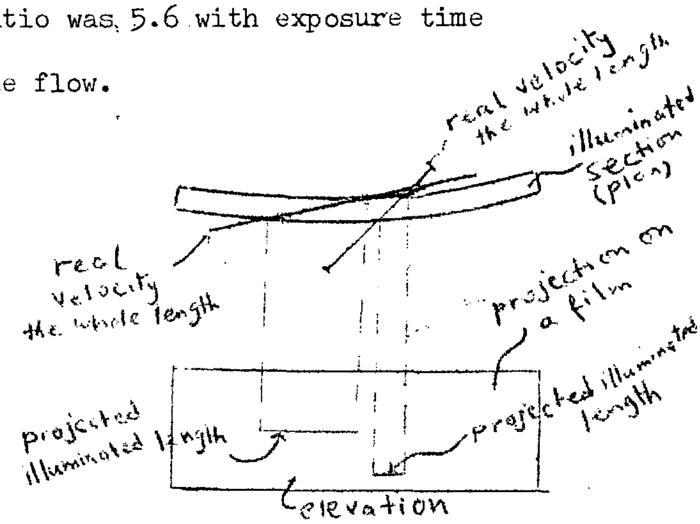

intensities along the flow depth, from the illuminated circumferential sections at which velocities were recorded, and, therefore, their projected images on a sensitive film do not really represent the flow velocities there. In order to measure the velocities, therefore, a small chopper was fitted on a small synchronised motor, Plate(III-3), of known constant speed of rotation, and the pathlines' images were then chopped into short dashes, as shown in Plate (IV-1). By photographing a scale at a particular section and then projecting the images on to a graphed sheet, the flow velocities were measured.

Two stations were chosen to record the three components of velocities: these were at $\theta = 30^{\circ}$ and $\theta = 150^{\circ}$. At each cross-section, measurements were taken at six locations over the width of the channel to record v_{θ} and v_z components, with the light projected from

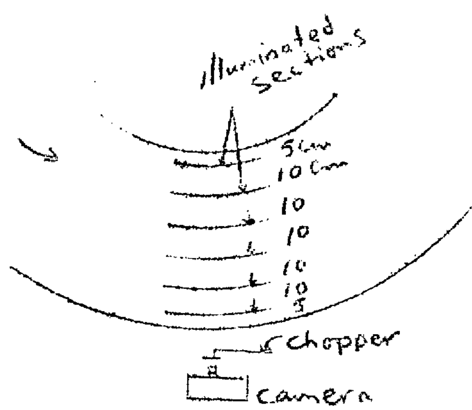

the top through a 1 cm. slit of 15 cm. long, and the camera mounted on a tripod perpendicular to the illuminated section; the chopper was introduced between the camera and the photo-

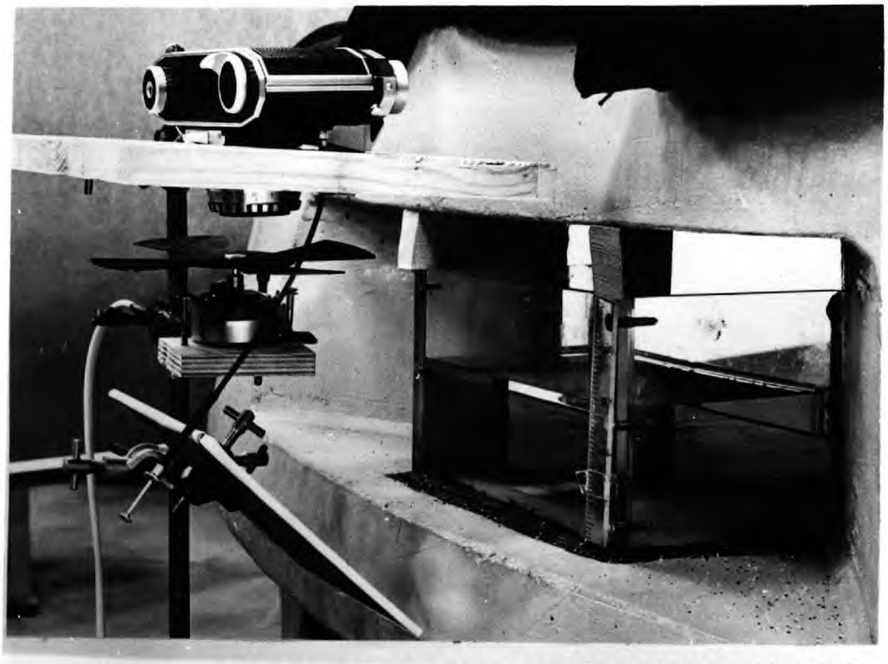

VELOCITY MEASUREMENTS(photographically)

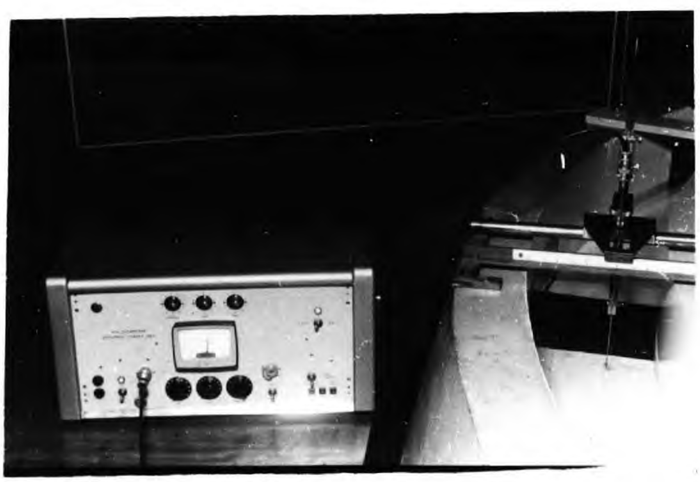

VELOCITY MEASUREMENTS (current meter)

FLOW MEASURING EQUIPMENT

PLATE (III_ 3)

graphed section.

For v_r measurements, the light was laterally projected through a 0.2 cm. slit, 15 cm. long, to illuminate the full width of the channel, and the camera and chopper were mounted at the top; sections parallel to the bed, at every 1.25 cm. from the bed upwards, were photographed. Owing to the very low speed of flow in this range, the secondary current components were of extremely small magnitudes, and could not, therefore, be measured very correctly due to the imperfect neutrality of the tracer material.

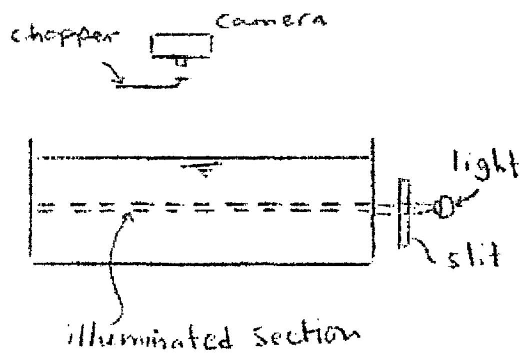

The photographic technique applied to the 22 sections mentioned above was, of course, tedious and time-consuming, and can only be recommended, therefore, when a very limited number of sections are to be studied and where there is no other alternative at hand to measure such very low-speed flow.

(ii) In high-speed flow (turbulent flow state), the photographic technique, using a different chopper and a motor of higher speed, was also applied at the same cross-sections for measuring the local mean tangential velocities.

However, due to turbulence effects, it was necessary to take many photographs at each section in order to know the local temporal mean values of velocities, an impracticability which led to discarding the technique in this state of flow and adopting a current meter method; the latter method enabled, moreover, the measurement of the v_θ distribution at many cross-sections around the bend where photography could not be applied. To this end, a miniature current meter, consisting of a small propeller of about 0.6 cm. diameter having five small rotating blades, was used; attached to an electronic counter unit, Dekatron, as shown in Plate (III-3), the number of rotations of the propeller during a particular period of time can be known. A calibration curve, Fig.(III-4), of this meter, giving the velocity of flow against the number of rotations in every 10 seconds, enabled the measurement of velocities down to 2 cm/sec. Obviously, due to turbulence there will be some differences in the number of rotations for repeated measurement at a point; the average of two readings at every point was considered, and the maximum deviation from the mean readings in this work did not exceed 3% at any point.

This technique was applied to study v_θ distribution along the depth and across the width of 15 cross-sections in both Channels I and III, starting from 0.50 m. before the bend entry and ending at 0.50 m. after the bend exit, at consecutive

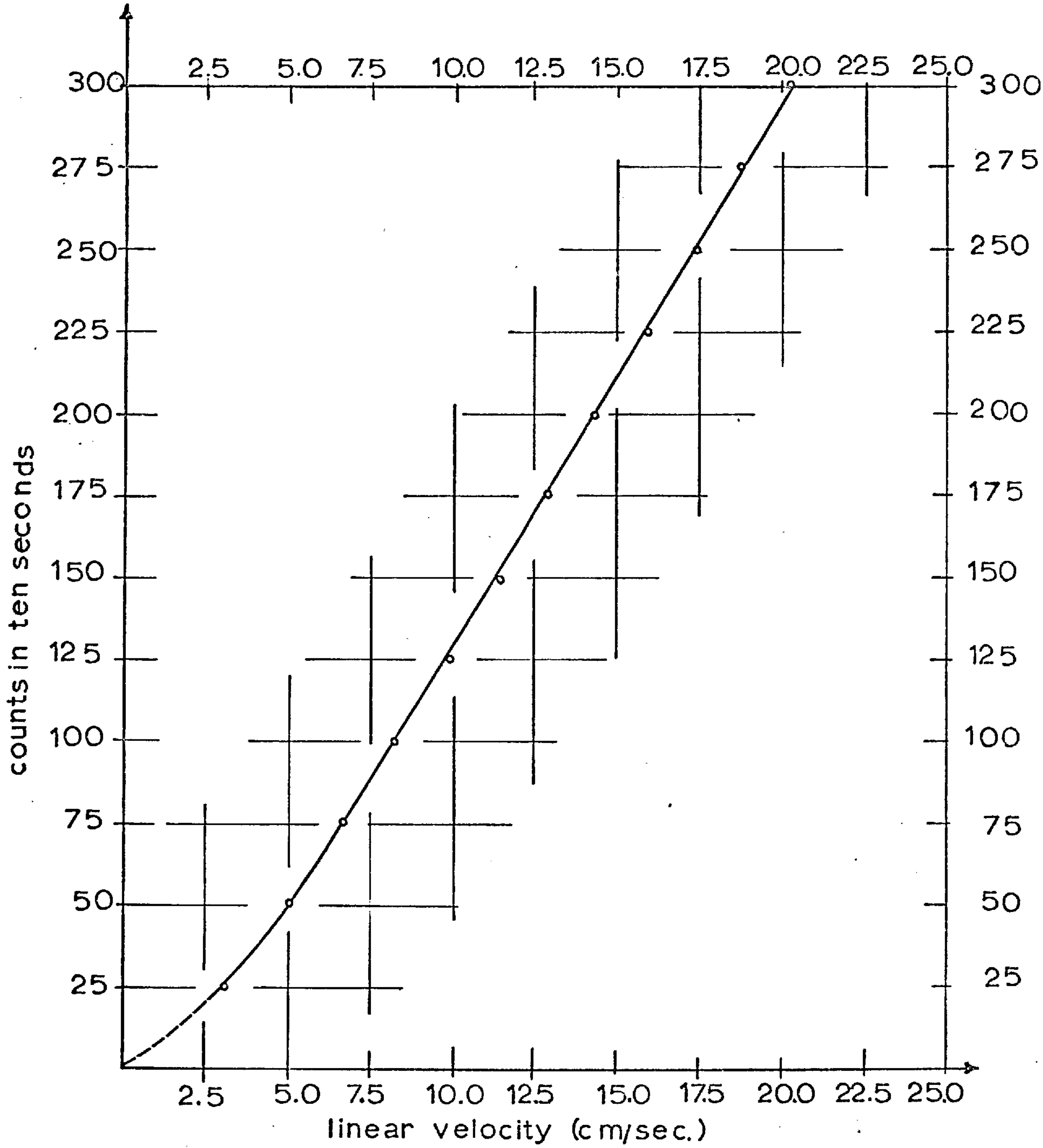

CALIBRATION CURVE FOR THE MINIATURE CURRENT METER

FIG III-4

sections every 15^{o} around the bend.

III.B.5 - Bed shear stress measurements. The distribution of bed shear stress around the bend was obtained by measuring the speed of small glass spheres, about 2 mm. in diameter, rolling on the bed. This simple technique has the advantage of enabling both longitudinal and radial bed shear stresses in the bend to be known. The glass spheres were calibrated first in a straight smooth flume, 0.56 m. wide and 12 m. long, in the laboratory. Uniform flow was maintained during calibration, and the velocity of the rolling grains, recorded over 1.8 m. distance at the mid-section of the flume, was plotted against the corresponding average bed shear stress in uniform flow, calculated as $\tau_o = \gamma h s$.

At every point in both the calibration flume and the two curved channels (Channels I and III), readings were repeated five times and the averages were considered. It is believed that no misleading results occur due to applying the calibration obtained from a straight flume to calculate bed shear in a curved one. The bed shear in the curved channel will have, due to the effect of secondary flow, a component in each of the tangential and radial directions.

III.B.6 - Bed-and-flow-angles measurements. The horizontal obliquity of the flow at any point in the bend relative to the circumferential direction gives an estimation of the intensity of secondary currents. This will be dealt with further in Chapter V.

The angles of deviations at the bed(bed angles) were measured around the bend in the three channels, and for different discharges and depths of flow. In laminar flow, the bed angles were visualized using crystals of Potassium Permanganate, and the resulting dye-streaks made angles α_o with the circumferential directions. Bed angles were measured by using a perspex pointer, 2.5 cm. thick, Plate (III-4), on the polished top and bottom faces of which two sharp lines were drawn on a vertical plane. The pointer was connected through a thin tube to a small indicator rotating on a horizontal protractor marked to 0.5 degree of arc. A reading of α_o at a point was recorded when the vertical plane passing through the two lines on the pointer passed tangential to the dye-streak at the bed. The Potassium Permanganate was chosen here because it is readily soluble and was therefore convenient in the present range of low-speed flow; on the other hand, it had the disadvantage of developing wide streaks on the bed, sometimes of 2 cm. width, and the location of the tangent to the dye-streak could only be estimated with an accuracy not higher than $\pm 1^o$.

In the case of turbulent flow, Process Black, another,

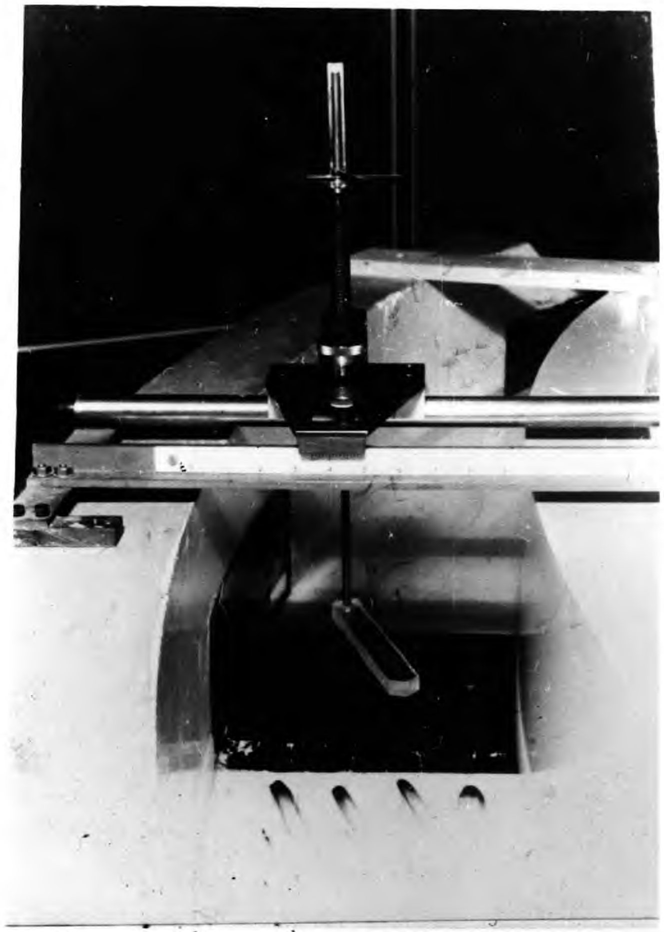

BED ANGLES MEASUREMENTS

FLOW ANGLES MEASUREMENTS

PLATE(III -4)

FLOW MEASURING EQUIPMENT

denser, dye, was chosen, and the resulting dye-streaks were fairly sharp, giving an accuracy of reading of $\pm 0.5^\circ$.

Flow angles (i.e., horizontal angles between real flow and circumferential directions along the depth in the main body of flow) were also measured around the bend in the three channels, but only in turbulent flow, by using a very thin tube, 1 mm. in diameter, to the lower end of which a thin black cotton thread of about 5 cm. length was attached. The horizontal deviation of the thread from the circumferential direction was read as in the previous bed angles measurements, Plate (III-4). Due to turbulence in the flow, the thread fluctuated within a range depending on the depth of the measured point, and average readings were considered with an accuracy ranging between $\pm 0.5^\circ \rightarrow \pm 1^\circ$.

III.B.7 - Secondary currents visualization. The patterns of secondary flow at $\theta = 30^\circ$ and $\theta = 150^\circ$ in the bend of Channels I and III only were recorded by photographing in a direction perpendicular to the cross-section concerned, illuminated tracer particles being fed in at the channel entry. It was not possible to photograph secondary currents in Channel II as the side windows were in a concave wall; the cross-sections were illuminated by a 1500 w. Phillips Lino-Lite lamp through about 2.5 cm. slit. The projection of pathlines of the illuminated particles on the plane of the cross-section gives the pattern of secondary flow. To define the direction of the secondary flow at every point, the rear (upstream) half of the slit width was covered with a strip of unexposed developed film, so that the brighter half of a particle pathline image on the picture showed the secondary flow direction at that point.

The same tracer (Telcon) was used for secondary currents measurements. In a trial to improve the quality of the pictures, another tracer was used, consisting of droplets of a mixture of 10 cc. of Nitrobenzene, 22 cc. of olive oil, and 15 cc. of water to bring the specific gravity to 1. Further details are given in Chapter V.

CHAPTER IV

VELOCITY DISTRIBUTION AROUND THE BEND

As was mentioned in Chapter III, the range of experimental values of local mean forward velocities in this study necessitated the use of two different techniques for measurements. These were: a photographic technique in laminar flow, and a miniature current meter in turbulent flow.

The following study, therefore, deals with these two states of flow separately.

IV - 1. Velocity distribution in laminar flow

The procedure for measuring the velocity distribution is described in Chapter III. At cross-sections $\theta = 30^{o}$ and $\theta = 150^{o}$ in Channel I (the only channel in which measurements in this state of flow were taken), measured profiles of forward velocity distributions are shown in Figs.(IV-1) and (IV-2) respectively. One value of flow depth equal to 7.6 cm. at $\theta = 30^{o}$ was studied for the three following values of Reynolds number :

$$Re = \frac{\bar{v}.m}{\nu} = 246, \quad 422, \quad 545$$

Examining these two figures, two main observations can be stated :

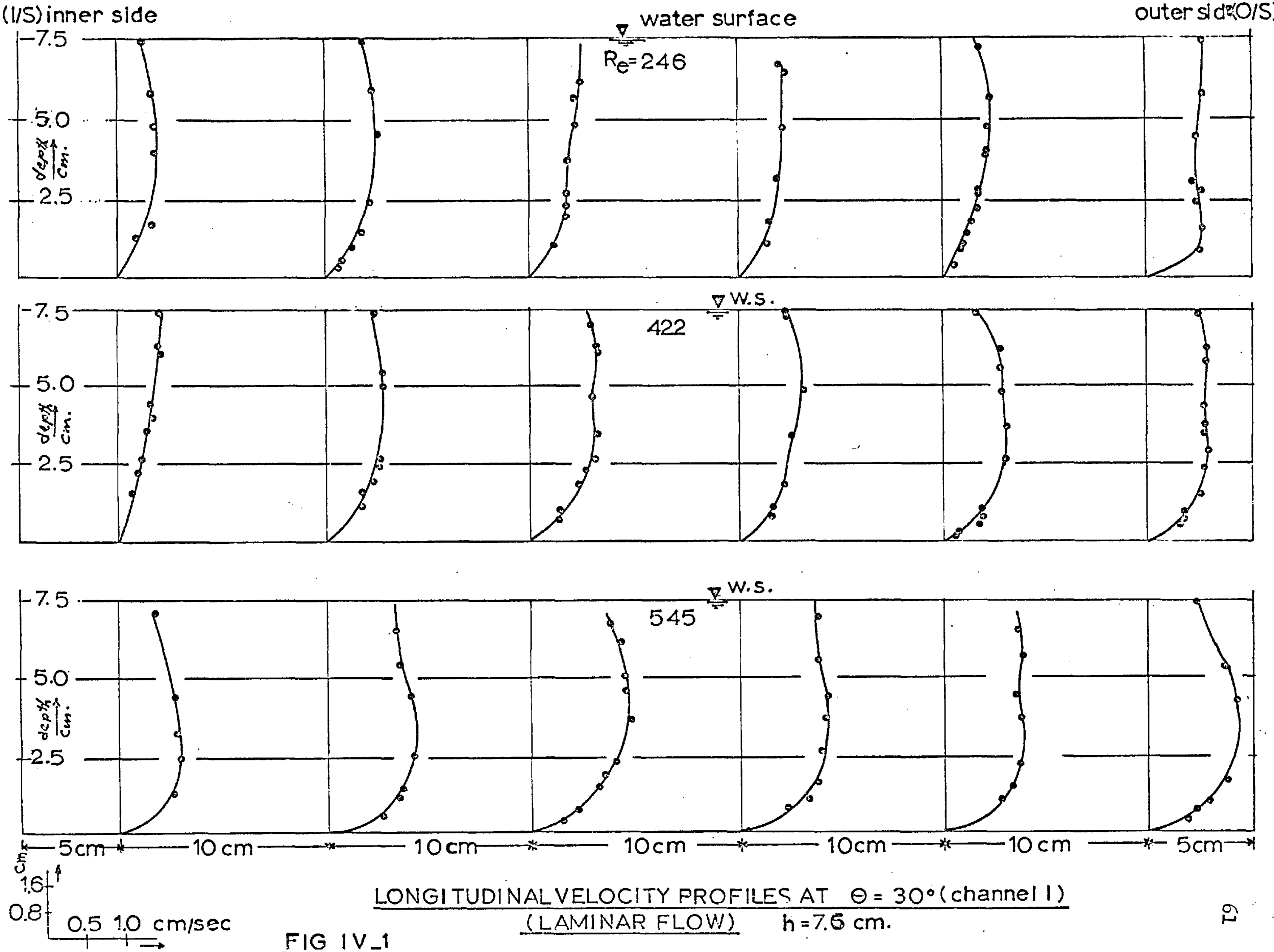

LONGITUDINAL VELOCITY PROFILES AT $\Theta = 30°$ (channel I)
(LAMINAR FLOW) h = 7.6 cm.

FIG IV_1

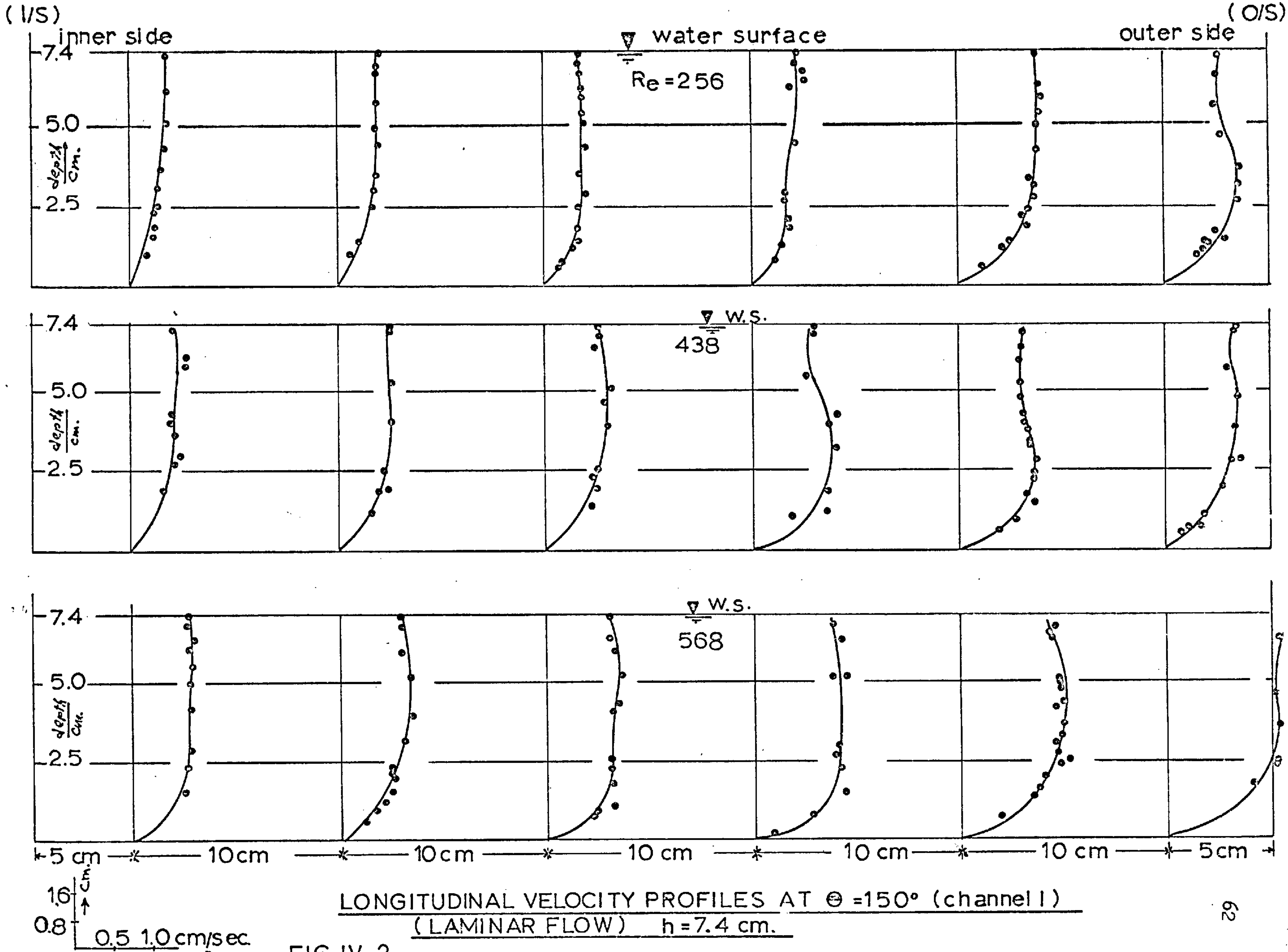

LONGITUDINAL VELOCITY PROFILES AT Θ =150° (channel I)
(LAMINAR FLOW) h = 7.4 cm.

FIG IV_2

1) The maximum forward velocity occurs near the outer-side of the channel in the two cross-sections, $\theta = 30^\circ$ and $\theta = 150^\circ$.

2) The maximum forward velocity occurs below the water surface (and at some regions far below the water surface, almost at the mid-depth of the flow).

As regards the first observation (which contradicts observations for turbulent flow in the early region of the bend, as will be shown later), the location of maximum velocity near the outer-side at $\theta = 30^\circ$ can be attributed to the effects of viscosity, which has the dominant role in this flow state. Contrary to the case of potential flow in bends, where free vortex phenomenon is a characteristic, the viscous flow in long bends is expected to behave as a forced vortex - with increasing velocity at increased radius. On the other hand, the momentum exchange due to secondary currents in bends, which is responsible in all cases for shifting the high velocity region towards the outer-side in curved flows, is stronger in laminar than in turbulent flow. It is shown in Chapter V that the relative magnitudes of secondary currents $\frac{v_r}{v_\theta}$ and $\frac{v_z}{v_\theta}$ are higher in the case of laminar than of turbulent flow. The forward acceleration which always takes place near the inner-

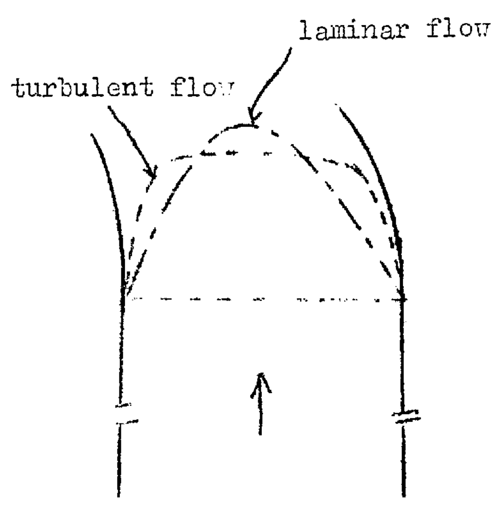

side when the flow enters a bend is not capable of overpowering the effect of outward flow due to centrifugal forces at the water surface, and the maximum forward velocity, originally at the centreline of the channel, will be shifted outwards.

However, such analysis as is proposed here needs to be checked by further experiments on several cross-sections in the early region of the bend.

Regarding the second observation, the depression of maximum velocity below the water surface can also be attributed to the exchange of momentum by secondary currents. Photographs to prove this second observation were taken in both laminar and turbulent flow states, and are reproduced in Plate (IV-1).

A trial was made to measure the secondary components of velocity v_r and v_z with this photographic technique. Plates (IV-1) and (IV-2) can be used to determine v_θ, v_z and v_θ, v_r respectively (see Chapter III). However, these plates show the extreme difficulty in measuring the secondary components because the latter are basically of very small magnitudes; in addition, the tracer (Telcon, with specific gravity about 0.95) used for velocity measurements was not exactly a neutral one. Another difficulty was encountered in illuminating parallel horizontal sections at short distances apart for measurement of v_r (see Chapter III).

The difficulties mentioned above led to discarding the

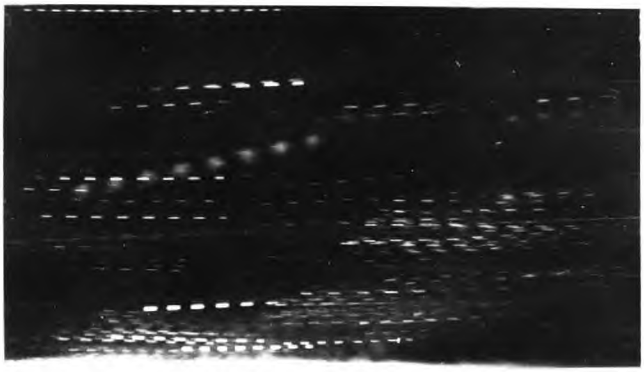

$\Theta = 30°$ 15 cm from o/s $Q = 0.2 \times 10^{-3}$ m^3/ sec.
laminar flow chopper I

$\Theta = 150°$ 15 cm from o/s $Q = 0.34 \times 10^{-3}$ m^3/sec
laminar flow chopper I

$\Theta = 150°$ Centreline $Q = 4.2 \times 10^{-3}$ m^3/sec
turbulent flow chopper II

VELOCITY DISTRIBUTION IN CHANNEL I ($r_c/b = 3$) V_Θ

d = 7.6 cm. (flow from left to right)
30°

PLATE (IV_1)

AT 1.25 cm DEPTH ABOVE THE BED

Chopper I

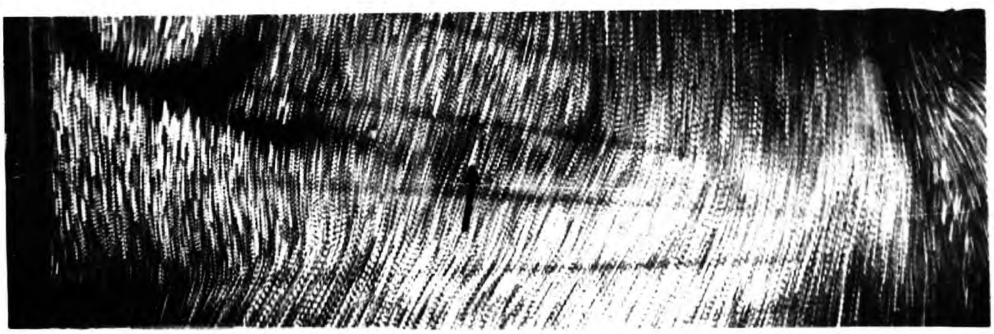

AT THE WATER SURFACE

Chopper II

VELOCITY DISTRIBUTION IN CHANNEL I ($r_c/b = 3$)

$d = 7.6$ cm. (flow from bottom to top)

$\theta = 150°$ (30°) $Q = 0.34 \times 10^{-3}$ m^3/sec

Pictures taken from the top.

PLATE (IV_2)

measurements of the secondary components v_r and v_z in this flow state. However, with improvements in lighting and the use of a tracer of neutral specific gravity, future research in this field seems worthwhile.

IV - 2. Turbulent flow

For the range of local velocities in this case (0.02 - 0.18 m/sec.), a miniature current meter was used to measure v_θ distribution around the bend of the two channels (I and III). Details of this instrument and its use are given in Chapter III.

The flow conditions in the two channels were :-

Channel	$Q(m^3/sec)$	$h_{\theta=30^o}(m)$	$\bar{v}_{\theta=30^o}(m/sec)$	$T(C^o)$	$Re=\frac{\bar{v}.m}{\nu}$
I	4.4×10^{-3}	0.076	0.0945	18.4	5460
III	2.75×10^{-3}	0.076	0.1450	18.7	6630

The measurements of temporal mean values of v_θ were taken at 15 cross-sections in each channel: in the bend, 13 cross-sections were chosen 15^o apart starting from the bend entry; one cross-section at 0.5 m. before and beyond each end of the bend was also chosen in the straight sections. Measurements of velocity in each cross-section were made over a total of 65 points in Channel I and 30 points in Channel III.

Along each vertical, measurements were taken, in the two channels, every 1.25 cm. Across the width, the verticals were located 5 cm. apart except nearest to the side walls, where the verticals were located at 1.25 cm. from each wall. Fig.(IV-3-1) represents a sketch of grid networks surrounding the points where measurements were taken.

To find the effects of secondary flow on the primary flow around the bend, a finite difference procedure was applied for solving the equations of motion in these two channels. An IBM 7094 computer with Fortran IV as language was used for the calculations and the steps taken were as follows :-

1) On the assumption of constancy of velocities along a small arc, $r\Delta\theta$, of the bend, and based on order of magnitude considerations (studied in Chapter II), the radial velocity components v_r were calculated from Eq.(II-17-a). The value of $\Delta\theta$ was chosen equal to 15°. In the two channels, the distribution of v_θ along the depth at several verticals chosen across the channel width at $\theta = 0$ conformed to the logarithmic profile as given by Von Karman, Eq.(II-13). Assuming the roughness coefficient n for the channel smooth surface equal to 0.011, for the range of depths tested in Channels I and III, an average value of Chezy's C equal to 70 (metric units) is assumed for calculations. Taking $\chi = 0.5$, then Eq.(II-13) transforms to :

$$\frac{v_\theta}{v_{\theta m}} = 1 + \frac{9.8}{0.5 \times 70}\,(1 + \ln\eta) \qquad \text{(IV-1)}$$

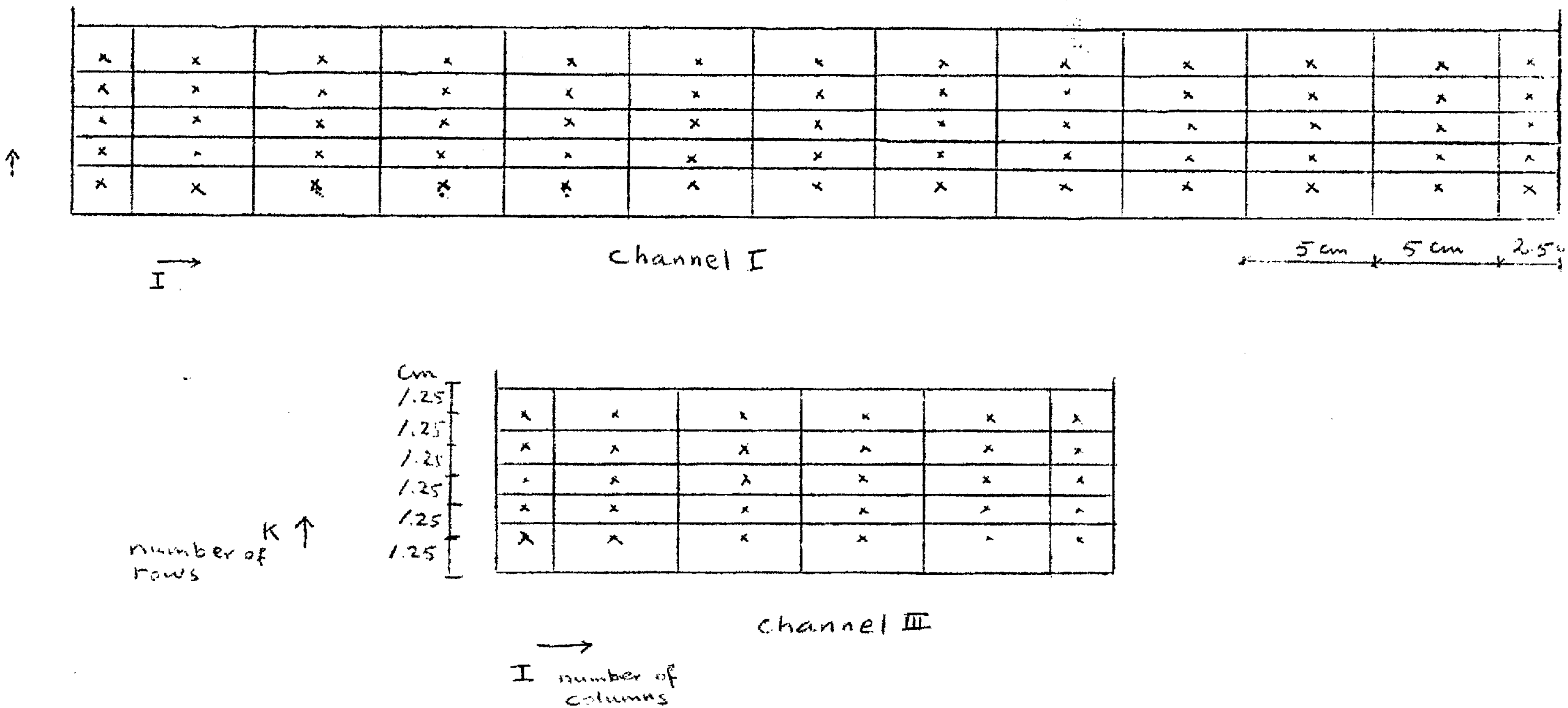

FIG. (IV-3-1)

Sketch representing the exact proportions of grid networks in channels I and III

X Locations where v_θ was measured.

Figure (IV-4-1) represents a plot of the measured values of v_θ along several verticals at the entry cross-section ($\theta = 0^{\circ}$) of both channels. Also plotted on the same figure (IV-4-1) is the profile for Eq.(IV-1); a good agreement between the measured profiles and that represented by Eq.(IV-1) can be seen. This led to considering Eq.(II-17-a) in the calculation of v_r.

2) In the side wall regions, the radial velocities v_r, after being calculated by Eq.(II-17-a), were reduced as follows (see Paragraph II-4) :-

Channel	distance from side wall	considered value of v_r
I	1.25 cm.	0.33 x v_r
I	5 cm.	0.66 x v_r
III	1.25 cm.	0.20 x v_r
III	5 cm.	0.60 x v_r

Values of v_r elsewhere in the cross-section were not considered under the effect of the side walls.

3) The vertical components of velocity v_z were calculated on the basis of continuity of flow :

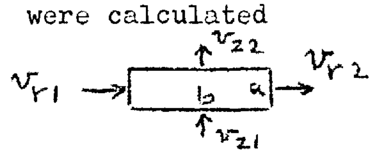

$$(v_{r2} - v_{r1}) \times a + (v_{z2} - v_{z1}) \times b = 0 \qquad \text{(IV-2)}$$

At the side walls, v_r=0, and at the channel bed and water surface, v_z=0. Starting from the channel bed v_{z1}=0 so that v_{z2} can be known.

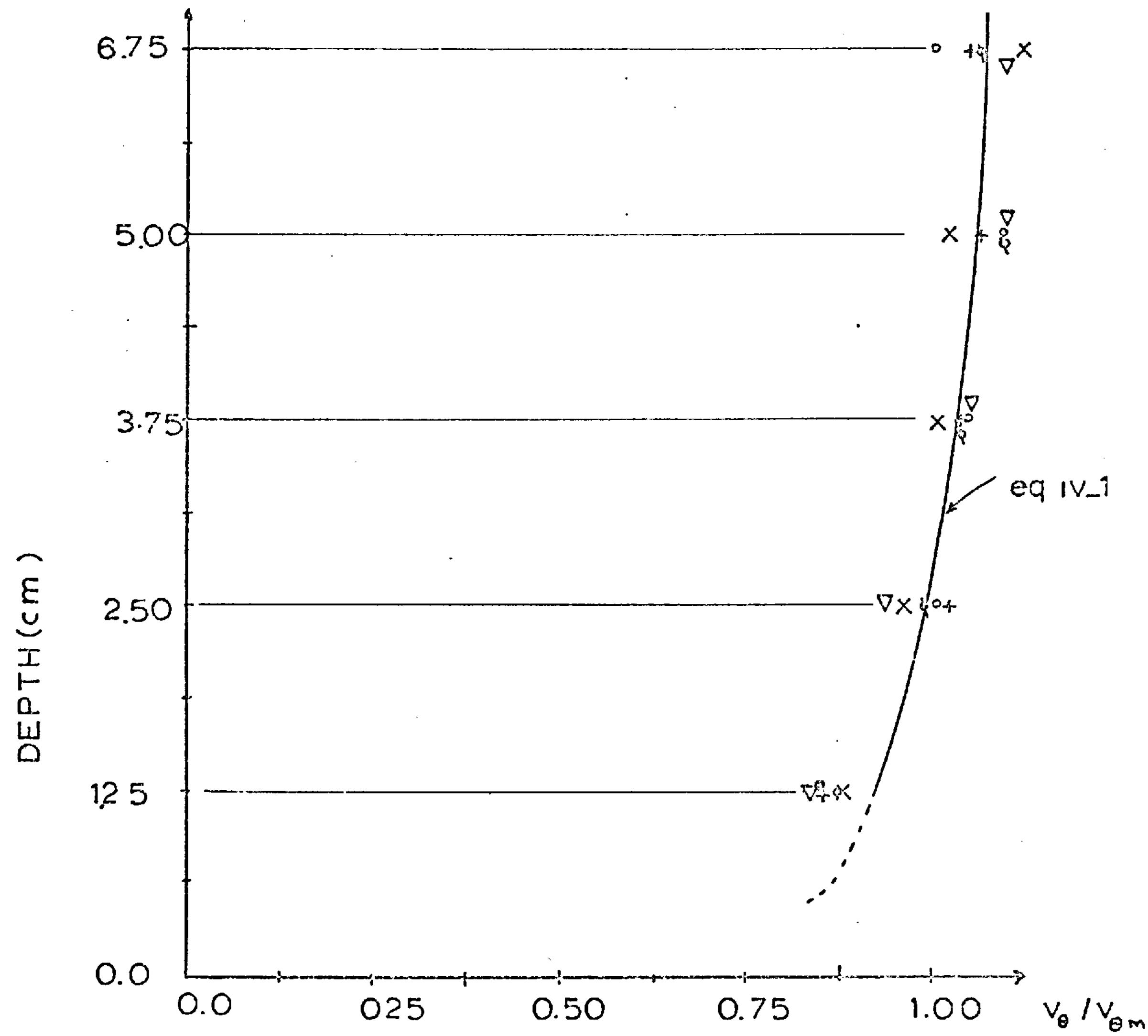

VELOCITY PROFILES AT THE BEND ENTRY

FIG IV-4-1

channel(I) [x at 10 cm l/s ; + " 30 " " ; o " 50

channel(III) [◊ at 10 cm l/s ; ∇ " 15 " "

Hence, corresponding components of v_z at the centres of the grids can be known from

$$v_z = (v_{z1} + v_{z2}) / 2 \qquad \text{(IV-3)}$$

4) Due to the calculated v_r and v_z, the tangential velocity component v_θ (assumed in a first step to be constant over $r\Delta\theta$) is actually modified as a result of momentum exchange.

To calculate the modified value of v_θ at the end of the arc $r\Delta\theta$, the calculated values of v_r and v_z were substituted into the second equation of motion, Eq.(II-19). In the steady state of flow, a balance between the frictional forces and gravity forces exists and the right-hand side of Eq.(II-19) becomes zero on the assumption of a linear distribution of shear stress along the flow depth, (rough approximation). In terms of finite differences, the last equation becomes:

$$v_r \frac{\Delta v_\theta}{\Delta r} + \frac{v_\theta}{r}\frac{\Delta v_\theta}{\Delta\theta} + v_z \frac{\Delta v_\theta}{\Delta z} + \frac{v_r v_\theta}{r} = 0 \qquad \text{(IV-4)}$$

This leads to :

$$\Delta v_\theta = -\frac{r\,\Delta\theta}{v_\theta}\left[v_r \frac{\Delta v_\theta}{\Delta r} + v_z \frac{\Delta v_\theta}{\Delta z} + \frac{v_r v_\theta}{r}\right] \qquad \text{(IV-5)}$$

Equation (IV-5) was solved for $\Delta\theta = 15^\circ$ over the whole of the grid networks of the two channels, I and III. The right-hand side of Eq.(IV-5) being known gives the value Δv_θ, and the new value of forward velocity in each grid at the end of step

$r \Delta \theta$ is :

$$v'_\theta = v_\theta + \Delta v_\theta \qquad \text{(IV-6)}$$

The values v'_θ are considered for calculating v_r and v_z in the next $\Delta \theta$ step, then v''_θ is calculated, and so on.

To solve for the average v_θ along the flow depth, Eq.(II-20) was used. In steady flow around gentle bends, it reduces to:

$$\frac{\partial v_{\theta m}}{\partial \theta} + \frac{0.75\sqrt{g}}{\chi^3 C} h \frac{\partial v_{\theta m}}{\partial r} + \frac{0.75\sqrt{g}}{\chi^3 C} v_{\theta m} \frac{\partial h}{\partial r} = 0 \qquad \text{(IV-7)}$$

Substituting $\frac{\partial h}{\partial r}$ with $\frac{v_\theta^2 m}{r}$, Eq.(IV-7) can be put in a finite difference form as :

$$\Delta v_\theta = -\Delta \theta \left[\frac{0.75\sqrt{g}}{\chi^3 C} h \frac{\Delta v_{\theta m}}{\Delta r} + \frac{0.75\sqrt{g}}{\chi^3 C} \frac{v_{\theta m}^3}{r} \right] \qquad \text{(IV-8)}$$

For a value of $\Delta \theta$ equal to 15°, the last equation was also solved around the bend by feeding into the computer the data from measurements at cross-section $\theta = 0^\circ$, and the new values of $v_{\theta m}$ are : $v'_{\theta m} = v_{\theta m} + \Delta v_\theta$ (IV-9)

Comparisons between measured and calculated values of v_θ in channels I and III are given in Figs.(IV-3-a→h) and (IV-4-a→d) respectively; those for the average values $v_{\theta m}$ in channels I and III are given in Figs.(IV-5-a) and (IV-5-b) respectively.

Programmes for the solutions of v_θ and $v_{\theta m}$ in both channels are given in Appendix B.

Discussion of results

Regarding the measured distribution of v_θ it can be seen

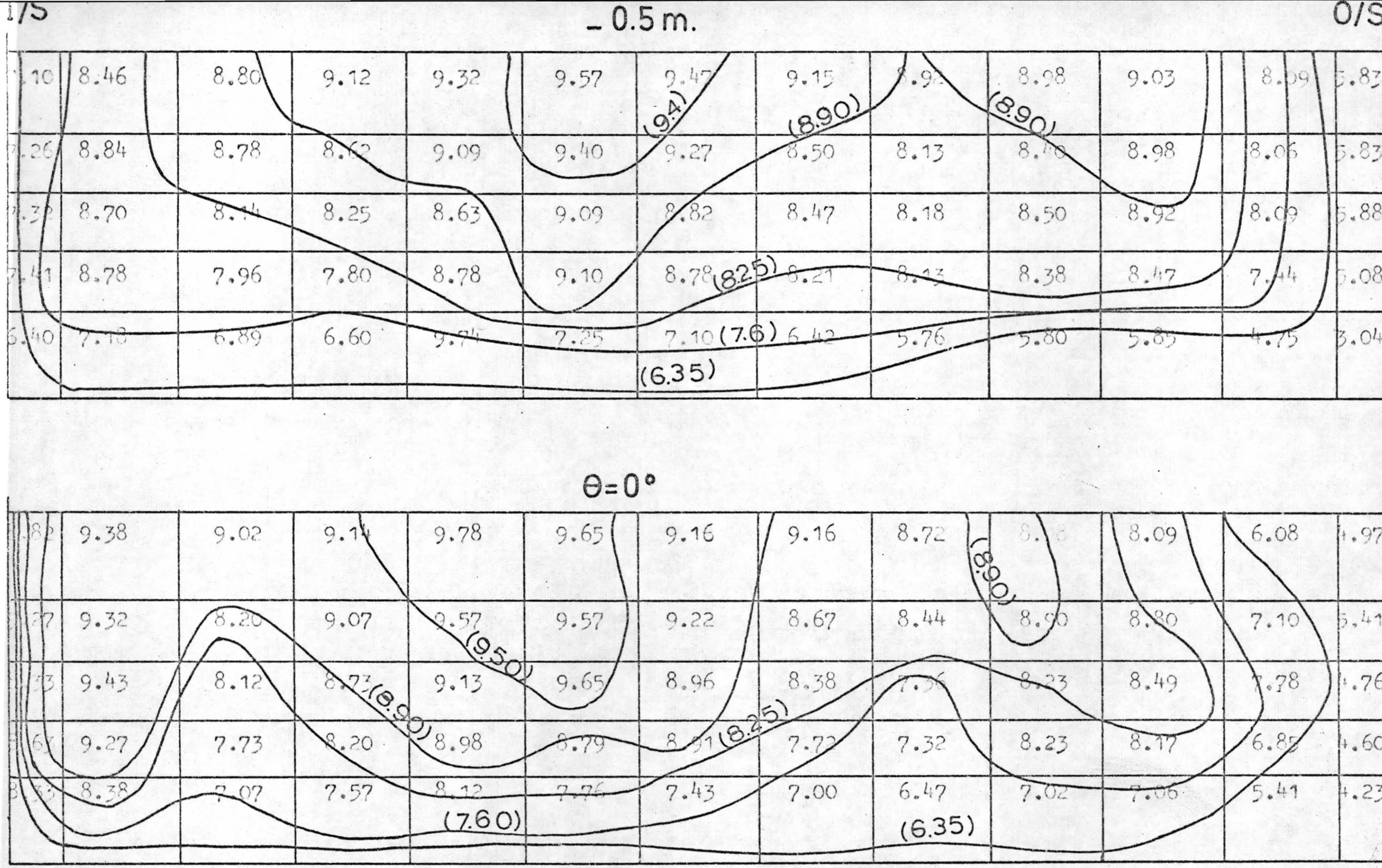

Figures in cm/sec.

FIG. IV_3_a

DESTRIBUTION OF TANGENTIAL VELOCITY (V_θ) IN CHANNEL I ($r_c/b=3$)

$Q = 4.4 \times 10^{-3}\ m^3/sec$
$h = 7.6$ cm

I/S $\theta = 15°$ O/S

08 71	10.10 8.76	10.15 8.68	9.96 8.79	9.96 9.41	10.28 9.29	9.96 8.83	9.34 8.46	9.05 8.43	8.76 8.67	8.81 7.80	7.10 5.95	4.67 4.92
08 09	10.21 9.16	9.98 9.14	9.80 8.90	10.10 9.38	10.15 9.38	7.12 9.06	9.06 8.52	9.05 8.30	8.46 8.75	8.96 8.68	6.81 7.04	5.08 5.38
7.23 33	10.42 8.38	9.80 9.02	9.60 8.71	9.96 9.11	9.90 9.65	9.38 8.96	8.50 8.37	7.78 7.36	8.46 8.22	8.62 8.47	7.46 7.79	4.54 4.67
7.86 8.70	9.80 8.39	9.10 9.09	9.13 8.39	9.67 9.15	9.34 8.97	8.46 9.08	7.46 7.87	7.75 7.45	7.79 8.37	7.40 8.32	7.11 6.93	5.58 4.75
6.90 7.88	8.80 8.06	8.13 8.66	8.38 7.74	8.40 8.52	8.12 8.15	7.40 7.72	6.85 7.33	6.55 6.77	7.11 7.35	6.59 7.41	6.09 6.26	4.49 5.01

$\theta = 30°$

6.61 8.58	9.23 8.51	9.18 8.29	9.14 8.43	9.14 9.04	9.44 8.93	9.14 8.50	9.02 8.16	8.18 8.16	8.12 8.38	8.66 7.52	6.11 5.79	3.77 4.87
5.09 9.03	9.49 9.04	9.50 8.96	8.85 8.73	9.04 9.20	9.38 9.21	9.00 8.90	8.43 8.37	7.78 8.16	7.70 8.60	8.09 8.45	5.83 6.99	4.39 5.36
5.00 8.33	8.92 8.38	8.85 9.02	8.25 8.71	8.46 9.11	8.11 9.64	7.79 8.95	7.16 8.37	5.85 7.35	5.54 8.21	6.58 8.46	3.73 7.79	2.67 4.76
4.25 8.77	8.08 8.52	6.59 9.29	6.48 8.57	7.38 9.34	7.51 9.15	6.59 9.25	5.81 8.08	5.16 7.59	6.09 8.52	6.26 8.46	5.08 7.07	2.74 4.72
3.55 8.02	6.59 8.33	6.09 9.07	6.13 8.12	5.71 8.91	4.39 8.53	3.56 8.08	4.14 7.66	3.78 7.07	4.36 7.66	4.39 7.71	3.04 6.42	2.66 5.47

FIG IV_3_b

I/S $\theta=45°$ O/S

5.80 8.45	5.83 8.26	8.46 7.91	7.91 8.07	7.88 8.67	7.65 8.57	7.66 8.16	7.42 7.86	6.07 7.88	5.23 8.09	5.58 7.24	5.96 5.64	5.55 4.82
5.39 8.79	8.18 8.92	10.15 8.78	10.20 8.57	9.98 9.03	10.15 9.04	9.95 8.74	9.58 8.22	8.96 8.03	8.38 8.46	7.77 8.40	7.10 6.89	5.83 [illegible].33
6.08 8.33	8.38 8.39	9.72 9.02	8.90 8.71	9.00 9.11	8.98 9.64	9.25 8.95	8.11 8.36	8.12 7.34	8.09 8.20	8.12 8.46	7.37 7.78	6.51 4.67
5.73 8.48	7.73 8.65	8.39 9.49	8.59 8.75	9.20 9.53	9.13 9.33	8.85 9.42	8.09 8.18	8.35 7.73	8.38 8.67	8.70 8.59	7.81 7.08	6.58 4.80
5.18 8.15	7.10 8.59	6.59 9.48	6.12 8.50	6.30 9.31	6.19 8.92	6.12 8.44	6.00 7.98	5.69 7.37	6.08 7.97	7.06 8.01	6.42 6.58	5.23 5.13

(9.00) (8.90) (8.25) (7.60) (6.35)

$\theta=60°$

5.20 8.32	5.08 8.01	8.75 7.52	8.55 7.71	8.80 8.29	8.50 8.22	8.46 7.83	8.85 7.55	8.63 7.60	7.88 7.80	7.35 6.96	6.11 5.49	4.86 4.76
5.94 8.91	5.29 8.81	7.35 8.61	8.50 8.40	8.09 8.85	8.22 8.87	8.46 8.58	8.18 8.08	7.86 7.89	7.35 8.32	6.83 8.26	5.42 6.81	4.62 5.30
6.09 8.[illegible]4	6.50 8.39	7.40 9.02	8.12 8.70	8.16 9.10	7.35 9.63	7.34 8.94	7.40 8.35	7.35 7.34	6.89 8.19	6.09 8.45	6.09 7.78	4.62 4.67
6.45 8.91	7.61 8.78	8.32 9.68	7.86 8.93	8.38 9.72	8.22 9.51	8.06 9.59	8.12 8.33	7.40 7.87	7.35 8.81	7.10 8.73	7.15 7.16	5.90 4.83
5.08 8.29	6.71 8.86	7.10 9.89	6.50 8.88	6.89 9.70	6.80 9.30	5.53 8.79	6.40 8.30	6.60 7.67	6.60 8.29	6.44 8.31	6.04 6.74	5.30 5.18

(8.25) (7.60) (6.35)

FIG IV_3_c

I/S θ=75° O/S

2.68 8.19	5.17 7.75	5.58 7.13	7.78 7.36	8.58 7.92	8.72 7.86	8.58 7.49	8.38 7.25	8.25 7.32	8.42 7.50	8.11 6.68	6.20 5.34	4.32 4.71
3.71 8.85	6.41 8.69	6.65 8.43	8.16 8.23	8.72 8.67	8.96 8.70	8.58 8.42	8.42 7.93	8.46 7.76	8.42 8.18	8.46 8.13	6.83 6.74	5.78 5.28
[illegible].52 8.34	7.10 8.39	7.63 [illegible].02	8.21 8.70	8.46 9.10	8.42 0.62	8.46 8.93	8.46 8.35	8.38 7.33	8.32 8.18	7.80 8.44	6.88 7.77	6.08 4.66
5.58 9.97	7.15 9.91	7.00 9.88	7.88 9.12	7.86 9.91	8.46 9.70	8.46 9.76	8.38 8.48	8.07 8.01	8.15 8.96	7.86 8.87	7.13 7.23	6.43 4.86
5.58 8.43	7.15 9.13	7.35 10.29	7.78 9.25	7.35 10.09	7.35 9.68	7.58 9.15	6.95 8.62	7.10 7.96	6.80 8.60	6.80 8.61	5.83 6.90	6.12 5.24

(8.90) (825) (7.60) (6.35)

θ=90°

4.12 8.06	5.02 7.50	5.67 6.74	6.90 7.00	7.60 7.55	8.10 7.50	8.40 7.16	8.46 6.95	8.86 7.04	8.77 7.21	8.62 6.40	9.70 5.19	6.08 4.65
3.88 8.79	6.38 8.58	6.86 8.25	7.70 8.06	8.16 8.50	8.50 8.52	8.67 8.26	8.72 7.78	8.80 7.62	8.62 8.03	8.46 7.99	9.70 6.67	6.12 5.25
5.08 8.34	7.06 8.39	7.30 9.01	7.90 8.70	8.80 9.09	8.72 9.62	8.96 8.93	8.80 8.34	8.88 7.32	8.96 8.18	8.46 8.43	7.42 7.75	7.10 4.66
6.35 9.04	8.62 9.04	8.43 10.08	8.96 9.30	9.23 10.10	9.22 9.88	9.43 9.93	9.38 8.63	9.38 8.15	9.61 9.10	9.61 9.01	8.46 7.30	8.11 4.88
6.13 8.56	7.83 9.39	7.91 10.70	8.41 9.63	8.21 10.49	8.50 10.06	8.55 9.54	8.42 8.95	8.96 8.26	8.90 8.91	8.76 8.91	7.86 7.07	7.58 5.30

(8.90) (9.40) (82.5) (7.60) (6.35)

FIG IV_3_d

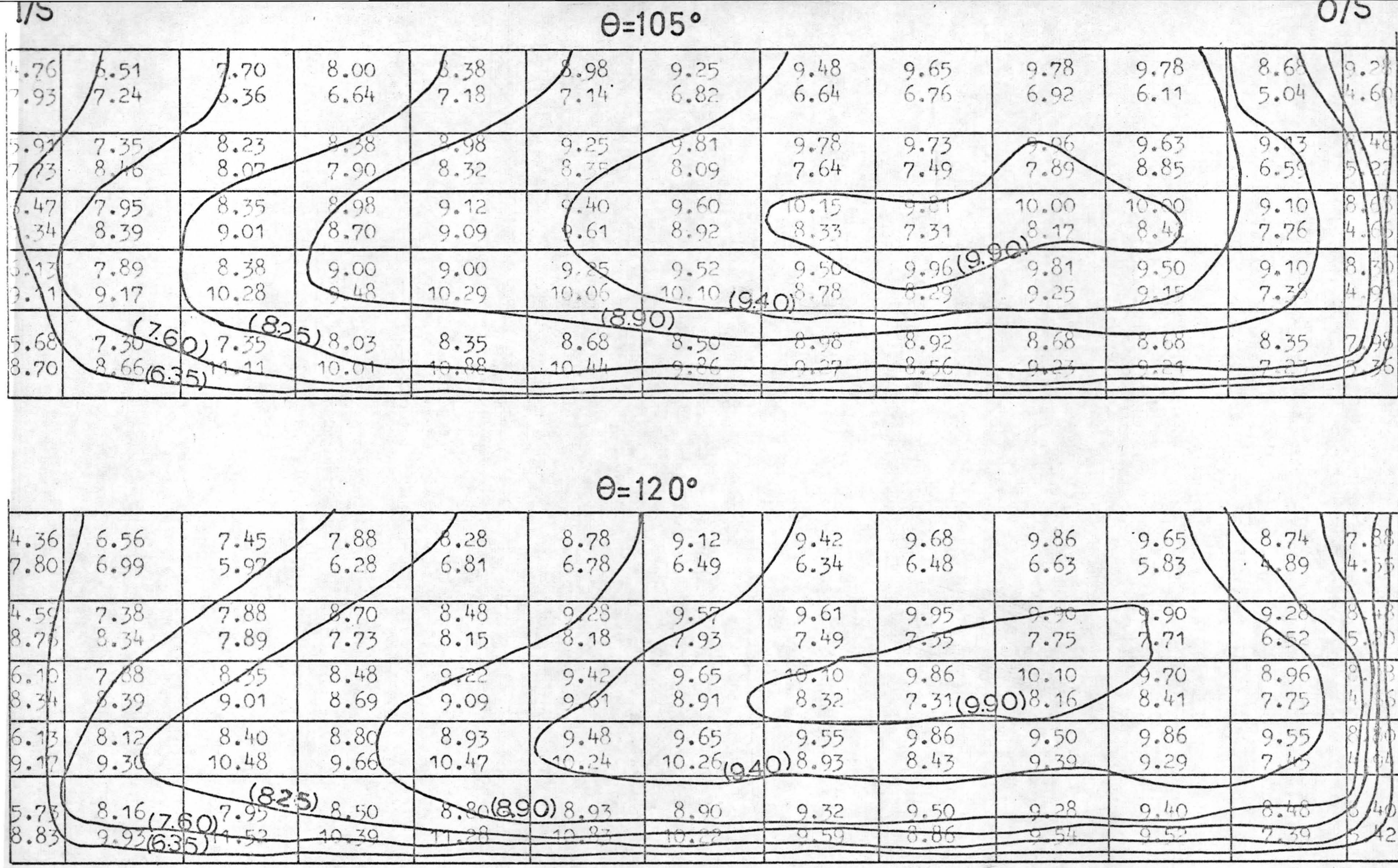

FIG IV_3_e

I/S

O/S

θ=135°

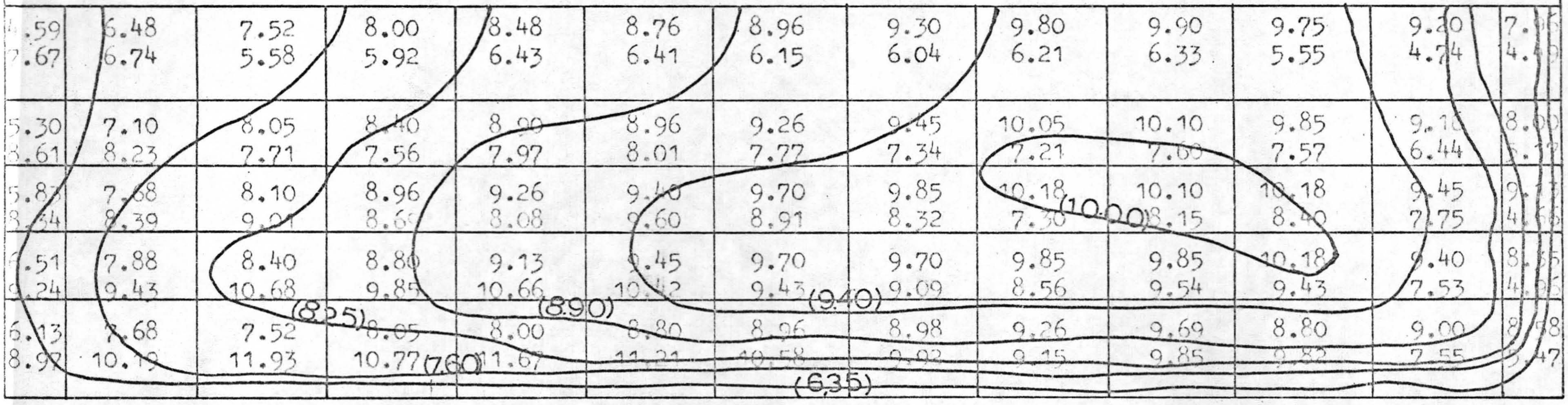

θ=150°

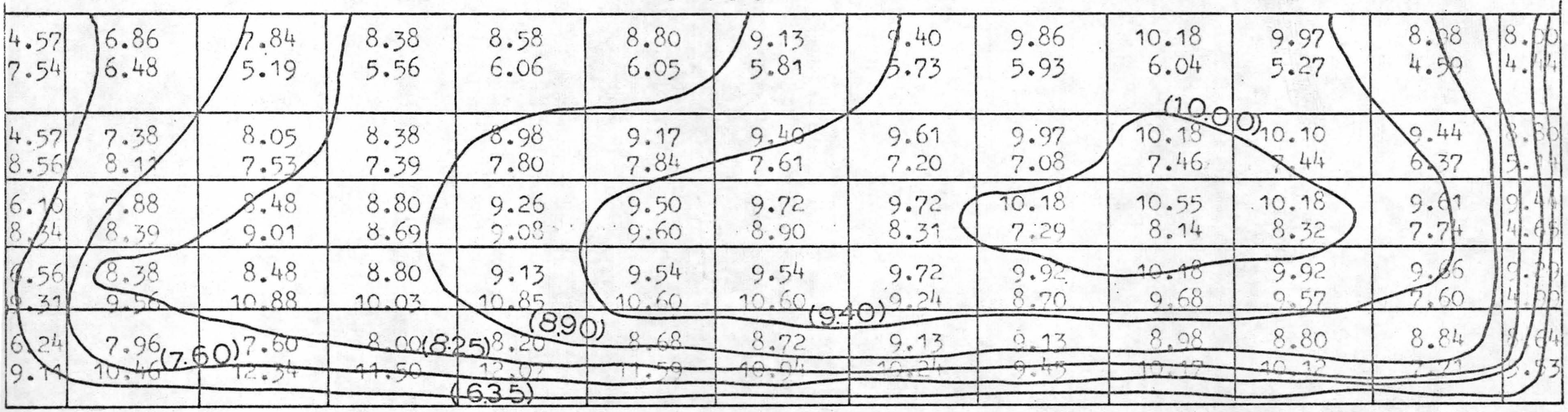

FIG IV_3_f

$\theta=165°$

4.30 7.41	6.42 6.23	7.66 4.80	8.11 5.20	8.71 5.69	8.71 5.69	9.02 5.48	9.46 5.43	9.85 5.65	10.24 5.75	10.24 4.99	9.40 4.44	8.[illegible] 4.[illegible]
5.20 8.50	7.19 7.99	7.92 7.35	8.71 7.23	9.02 7.62	9.28 7.67	9.46 7.45	9.50 7.05	9.97 6.94	10.42 7.32	10.46 7.30	9.81 6.29	8.[illegible] 5.[illegible]
5.55 8.34	7.62 8.40	8.34 9.01	8.92 8.69	9.24 9.07	9.32 9.59	9.66 8.89	9.81 8.30	10.20 7.28	10.46 8.13	10.42 8.38	9.85 7.74	9.[illegible] 4.[illegible]
6.58 9.38	7.88 9.69	8.48 11.08	8.92 10.21	9.02 8.04	9.24 10.79	9.66 10.77	9.81 9.39	10.07 8.84	10.24 9.83	10.20 9.71	10.16 7.68	8.[illegible] 5.[illegible]
5.34 9.24	7.92 10.73	8.44 12.79	8.58 11.53	8.15 12.46	8.62 11.98	8.58 11.30	9.40 10.57	9.36 9.75	9.40 10.48	9.24 10.42	9.26 7.87	8.[illegible] 5.9[illegible]

(6.35) (7.60) (8.25) (8.90) (9.40) (10.00)

$\theta=180°$

3.37 7.28	5.66 5.97	7.28 4.41	8.62 4.84	8.82 5.31	8.83 5.33	9.13 5.14	9.46 5.12	10.10 5.37	10.56 5.45	10.65 4.71	10.52 4.29	9.5[illegible] 4.[illegible]
3.68 8.44	6.15 7.88	7.28 7.17	8.20 7.06	8.46 7.44	8.98 7.49	9.17 7.29	9.46 6.90	9.97 6.81	10.60 7.17	10.68 7.16	10.48 6.22	10.[illegible] 5.[illegible]
4.94 8.35	6.87 8.40	7.66 9.01	8.46 8.68	8.78 9.07	9.17 9.58	9.42 8.89	9.17 8.30	9.97 7.27	10.60 8.12	10.90 8.37	10.90 7.73	10.[illegible] 4.[illegible]
5.38 9.44	7.10 9.83	8.01 11.28	6.89 10.40	8.78 11.23	9.42 10.27	8.56 9.94	9.86 9.54	10.18 9.98	10.68 9.97	10.52 9.85	10.56 7.75	10.[illegible] 5.[illegible]
4.72 9.38	6.90 11.00	7.28 13.16	8.20 11.91	8.58 12.86	7.94 12.36	8.52 11.66	9.13 10.89	9.21 10.05	9.46 10.80	9.86 10.72	9.90 8.04	9.[illegible] [illegible]5

(6.35) (7.60) (8.90) (10.00) (10.80)

FIG IV_3_g

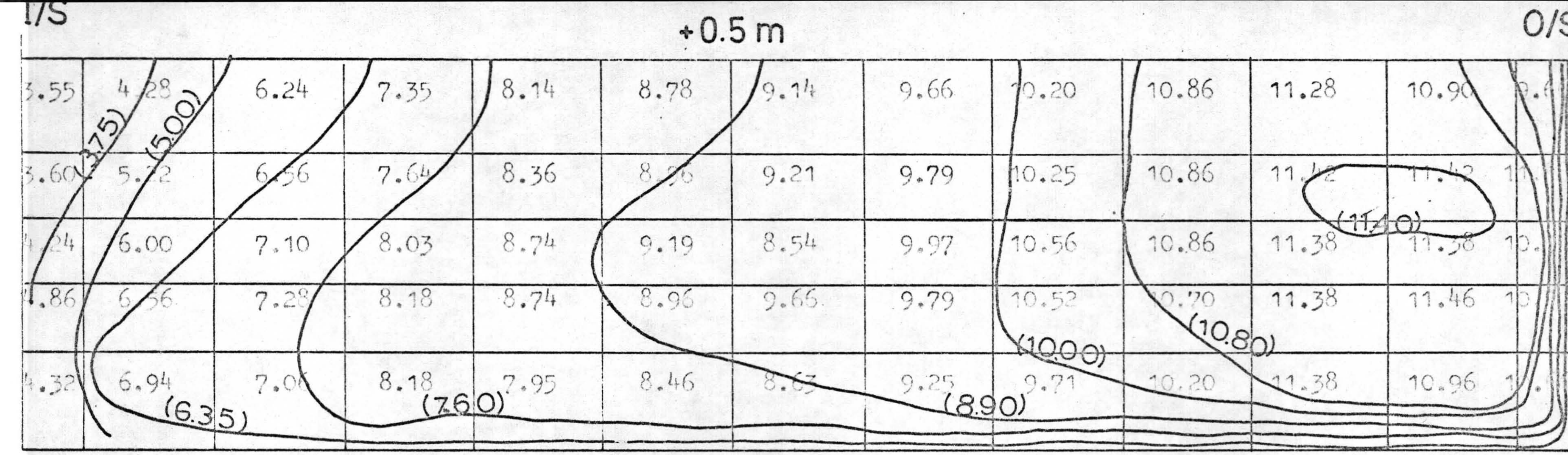
I/S
+0.5 m
O/S
4.28 6.24 7.35 8.14 8.78 9.14 9.66 10.20 10.86 11.28 10.90
3.60 5.22 6.56 7.64 8.36 9.21 9.79 10.25 10.86
6.00 7.10 8.03 8.74 9.19 8.54 9.97 10.56 10.86 11.38
6.56 7.28 8.18 8.74 8.96 9.66 9.79 10.52 10.70 11.38 11.46
6.94 8.18 7.95 8.46 9.25 9.71 10.20 11.38 10.96
(3.75)
(5.00)
(6.35)
(7.60)
(8.90)
(10.00)
(10.80)
(11.40)

FIG IV_3_h

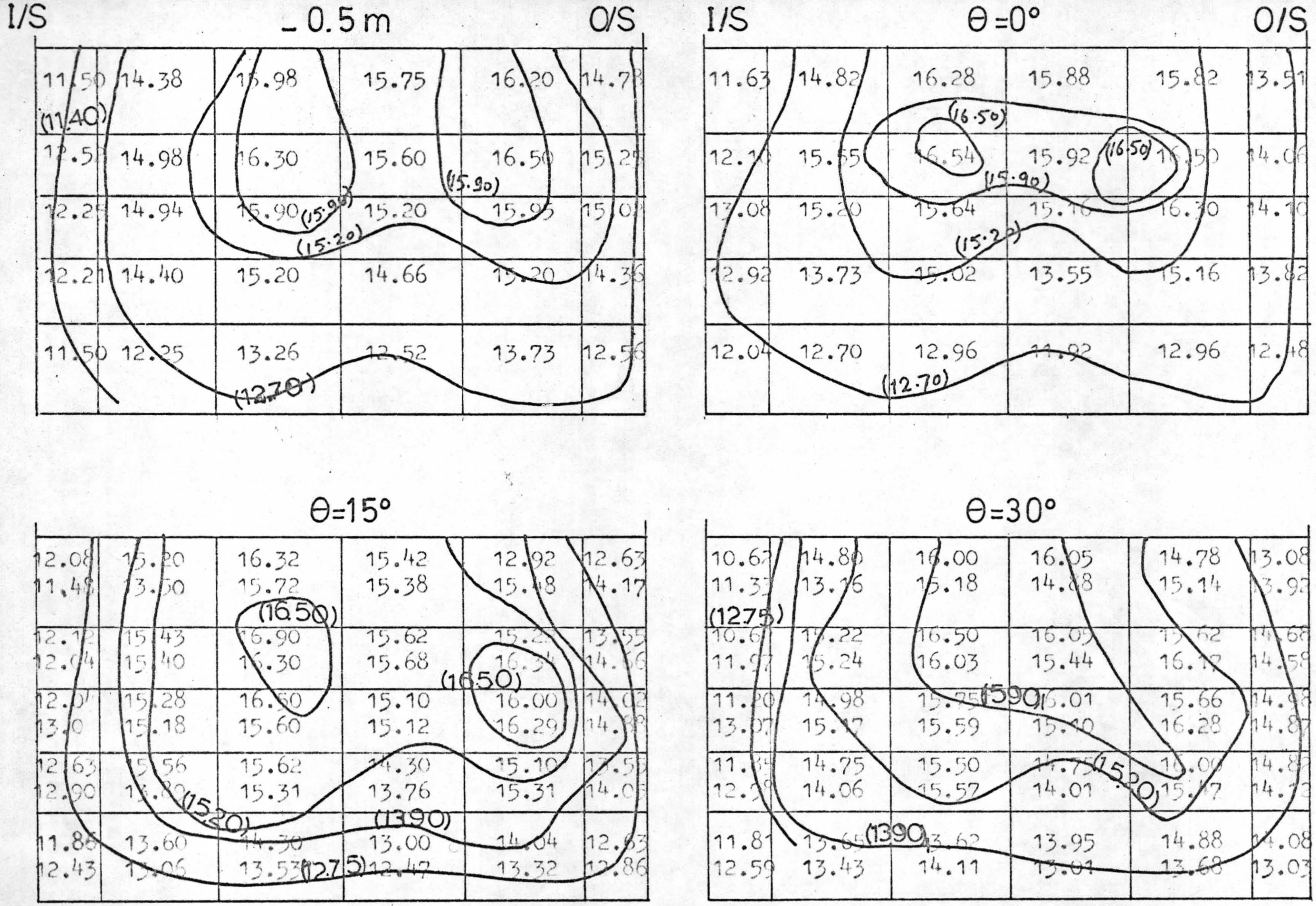

Figures in cm/sec.

FIG IV_4_a

DISTRIBUTION OF TANGENTIAL VELOCITY(V_θ)
IN CHANNEL III ($r_c/b = 7.9$)

$Q = 2.75 \times 10^{-3}\ m^3/sec$
$h = 7.60$ cm

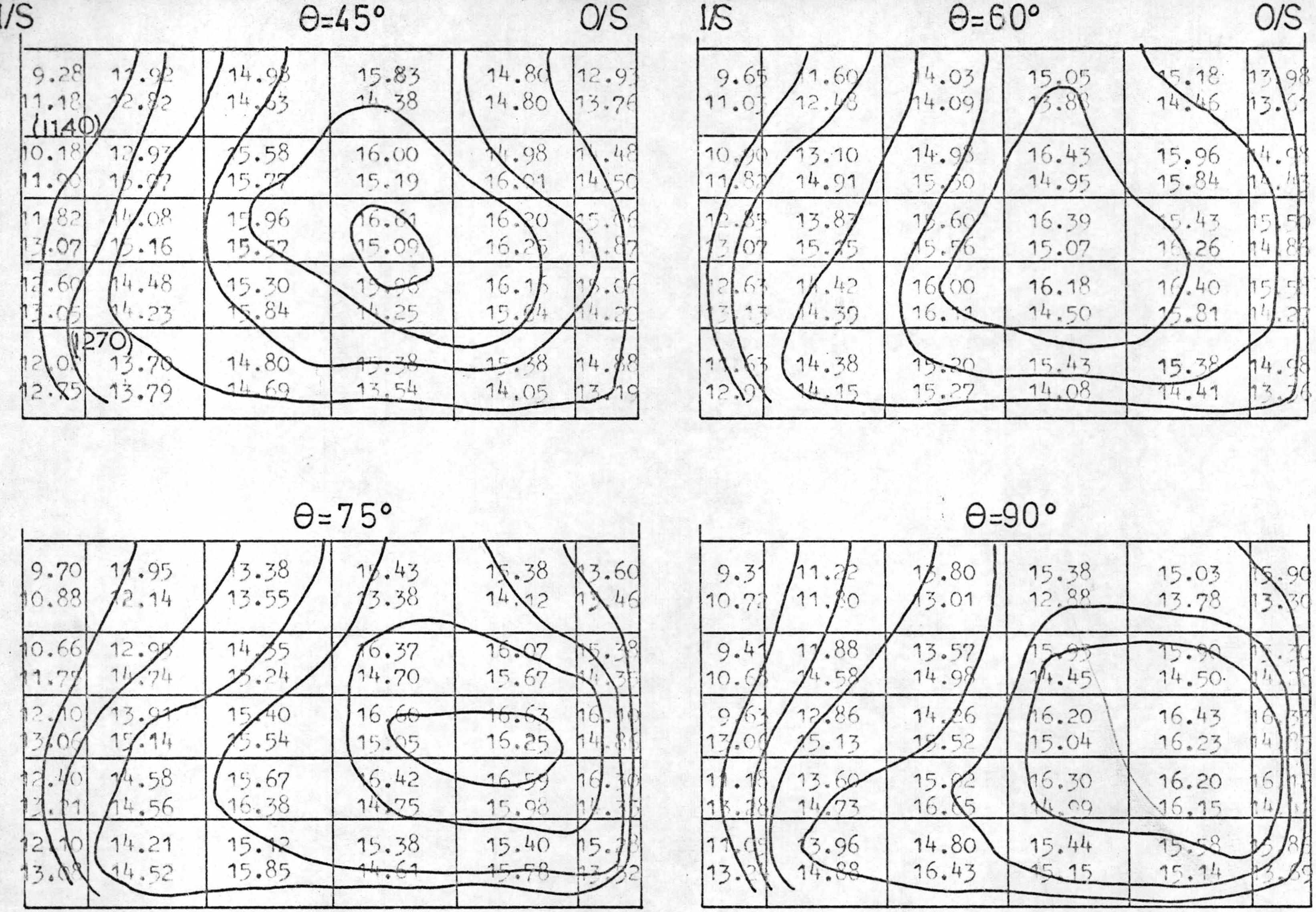

FIG IV_4_b

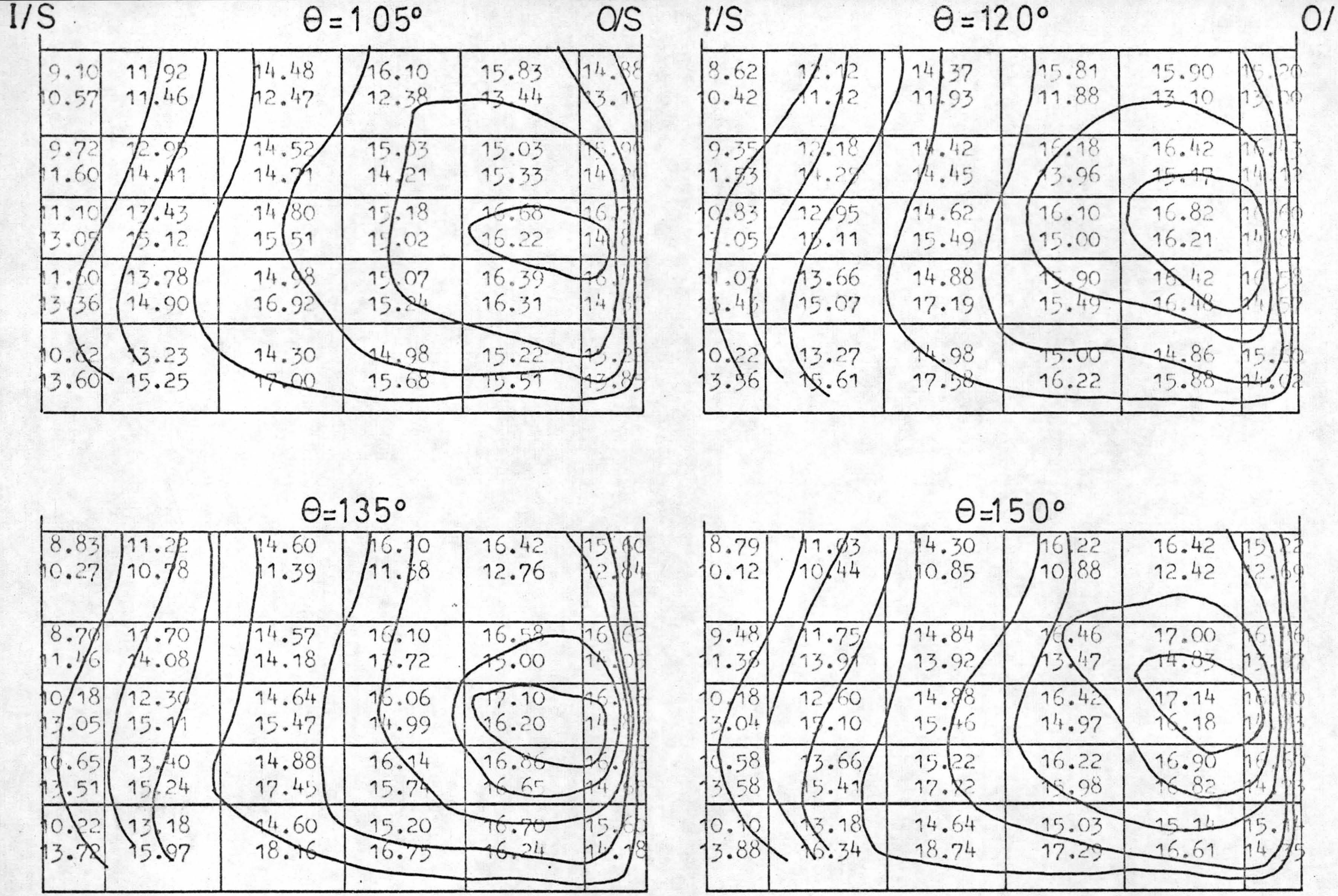
I/S
θ=105°
O/S
9.10 11.92 14.48 16.10 15.83
10.57 11.46 12.47 12.38 13.44
9.72 12.95 14.52 15.03 15.03
11.60 14.41 14.21 15.33
11.10 13.43 14.80 15.18 16.68
13.05 15.12 15.51 15.02 16.22
11.60 13.78 14.98 15.07 16.39
13.36 14.90 16.92 15.24 16.31
10.62 13.23 14.30 14.98 15.22
13.60 15.25 17.00 15.68 15.51
I/S
θ=120°
O/S
8.62 12.12 14.37 15.81 15.90
10.42 11.12 11.93 11.88 13.10
9.35 12.18 14.42 16.18 16.42
11.53 14.29 14.45 13.96 15.47
10.83 12.95 14.62 16.10 16.82
11.05 15.11 15.49 15.00 16.21
11.07 13.66 14.88 15.90 16.42
13.46 15.07 17.19 15.49 16.48
10.22 13.27 14.98 15.00 14.86
13.56 15.61 17.58 16.22 15.88 14.02
θ=135°
8.83 11.22 14.60 16.10 16.42 15.60
10.27 10.78 11.39 11.58 12.76 12.84
8.70 11.70 14.57 16.10 16.58
11.46 14.08 14.18 13.72 15.00
10.18 12.30 14.64 16.06 17.10
13.05 15.11 15.47 14.99 16.20
10.65 13.40 14.88 16.14 16.86
13.51 15.24 17.45 15.74 16.65
10.22 13.18 14.60 15.20 16.70 15.60
13.72 15.97 18.16 16.75 16.24 14.18
θ=150°
8.79 11.03 14.30 16.22 16.42 15.22
10.12 10.44 10.85 10.88 12.42 12.69
9.48 11.75 14.84 16.46 17.00
11.38 13.91 13.92 13.47 14.83
10.18 12.60 14.88 16.42 17.14
13.04 15.10 15.46 14.97 16.18
10.58 13.66 15.22 16.22 16.90
13.58 15.41 17.72 15.98 16.82
10.10 13.18 14.64 15.03 15.14
13.88 16.34 18.74 17.29 16.61 14.35

FIG I.V_4_c

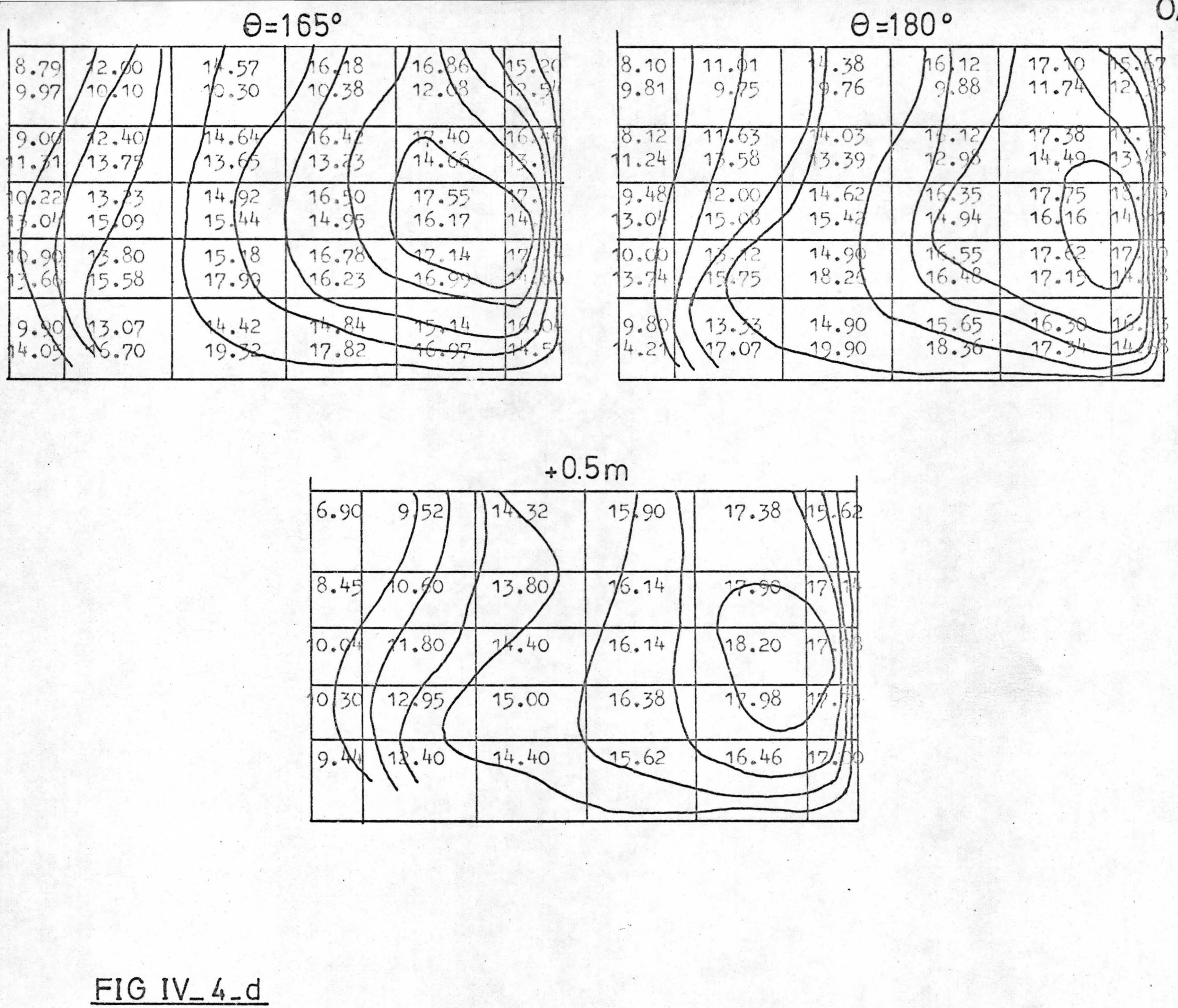
O/S
θ=165°
θ=180°
+0.5m
6.90
9.52
15.90
17.38
8.45
10.60
13.80
16.14
16.14
18.20
15.00
16.38
14.40
15.62
16.46

FIG IV_4_d

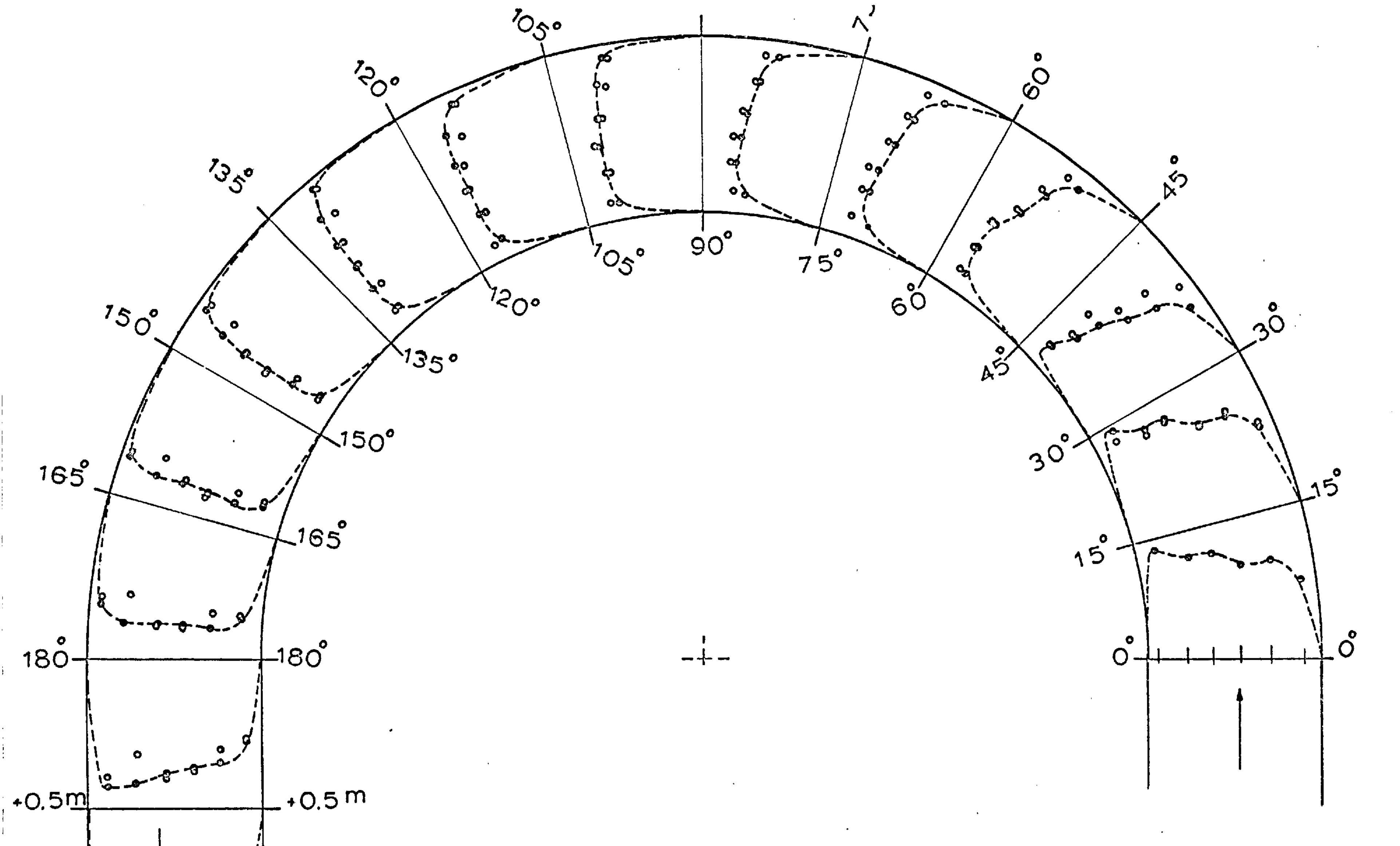

TANGENTIAL VELOCITY DISTRIBUTION($V_{\theta m}/\bar{V}_0$)

CHANNEL I ($r_c/b = 3$)

$b = 0.61$ m $h = 7.6$ cm $\bar{V}_0 = 9.45$ cm/sec

FIG IV_5_a

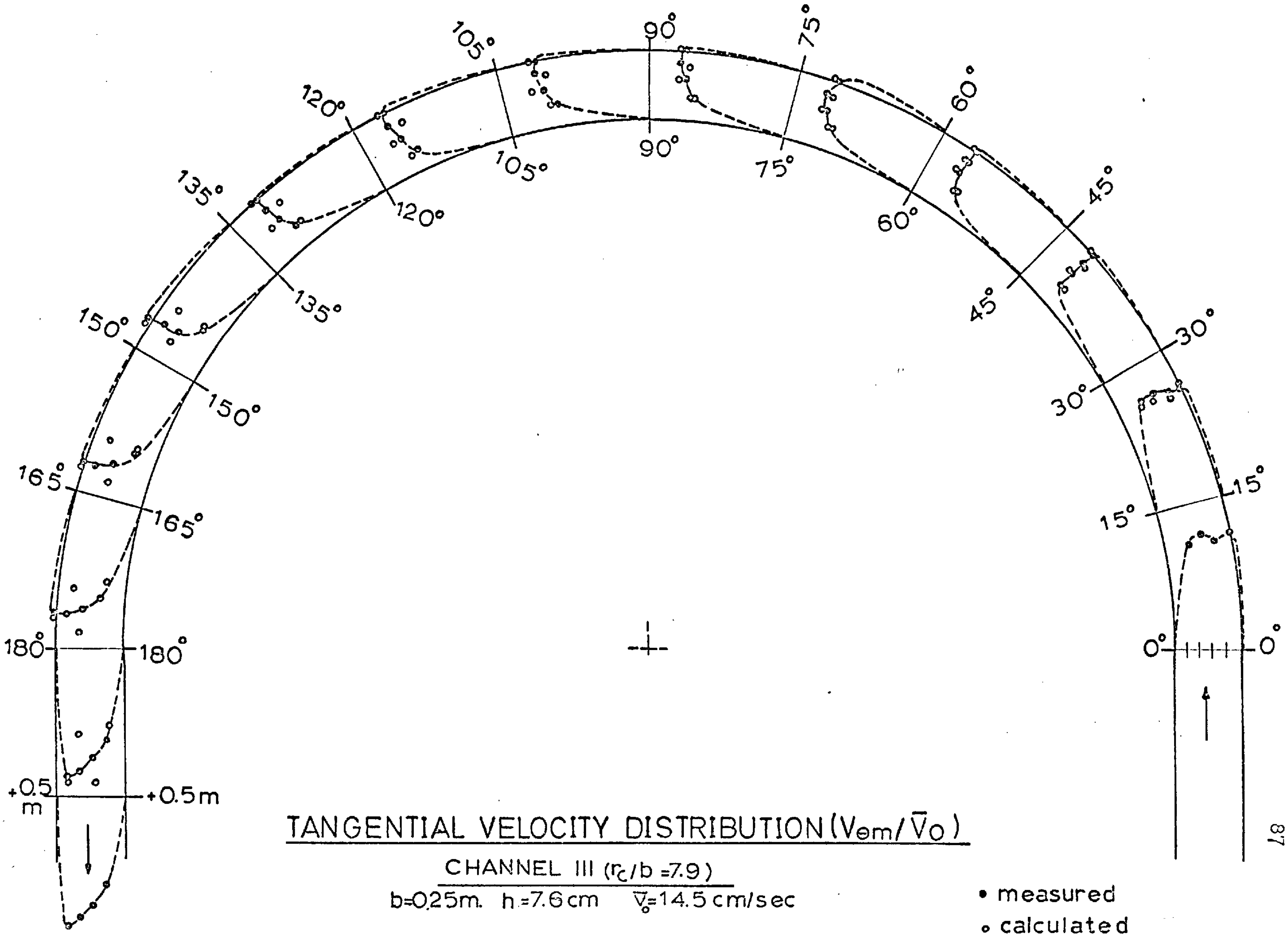

TANGENTIAL VELOCITY DISTRIBUTION $(V_{\theta m}/\bar{V}_0)$

CHANNEL III $(r_c/b = 7.9)$

b=0.25m. h=7.6cm $\bar{V}_0$=14.5 cm/sec

FIG IV-5-b

from Figs.(IV-3-a) to (IV-3-h) for Channel I that the maximum velocity region prevails near the inner-side from the bend entry down to $\theta = 45^\circ$, after which it gradually shifts towards the outer-side with increasing magnitude. The overall maximum local velocity is found to be near the outer-side and below the water surface at cross-section 0.5 m. downstream of the bend exit. In the case of Channel III, Figs.(IV-4-a) to (IV-4-d) reveal that the maximum velocity location at the channel entry is close to the centreline and does not approach the inner-side at any section around the bend. It starts shifting to the outer-side in the region $\theta = 15^\circ - 30^\circ$ with increased magnitude of velocity. The overall maximum v_θ is also found very near the outer side, at cross-section + 0.5 m. downstream of the bend exit.

For the sake of comparison between calculated and measured v_θ distribution around the bend, the numerical values of v_θ in cm/sec. in Channels I and III are written in each grid rectangle, Figs. (IV-3-a) to (IV-3-h) and Figs.(IV-4-a) to (IV-4-d). The top values in ~~the~~ each grid represents the measured value and the bottom one represents the calculated value.

Examining these figures, it can be seen that some agrrement (in some places, very good agreement, with discrepancies less than 5 %) exists between the two values.

The most serious limitations in the present calculation can be summed up as follows :

1) The grid network on the vertical section is large and irregular. When approaching the boundaries at which steep gradients of velocities occur in reality, and where discrepancies between measured and calculated values grow much higher, the size of the grid should be much smaller than that for the remainder of the flow.

2) The increment $\Delta\theta$ along the length should be reduced, in order to obtain better approximation.

3) Discrepancies can also be attributed to the non-uniformity of velocity distribution across the width of the entry cross-section. This is particularly noticeable in Channel I.

4) Derivation of Eq.(II-17-a) was also based on a gentle curvature, i.e., b/r_c is much smaller than one. In Channel I, where the discrepancies are higher than in Channel III, the value $b/r_c = 0.33$ ~~and~~ is not much smaller than unity.

It is believed that all the discrepancies mentioned above could be greatly reduced if such limitations were removed.

Since the present calculation represents a trial in applying a finite difference procedure for a numerical solution of the equations of motion, much scope is available in elaborating this technique to obtain closer results in the light of the suggestions outlined above. Moreover, since the primary interest has been concerned with the application of computer programming to solve numerically the equations of motion in curved channel flow, no regard was given to factors affecting the flow other than the channel curvature and velocity distribution at the bend entry.

CHAPTER V

CHARACTERISTICS OF SECONDARY CURRENTS IN CURVED OPEN CHANNEL FLOW

The onset of secondary currents when a stream enters a channel bend depends only upon the interaction between the radial gradient of pressure across the stream and the variation of centrifugal force from bottom to top of the cross-section. The pressure excess is constant at all levels, so that near the bottom there is a net inward force (and so, a flow) and at the top an outward force (and hence, a flow), as represented in Fig.(V-1) below.

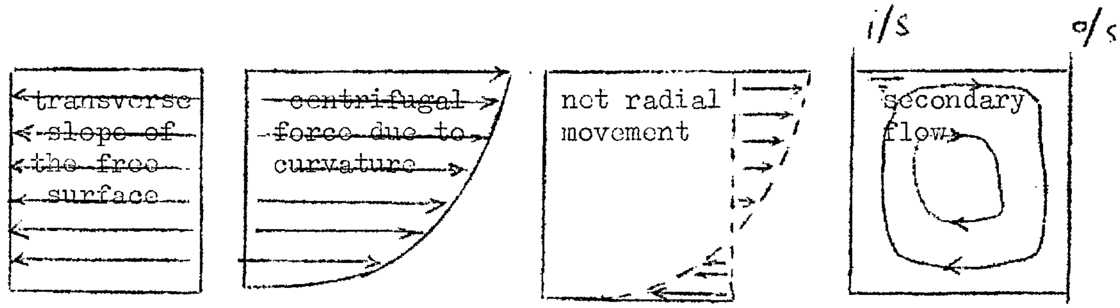

Fig.(V-1)

The secondary flow, so developed, combines with the primary, or main flow, to result in a helical, or spiral, type of motion around the bend. This spiral motion persists, in most cases, for some distance downstream of the bend exit depending on the flow conditions.

In all practical cases of spiral motions around channel bends, no steady fully developed state of flow can be reached except, perhaps, when the bend is a very long one, i.e., $r_c/b \gg 1$. Therefore, the spiral motion undergoes, in reality, two consecutive stages :- a gradual development, then a gradual decay. To date, this very complicated nature of the flow has been analysed by methods of successive approximations or finite difference techniques based on simplified equations of motion around the bend (<u>vide</u> Kozovskii, Ananyan, etc.) 1 . [illegible].)

The characteristics of flow in curved channels can be summarized in the following main features :

1) Superelevations of the water surface due to centrifugal force and the reaction of the side walls.

2) Helical motion as a result of the combination of secondary and main flows.

3) Redistribution of velocities around the bend and across the channel width.

4) Flow separation from the sides in bends of sharp curvature, and the development of surface waves in supercritical flow.

5) Additional energy losses due to the helical motion above those occurring in straight channel flow.

The third feature has been examined in Chapter IV. The fourth feature, i.e., flow separation and the development of surface waves, is excluded from the present study due to the relatively mild curvature and low speed of the investigated flow. The fifth feature, i.e., additional energy losses, is interpreted in terms of an increase in friction factor C_f (presented originally by Darcy-Weisbach for straight flow) in curved flow above that in straight flow with the same conditions. This is briefly studied and reported in Appendix A.

The first and second features are examined in the following discussion.

V - 1. Superelevation of the water surface in the radial direction

The radial slope of the water surface I_r in the cross-section can be calculated from the first equation of motion, Eq.(II-9), if the other terms are known. The total super-elevation over the channel width can be given as :

$$\Delta h = \int_{r_i}^{r_o} \frac{v_\theta^2}{gr} \, dr \qquad \text{(V-1)}$$

Leopold et al (1960) stated that the value of Δh for a particular bend is independent of the radial distribution of v_θ. This is particularly true when the channel curvature is small (i.e., $r_i \cong r_o$).

Radial as well as longitudinal water surface profiles were measured in Channel I only, through the static pressure tappings at the bed referred to a still water level. Accuracy of measurement was 0.0025 mm. (see Chapter III).

Figures (V-2) and (V-3) represent the longitudinal and radial water surface profiles respectively, as taken for different flows under almost the same depth.

To check the independence of the total superelevation Δh upon the radial distribution of v_θ the following three cases were examined :

a) A free vortex distribution $v_\theta r$ = constant (c); substituting this in Eq.(V-1) gives :

$$\Delta h = \frac{1}{g} \int_{r_i}^{r_o} \frac{C^2}{r^3} dr = \frac{C^2}{2g} \left[- \frac{1}{2r^2} \right]_{r_i}^{r_o} = \frac{C^2}{2g} \left(\frac{1}{r_i^{\,2}} - \frac{1}{r_o^{\,2}} \right) \qquad \text{(V-2)}$$

The constant C was calculated by Ippen <u>et al</u> (1960), on the assumption of irrotational flow in which the specific head $H = y + \frac{v_\theta^2}{2g}$ is constant. They concluded the value of C as :

$$C = \bar{v}_\theta \sqrt{r_o \, r_i}$$

in which $\bar{v}_\theta$ is the velocity corresponding to the mean depth of flow $\bar{y}$ in the cross-section.

b) A forced vortex distribution $\frac{v_\theta}{r}$ = constant (c): Equation (V-1) gives :

$$\Delta h = \frac{1}{g} \int_{r_i}^{r_o} C^2 r dr = \frac{C^2}{g} \left[\frac{r^2}{2} \right]_{r_i}^{r_o} = \frac{C^2}{2g} (r_o^{\,2} - r_i^{\,2}) \qquad \text{(V-3)}$$

The value of C was also calculated by Ippen <u>et al</u> (1960)

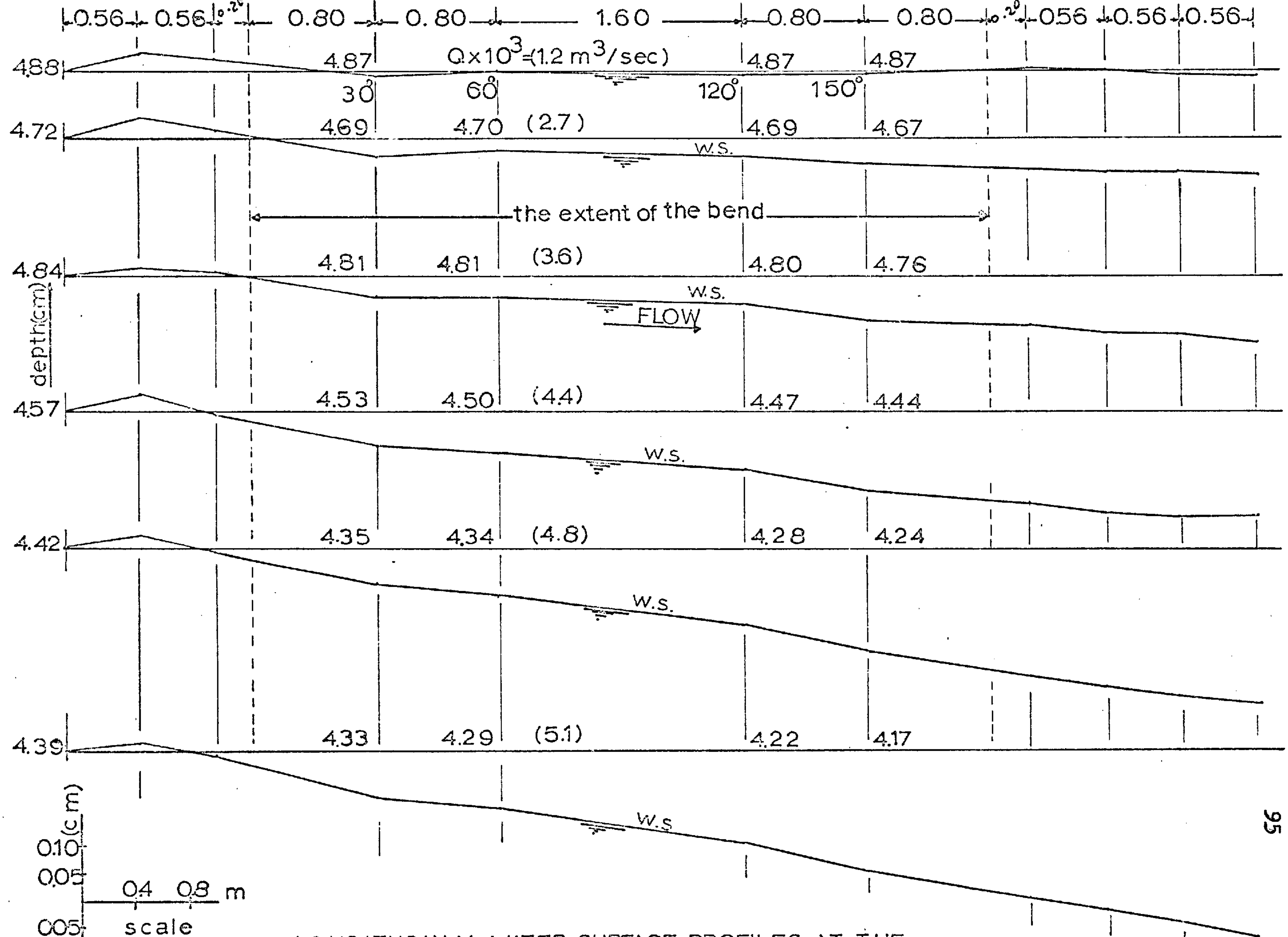

FIG V-2 LONGITUDINAL WATER SURFACE PROFILES AT THE CENTRELINE OF CHANNEL I ($r_c/b = 3$)

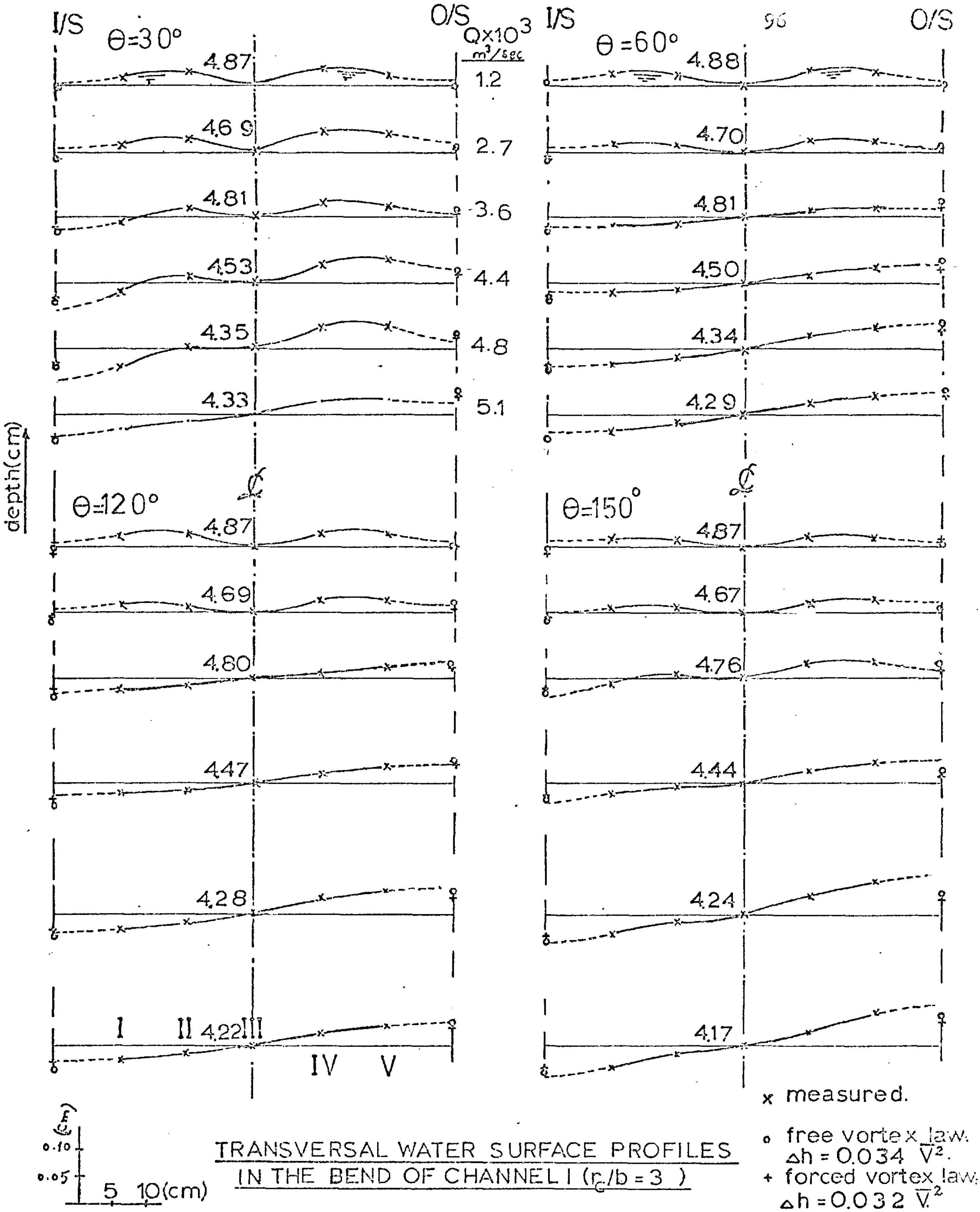

TRANSVERSAL WATER SURFACE PROFILES IN THE BEND OF CHANNEL I ($r_c/b = 3$)

FIG V_3

and found to be :

$$C = \left[\frac{3\bar{v}_\theta^{\,2}}{r_o^{\,2} + r_o r_i + r_i^{\,2}} \right]^{\frac{1}{2}}$$

c) One-dimensional analysis where v_θ = constant everywhere with constant r (= r_c) :

Equation (V-1) gives :

$$h = \frac{\bar{v}_\theta^{\,2}(r_o - r_i)}{g\, r_c} \qquad \text{(V-4)}$$

Substituting into Eqs.(V-2),(V-3) and (V-4) the values of g, r_c, r_o, r_i and C (in metric units) of Channel I, the following equations can be obtained :

a-1) Free vortex : $h = 0.034\ \bar{v}_\theta^{\,2}$ (V-5)

b-1) Forced vortex : $h = 0.0032\ \bar{v}_\theta^{\,2}$ (V-6)

c-1) Constant v_θ and $r = r_c$: $h = 0.0030\ \bar{v}_\theta^{\,2}$ (V-7)

In Figure (V-3) the values of Δh_{as} calculated from Eqs.(V-5) and (V-6) are plotted, assuming the rise at the outer side over the mean flow depth (assumed to be at the centreline) to be equal to the drop at the inner side from the mean flow depth. The values of $\bar{v}_\theta$ (in m/sec.) were calculated on the basis of measured mean depths of flow at the centreline for the cross-sections $\theta = 30^\circ$, 60°, 120° and 150°. The mean depths were taken from the longitudinal water surface profiles as represented in Fig.(V-2).

From the present experiments it can be seen that the radial water surface profiles conform to neither of the previous formulae when the flow is small. The profiles, in this case, show a hump on each side of the centreline; the cause of this peculiar shape can be attributed to the effect of secondary currents which presumably constitute two cells of secondaries in the cross-section. This has also been observed by Ali (1964) in field measurements. When the flow speed increases, the radial profiles gradually take the shape of a straight line.

Regarding the longitudinal water surface profiles, Figure (V-2) shows, in all flows investigated, a constant rise in the water surface at tapping point 0.8 m. before the bend entry. This rise in water surface before the bend can be ascribed to the existence of the bend itself, which acts as an obstacle to the flow with a backwater effect. (The present experiments were all in the sub-critical flow condition and the Froud number $F = \frac{\bar{v}}{\sqrt{gh}}$ was far less than 1). An M1 curve of the water surface is expected to develope upstream of the bend. This was not checked, due to the rather short straight approach section of the bend. With increasing flow velocities, this rise before the bend decreases, and the longitudinal gradient of the water surface in the bend and downstream of it increases.

V - 2. Helical motion in curved channel flow

The helical motion around channel bends is primarily dependent on the intensity of secondary currents; therefore, the characteristics of these currents are investigated, as a first step, in order to assist the understanding of the nature of the problem.

It is convenient to interpret the intensity of secondary currents in terms of the deviation of the flow from the circumferential direction around the bend. Because the vertical deviation from this direction is basically of a negligible magnitude except near the side walls, the intensity of secondary flow, which produces the helical motion, can be represented, in the case of a wide stream, by the horizontal deviation of the pathlines from the circumferential direction. At the channel bed, the deviation of the pathlines from the circumferential direction is represented by an angle α_o, designated the bed angle, whereas at the remainder of the stream it is represented by an angle α and designated the flow angle. Measuring devices for α_o and α are described in Chapter III.

<u>i) Bed angles</u>. At six points across the width of Channel I, the bed angles were measured for different depths of flow and the same discharge at $\theta = 60^o$ and 120^o, Fig.(V-4). It can be seen from this figure that maximum α_o for a particular flow depth occurs near the centreline. The same figure (V-4) shows that α_o increases with decreasing aspect ratio b/h (see Table 6 in Appendix C for numerical values).

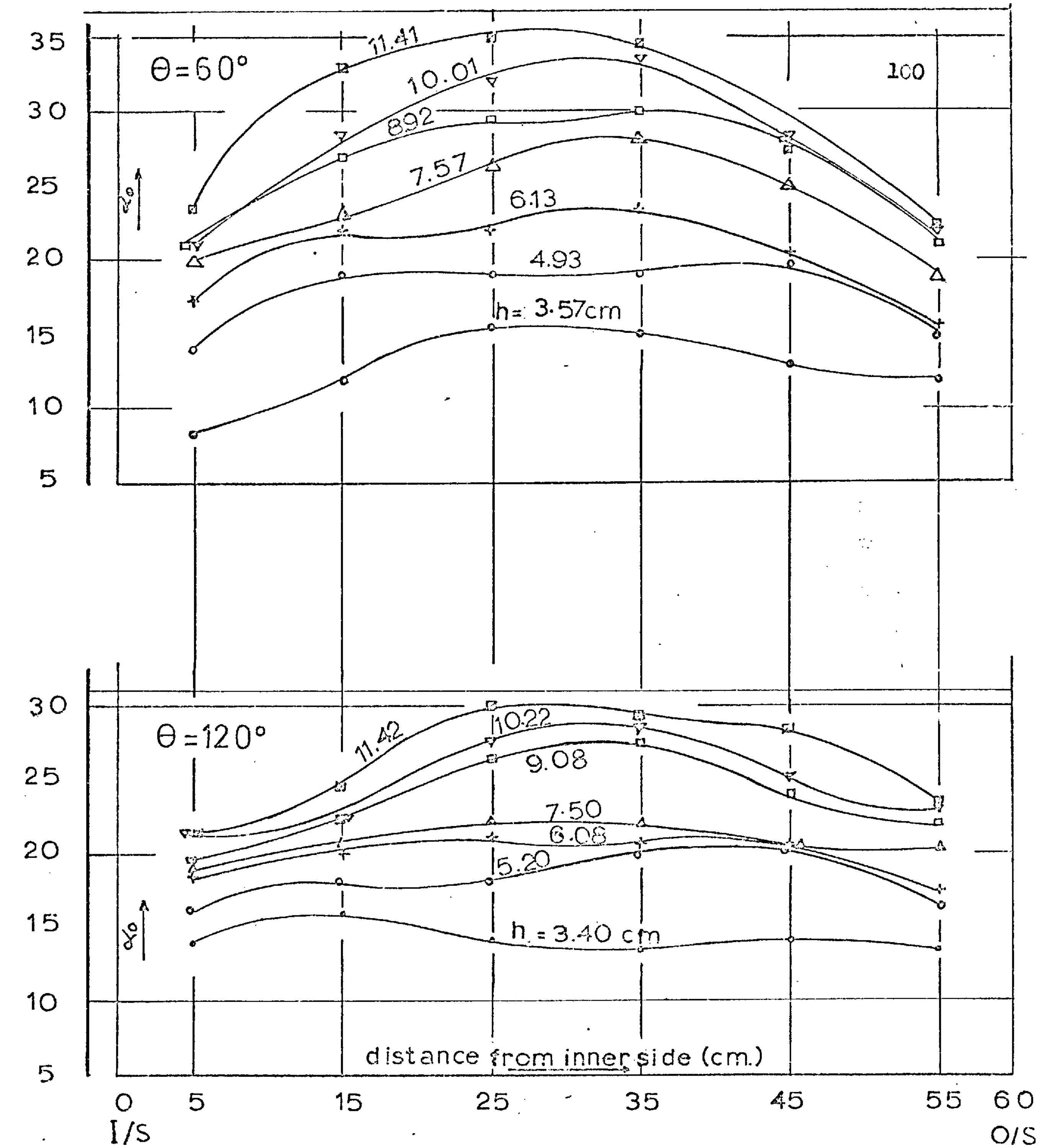

FIG V-4 BED ANGLES ACROSS THE WIDTH FOR DIFFERENT DEPTHS OF FLOW (channel I); Q=4.3×10^{-3}m/sec.

The effect of channel curvature on the bed angles is revealed by measuring α_o in the three channels at $\theta = 60^o$ and $\theta = 120^o$ under the following flow conditions :

Channel	b/r_c	h(cm)	$Q \times 10^3$ m^3/sec	
I	0.333	3 - 12 (7 depths)	4.3	giving same Re
II	0.154	"	2.72	
III	0.127	"	2.72	

The measurements as plotted in Fig.(V-5), in terms of $\tan\alpha_o$ vs. h/r_c, show a straight line distribution. A relation of the form :

$$\tan\alpha_o = K.\ h/r_c$$

is obtained, in which K is a factor whose numerical magnitude depends on the channel curvature and cross-section location. From the present measurements, K is given as :

Channel	cross-section	K
I	60^o	11.6
I	120^o	10
II,III	60^o	7.5
II,III	120^o	6.5

Field as well as laboratory measurements on different bends by Rozovskii (1957) gave the factor K as between 10 - 12.

These measurements confirm the previous conclusion that α_o increases with h (or with decreasing aspect ratio), and

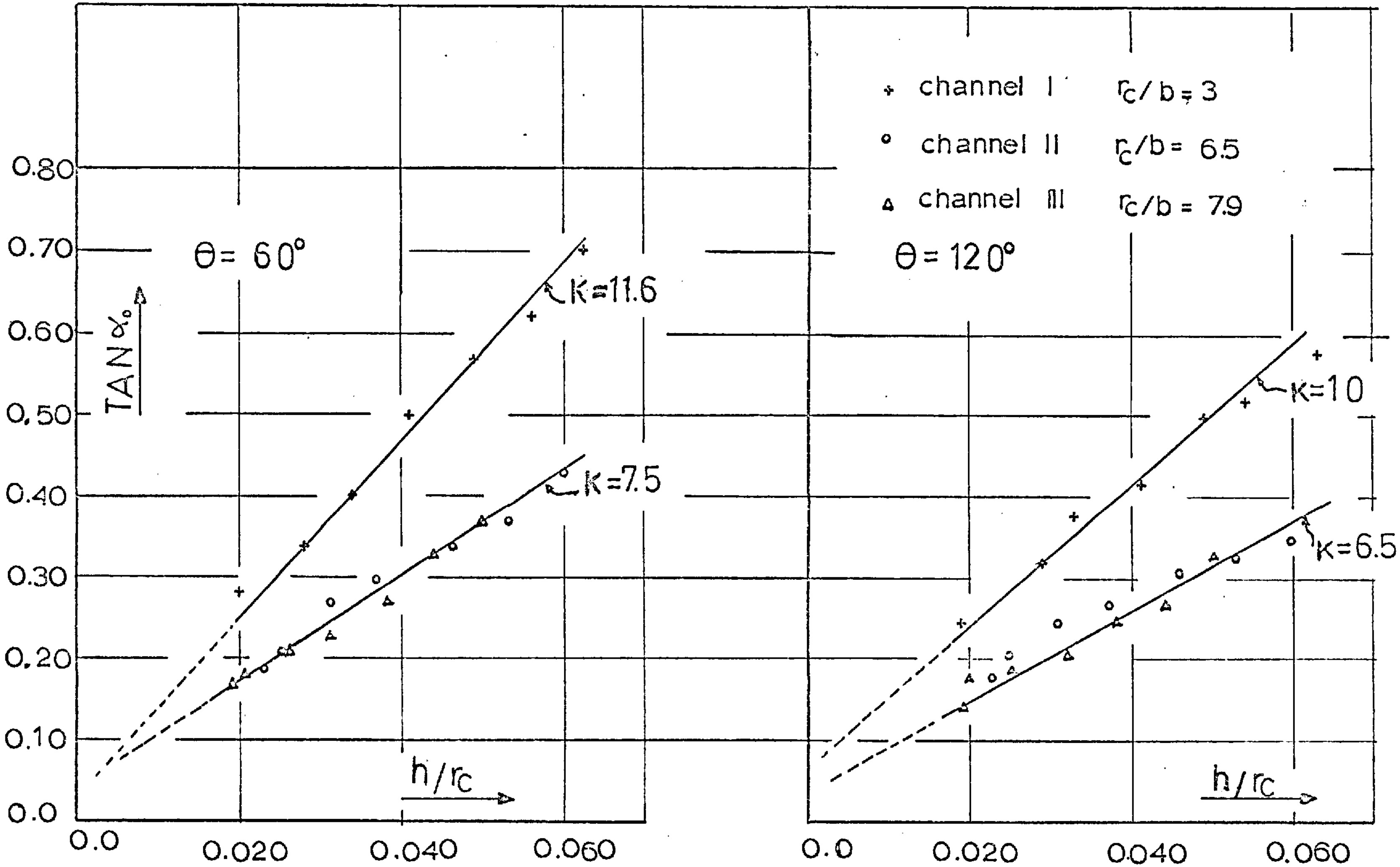

$$\tan \alpha_o = K\,(h/r_c)$$

FIG V_5

BED ANGLES VS. d/r_c AT CENTRELINE
(turbulent flow)

from them it can be concluded that increasing curvature b/r_c increases α_o. The factor K, however, is not a universal one, as suggested by Rozovskii, for all bends and all cross-sections around the bend, but is expected to change with these parameters.

The effect of Reynolds number on the magnitude of α_o is revealed by measuring the bed angle in the three channels at the centreline of several cross-sections around the bends. Examining Fig.(V-6) confirms the previous result that α_o increases with increasing curvature b/r_c, and gives the conclusion that the maximum α_o occurs at the early region of the bend when curvature is high (in Channel I, $\alpha_{o\,max}$ occurs at $\theta = 30^o \rightarrow 60^o$) and moves towards the middle region of the bend for decreasing curvature. From the same figure (V-6), it can also be concluded that α_o decreases with increasing Reynolds number, whatever the channel curvature is (see Table 7 in Appendix C).

The strength of secondary flow was defined by Malouf (1950) as the magnitude of $\tan\alpha_o$, and he correlated this to $(h/r_c)^{\frac{1}{2}}(Re)^{-\frac{1}{4}}$ as h and Re are the most effective factors governing α_o. In the present experiments a similar correlation was plotted in Fig.(V-7), which shows that

$$\tan\alpha_o = A \cdot (h/r_c)^{\frac{1}{2}} (Re)^{-\frac{1}{4}} - C \qquad \text{(V-9)}$$

The value of A as obtained by Malouf (1950) on a 90^o bend was

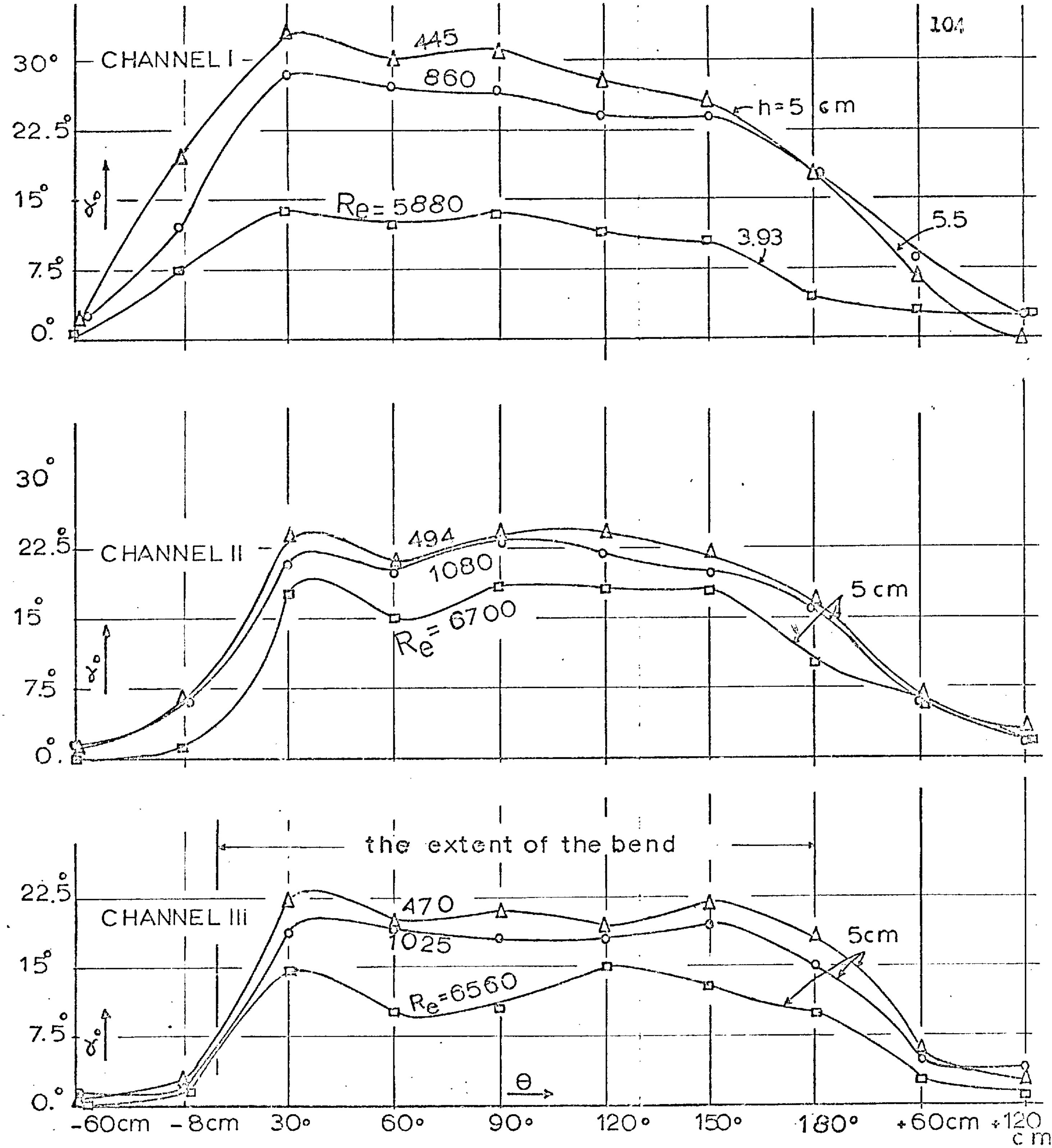

FIG V_6 BED ANGLES AROUND THE BEND FOR DIFFERENT REYNOLDS NOS.

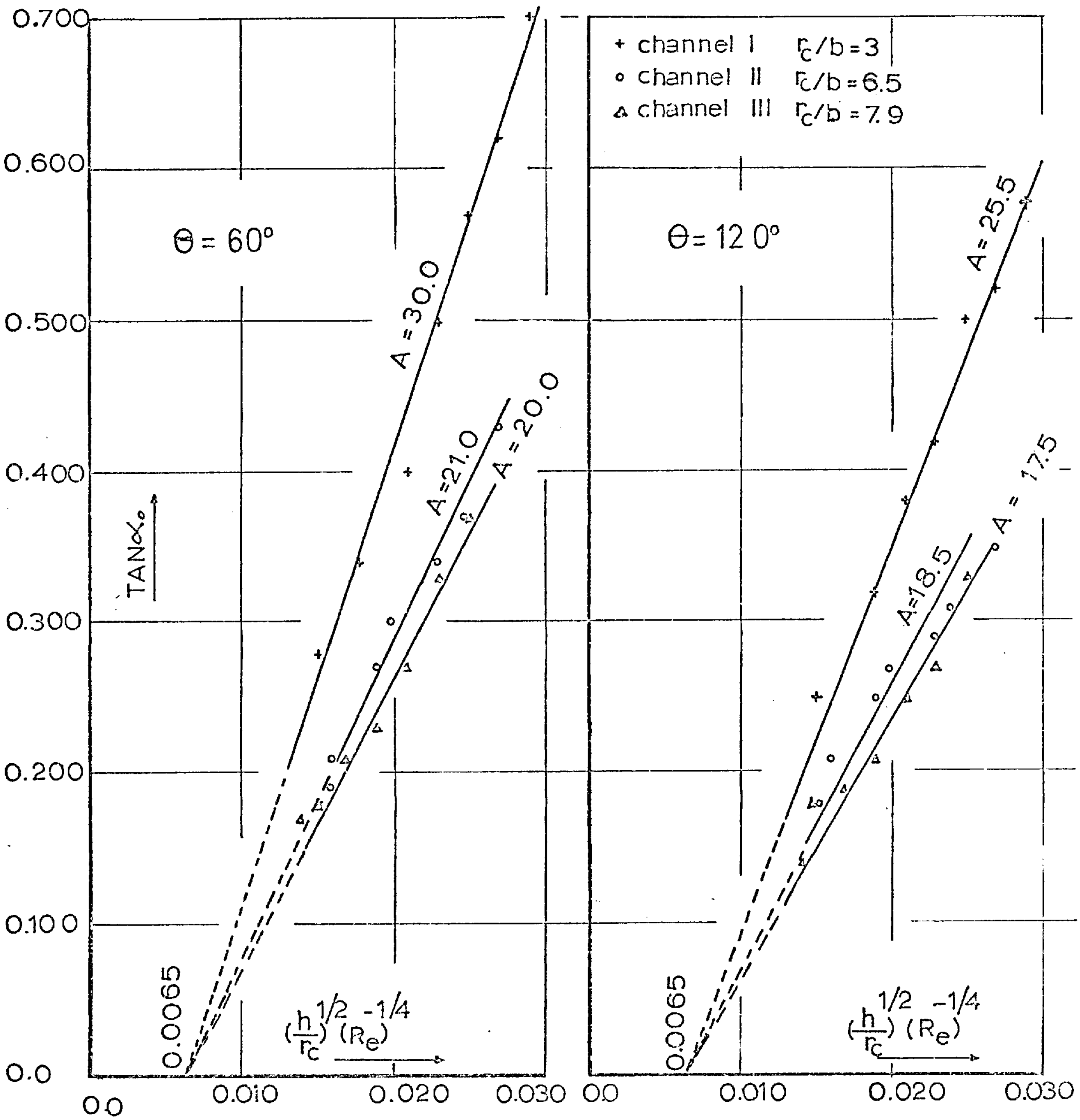

$$\mathrm{TAN}\,\alpha_o = A\left[\left(\frac{h}{r_c}\right)^{1/2}(R_e)^{-1/4} - C\right];\ C = 0.0065$$

FIG V_7 BED ANGLES VS. $(h/r_c)^{1/2}(R_e)^{-1/4}$ AT CENTRELINE (turbulent flow) equal to 23.4, whereas that obtained by Wadekar (1956) was equal to 25.4 (see Chapter I). In the present experiments in the three channels, the factor A is seen to change around the bend and also for different channel curvatures (Wadekar and Malouf each experimented on one bend). It is interesting to find that the value of C in Eq.(V-9) is constant for the three channels. From the present experiments, the factors A and C can be given as (Fig.(V-7) and Table 8, Appendix C) :

Channel	cross-section	A	C
I	60°	30.0	0.0065
I	120°	25.5	"
II	60°	21.0	"
II	120°	18.5	"
III	60°	20.0	"
III	120^{c}	17.5	"

To confirm the previous conclusion, particularly the effect of depth and curvature, photographs were taken at several cross-sections in the three channels for different depths of flow. These are reproduced in Plates (V-1) to (V-5), and show the increase in α_o with increased depth, increased curvature and decreased Reynolds numbers.

Occasionally, measurements near the inner-side of the bed angles of the regions $30^{\circ} < \theta < 60^{\circ}$ of Channel I exhibited a reverse direction of α_o, i.e., towards the outer-side. Such

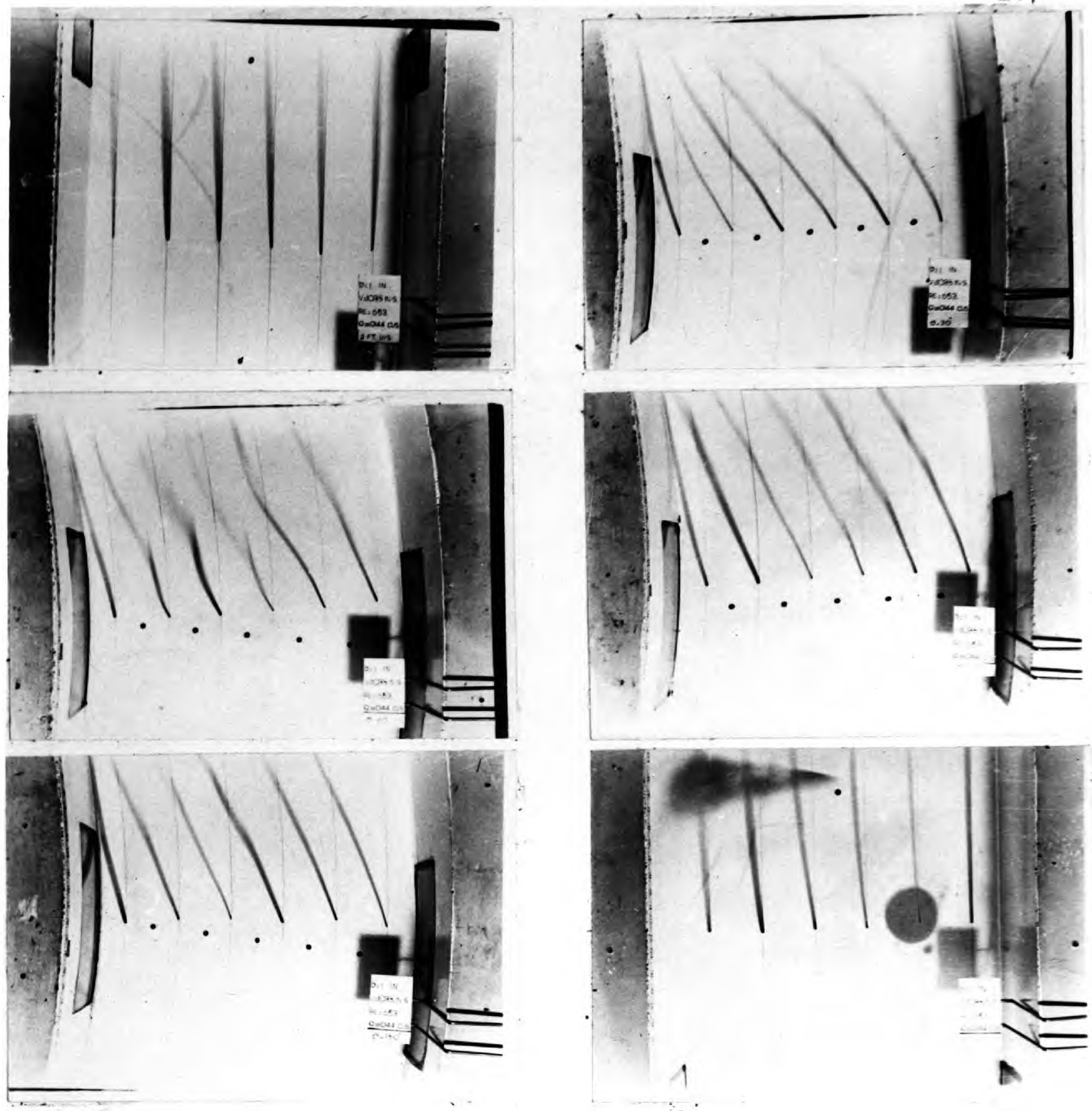

BED ANGLES IN CHANNEL I ($r_c/b=3$)

d = 2.5 cm. Re = 653

PLATE (V_1)

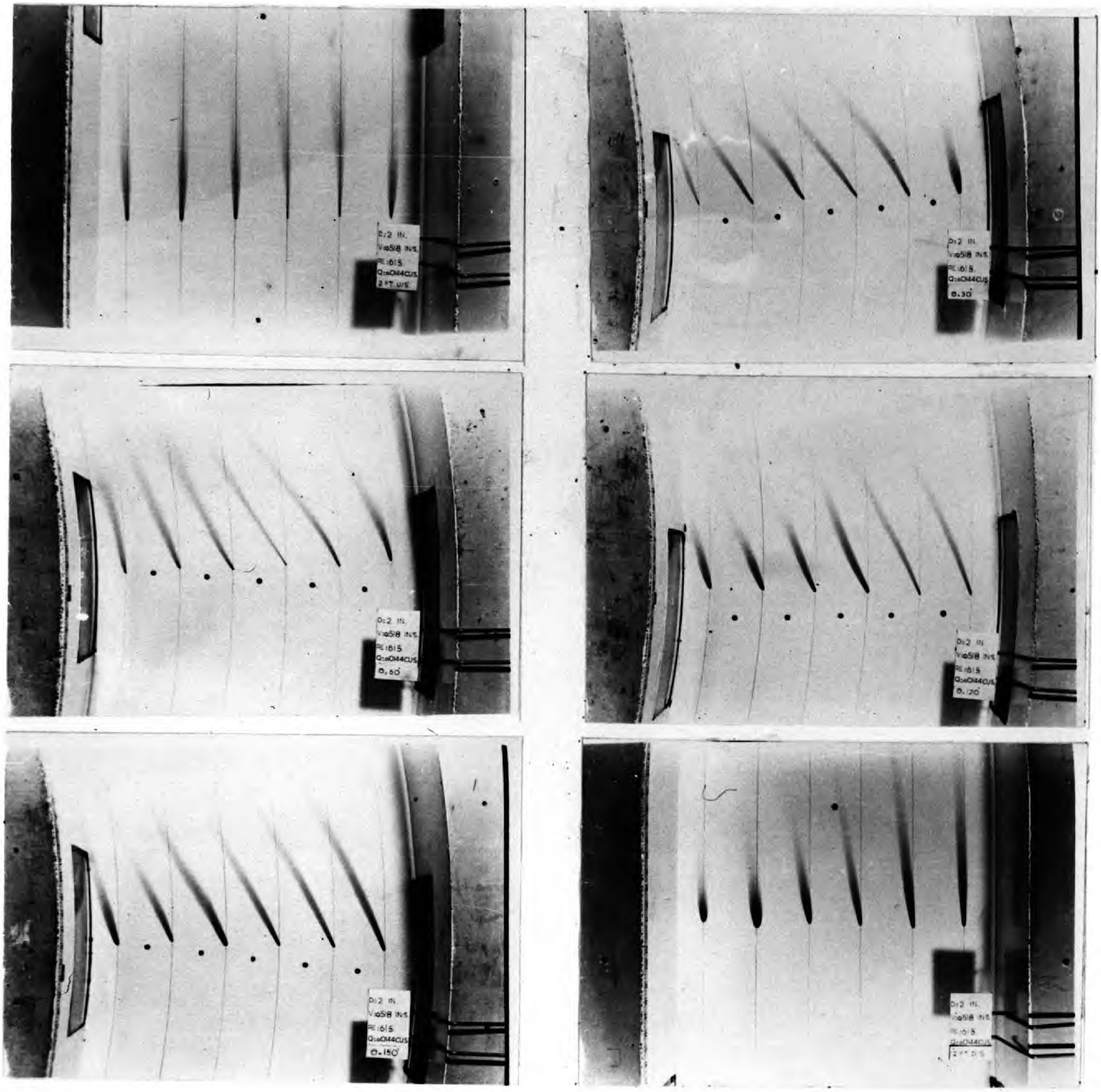

BED ANGLES IN CHANNEL I ($r_c/b = 3$)

d = 5 cm. Re = 615

PLATE (V_2)

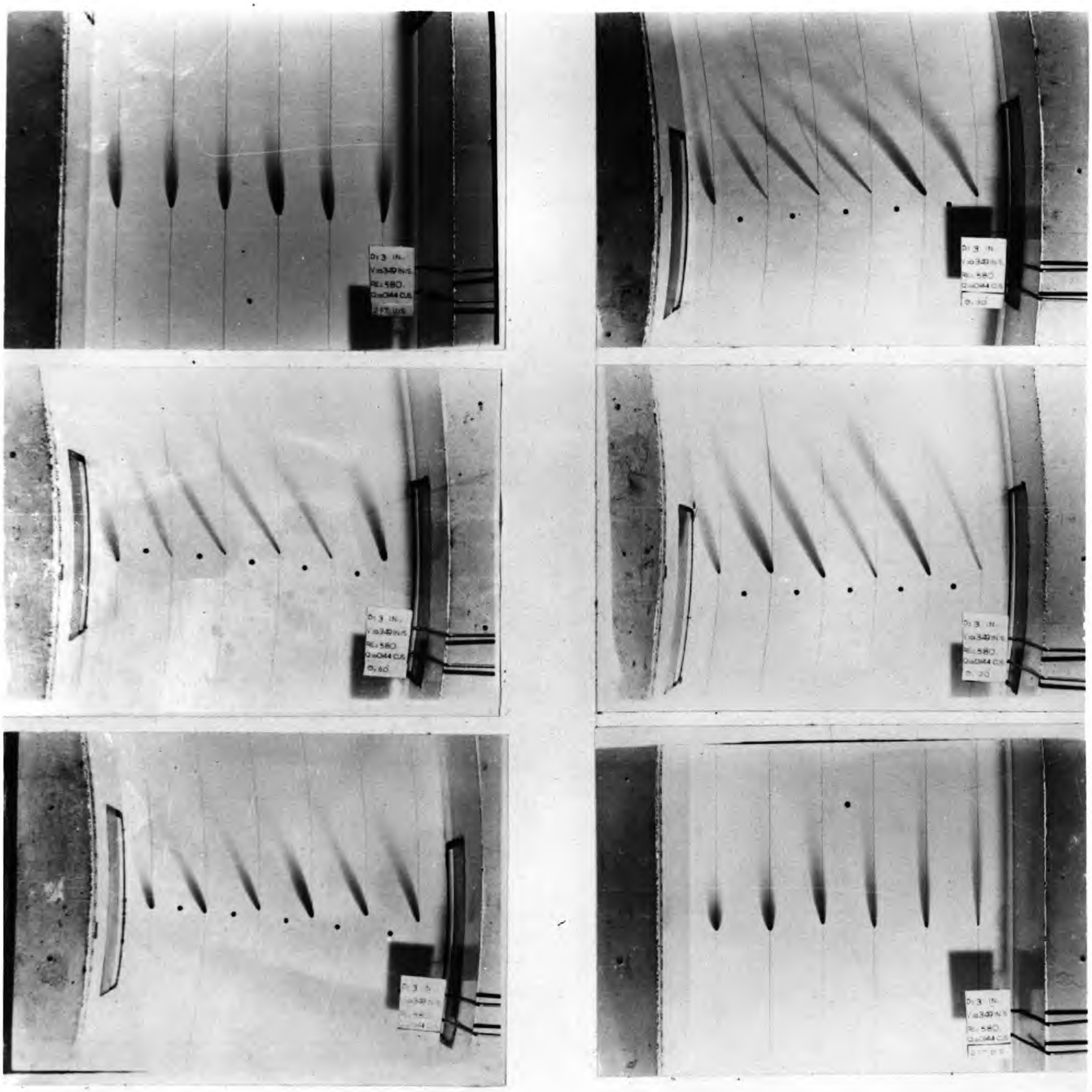

BED ANGLES IN CHANNEL I ($r_c/b=3$)

d = 7.6 cm. Re = 580

PLATE (V_3)

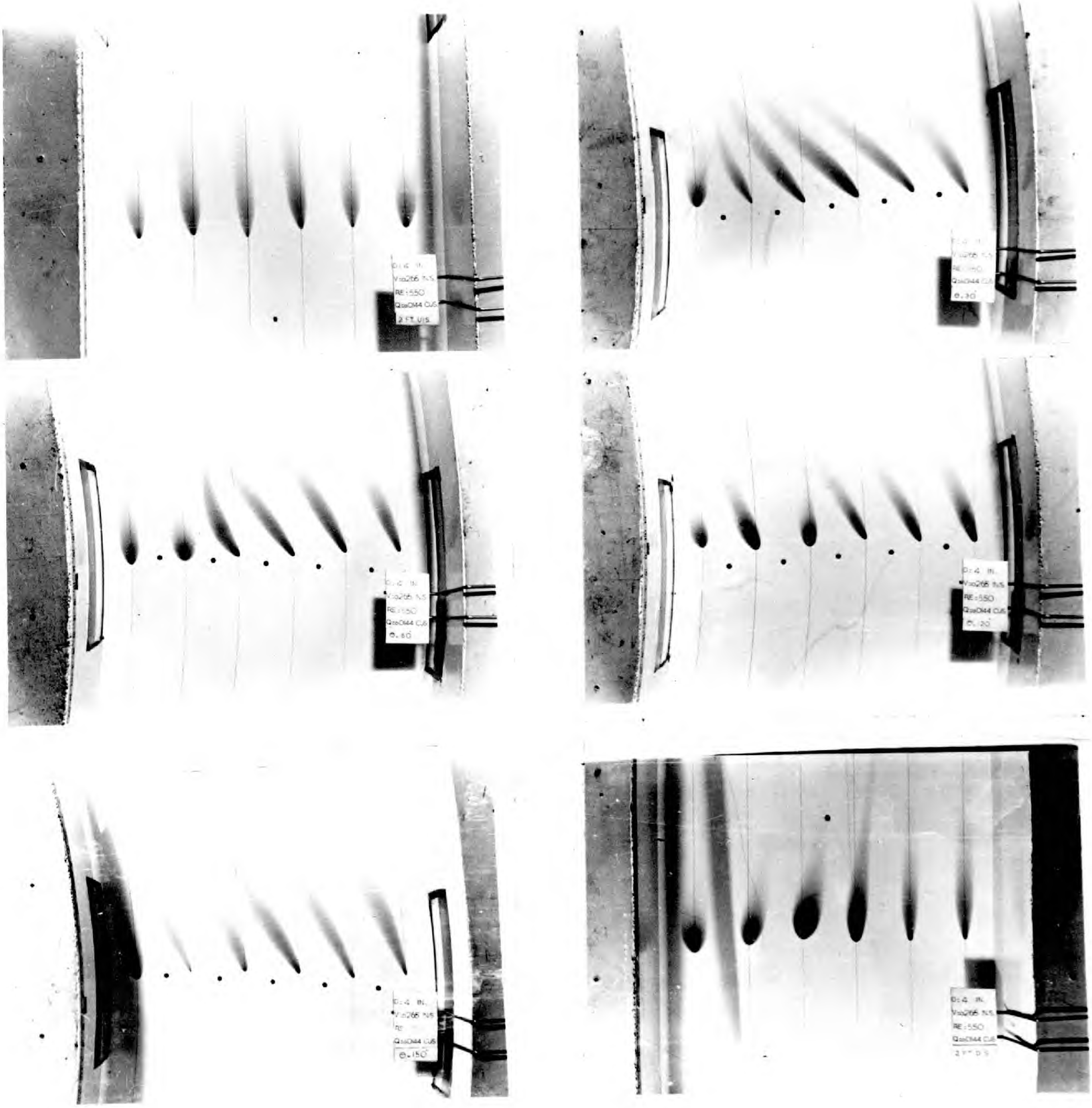

BED ANGLES IN CHANNEL I ($r_C/b = 3$)

$d = 10$ cm $Re = 550$

PLATE (V_4)

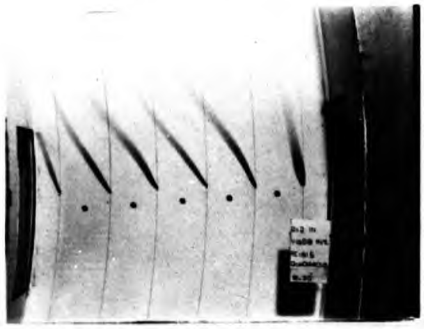

channel
I

θ= 30°

θ=150°

II

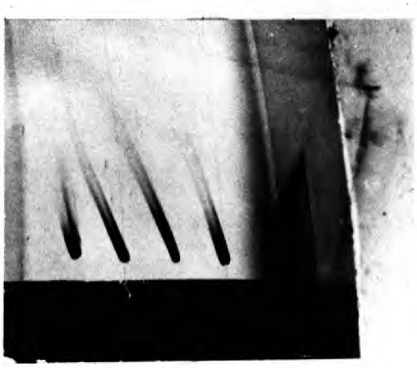

III

BED ANGLES AT θ=30° & 150° IN THE THREE CHANNELS

d = 5 cm. $Q = 0.4 \times 10^{-3}$ m3/sec.

PLATE (V_5)

a deviation was often of the order of 10° to 15°; the slower the flow or higher the depth, the higher the deviation.

Flow disturbances could not be considered as a sufficient reason, for, in some instances, this reversed deviation of α_o, though variable in magnitude, persisted even after three hours from the commencement of the experiment. It was then thought that differences in temperature across this wide channel could be a probable reason. To check this possibility further, the water in the inner region of the channel was cooled externally with crushed ice at the four inner-side windows around the bend. Five minutes later, photographs were taken of the flow-lines, with the aid of potassium permanganate streaks. These photographs are reproduced in Plate (V-6) The outward deviation of the bed angles can be seen, much intensified. At 5 cm. from the inner-side at $\theta = 60^{\circ}$, α_o was measured and found to be equal to about 65° outward. The temperature at $\theta = 60^{\circ}$ was immediately measured after measuring α_o and was as follows :

near the i/s — $T = 17.4^{\circ}$ C.

near the o/s — $T = 18.5^{\circ}$ C.

which shows that a small difference in the water temperature causes a considerable change in the flow pattern. After removing the crushed ice from the inner side windows, the outward deviation slowly decreased over a short period of time. This could then be one of the reasons for the development of

θ= 30°

θ= 60°

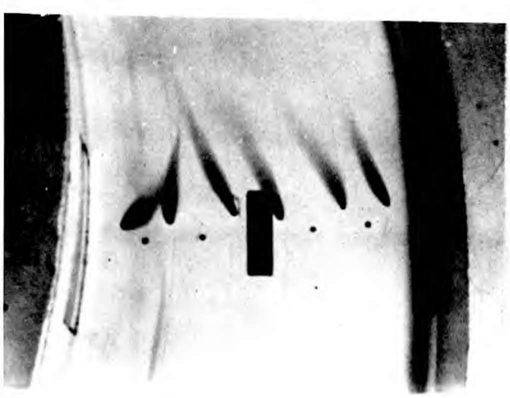

θ= 120°

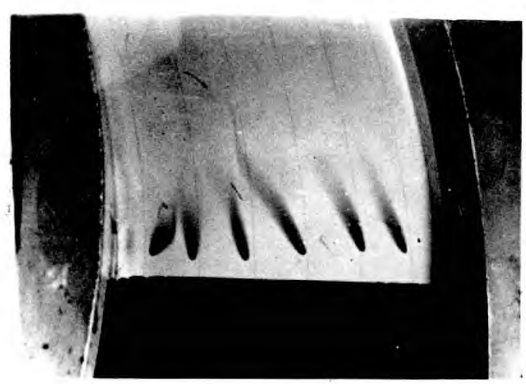

θ= 150°

BED ANGLES WITH ICE AT THE INNER SIDE WINDOWS

channel I ($r_c/b=3$) $d=7.6$ cm. $Q=0.36\times10^{-3}$ m^3/sec.

PLATE (V_6)

multi-cell spiral flow around river bends. This last fact is investigated again later in this chapter.

ii) Flow angles. At several cross-sections around the three channel bends, the flow angles at five points along the depth were measured at three verticals in each cross-section. These were :

5 cm. from i/s   Centreline C.L.   5 cm. from o/s

Conditions of flow were :

Channel	h(cm)	$Q \times 10^3\ m^3/sec$	
I	7.6	4.3	→ giving same Re
II	"	2.72	
III	"	2.72	

Figures (V-8),(V-9) and (V-10) represent the distribution of α around the three channels at the vertical 5 cm from i/s, C.L. and 5 cm from o/s respectively. The effect of channel curvature on α is clearly seen :- increased curvature increases α .

At the vertical 5 cm. from o/s, the existence of a small reversed vortex at the top corner, as first revealed by Einstein and Harder (1954), is also detected in these experiments ,Fig(V-10). In Channel I, this small vortex starts developing at sections as early as 15° from the bend entry; for decreasing curvature it is not detected before the cross-section $\theta = 75^{\circ}$ from the bend entry. In all three channels, this small reversed vortex

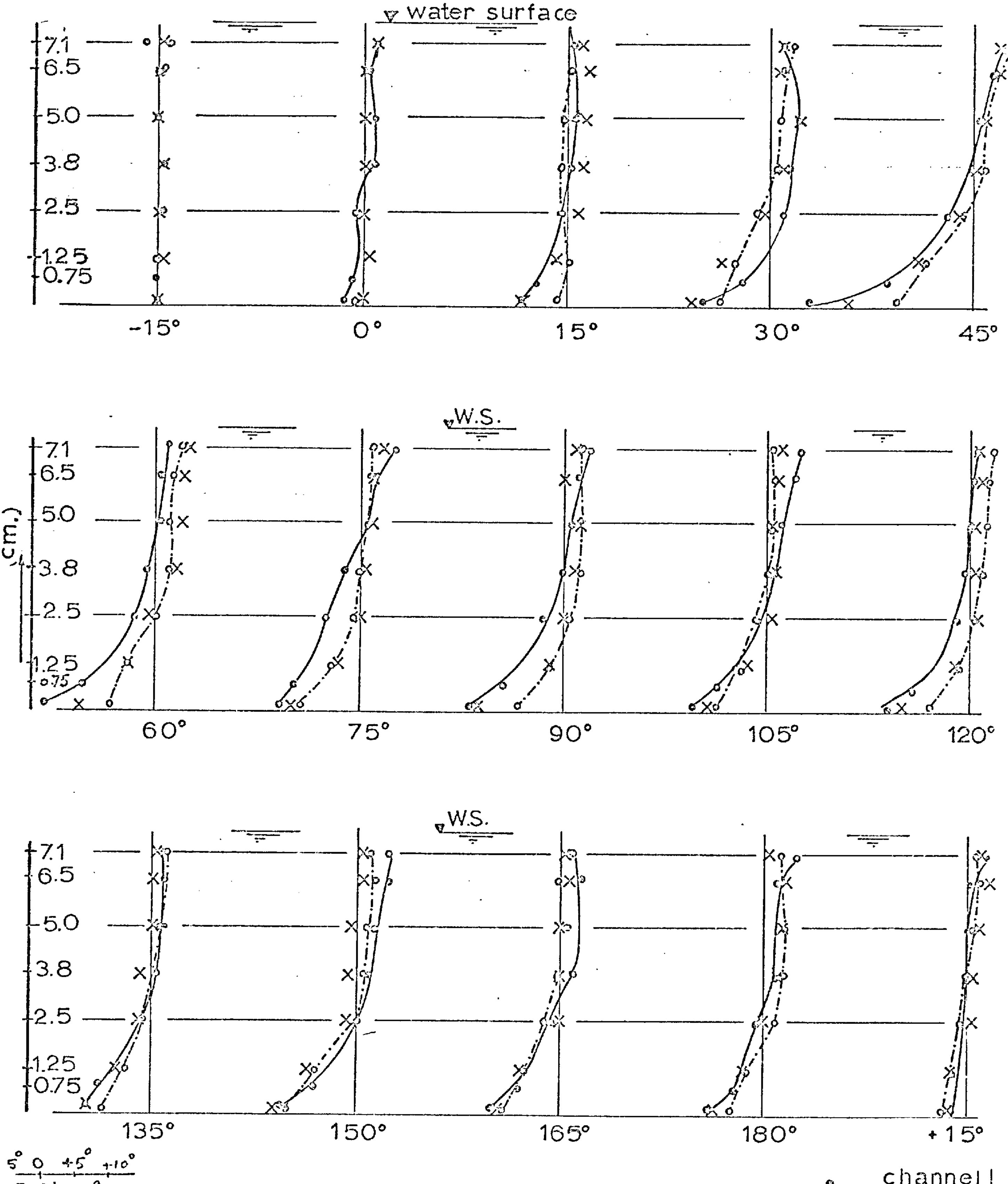

FLOW ANGLES AT 5cm FROM THE (I/S).

$Q_{(I)} = 4.4 \times 10^{-3}$ m³/sec, $Q_{(III)} = 2.75 \times 10^{-3}$

FIG V_8

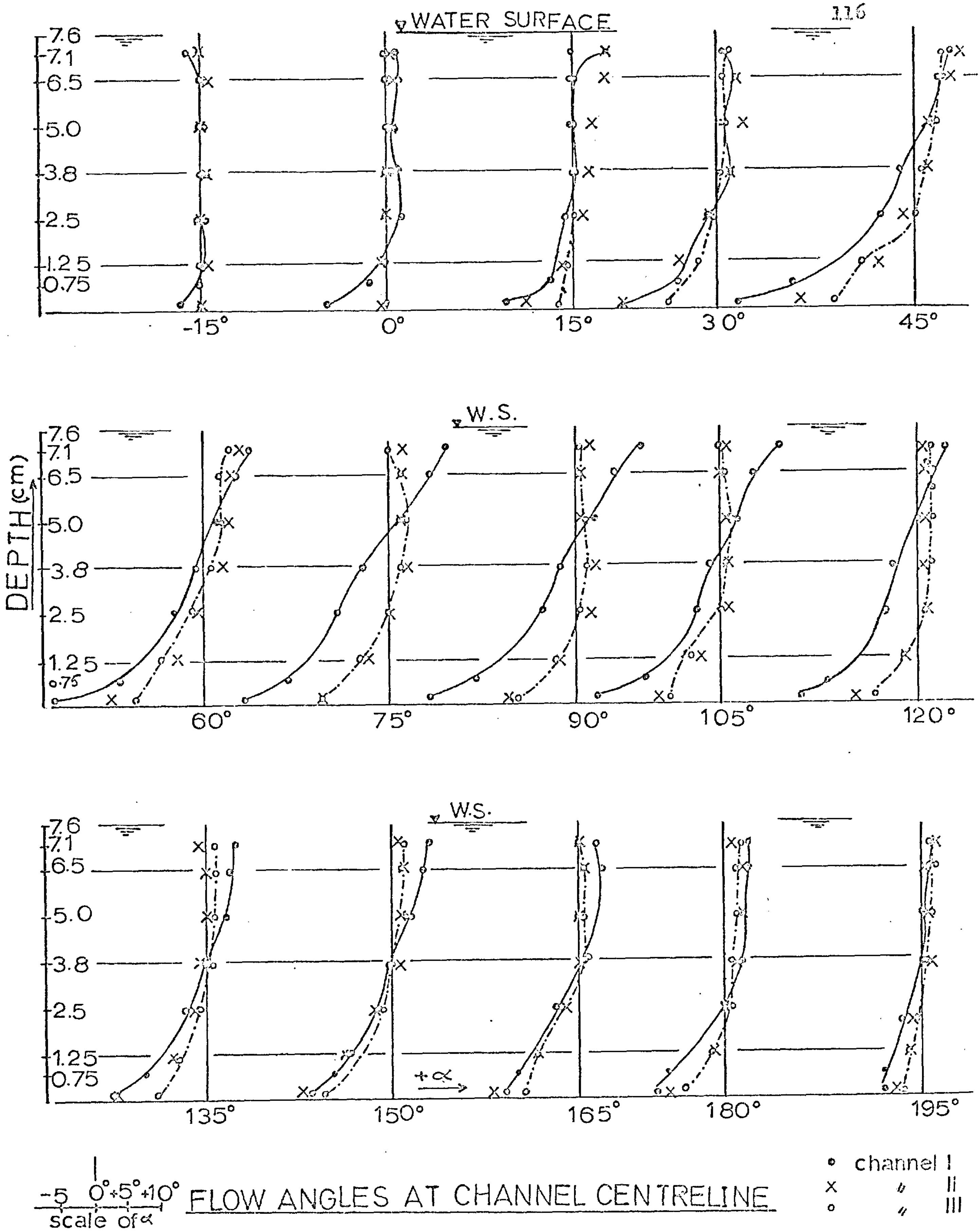

FLOW ANGLES AT CHANNEL CENTRELINE

FIG V_9

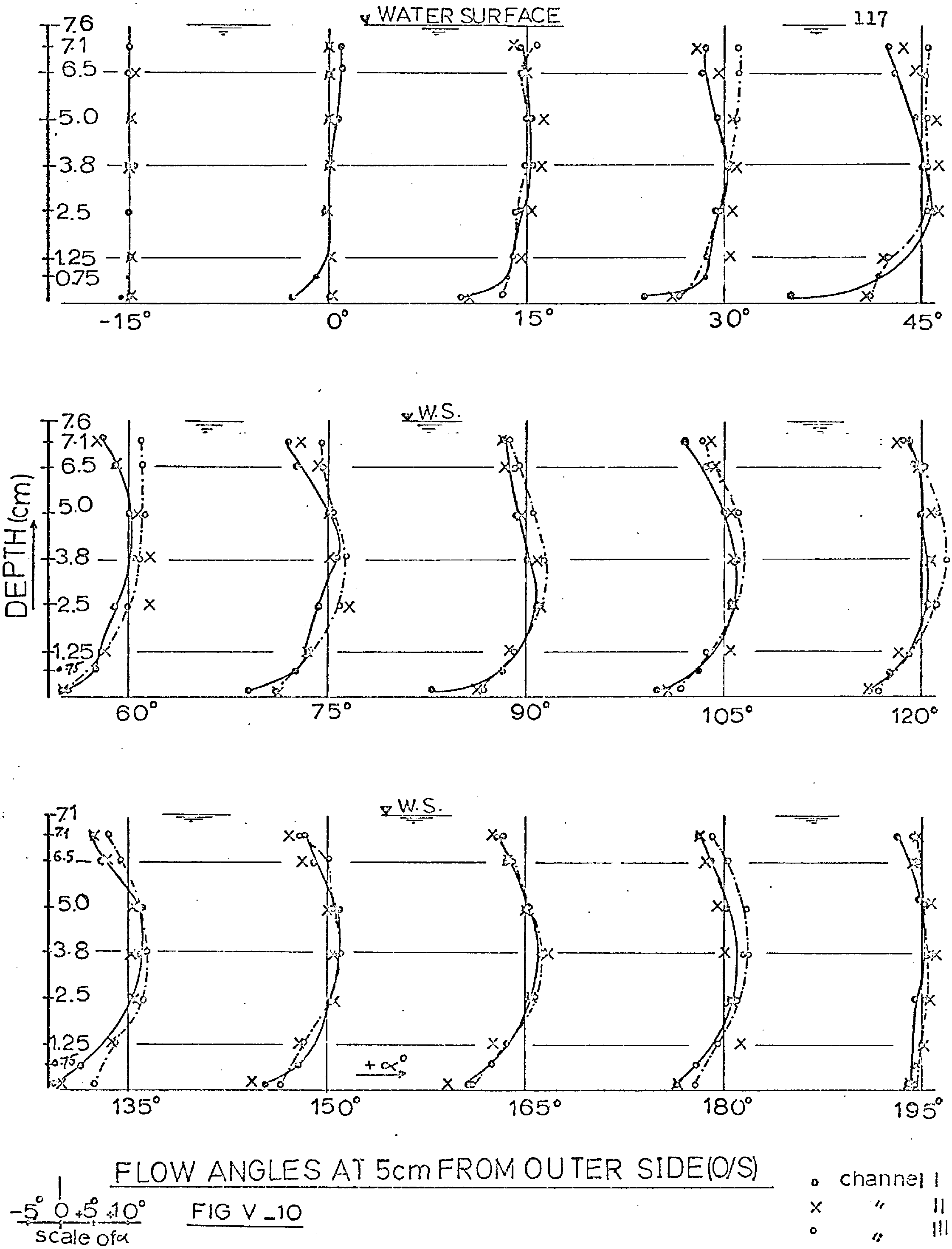

FLOW ANGLES AT 5cm FROM OUTER SIDE (O/S)

FIG V-10

o channel I
x " II
o " III

persists^{ed} for some distance downstream of the bend exit, at distances 1 to 3 times the channel width. The lower photograph on Plate (IV-2) shows one such reversed vortex at the outer-side at $\theta = 15^\circ$ of Channel I.

To explore the pattern of helical motion in Channels I and III for two depths of flow $h = 7.5$ cm. and $h = 3.75$ cm. pathlines of tracer particles of a density very close to that of water (Telcon s.g. = 0.95, see Chapter III) were photographed perpendicularly to the flow cross-section. Slightly improved photographs were later obtained using a mixture of Nitrobenzene, olive oil and water at suitable proportions (s.g. = 1) as a flow tracer , (see Chapter III) Plates (V-7) and (V-8) were taken with Telcon, whereas Plates (V-9) tO (V-11) were taken with droplets of the other tracer mentioned above. These photographs do not exactly represent the full width of the channel, due to the limitations of the windows; it was not possible to photograph the region about 5 cm. near the outer side. At cross-section $\theta = 30^\circ$, the left-hand side of the plate represents the outer side of the bend, wheareas the right-hand side represents the inner side; at $\theta = 150^\circ$, the opposite situation is the case. The difficulties in exploring the helical motion were too great to obtain better photographic records of this, although, examining these photographs, a general trend of the flow towards the outer side at the water surface can be seen. The multi-cell pattern of the secondary

On the plates opposite, the
left-hand side is the outer
side of the bend.

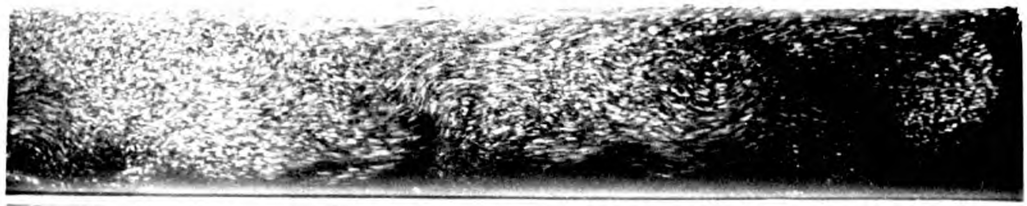

channel I Re = 246

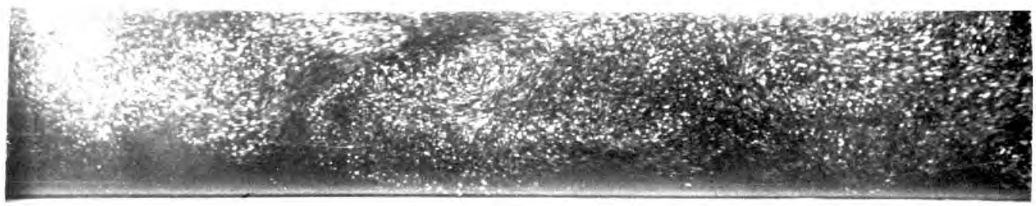

I 545

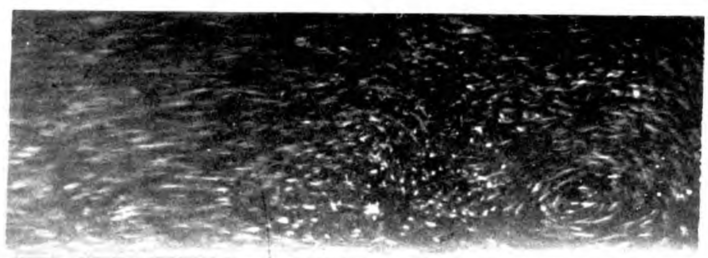

III 2000

SECONDARY CURRENTS AT $\theta = 30°$

flow depth = 7.5 cm

PLATE (V_7)

On the plates opposite, the right-hand side is the outer side of the bend.

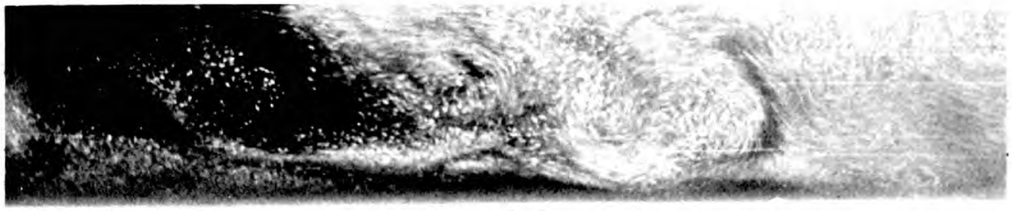

channel I Re = 246

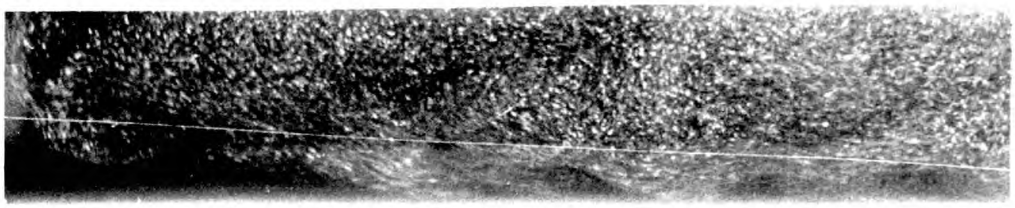

I 545

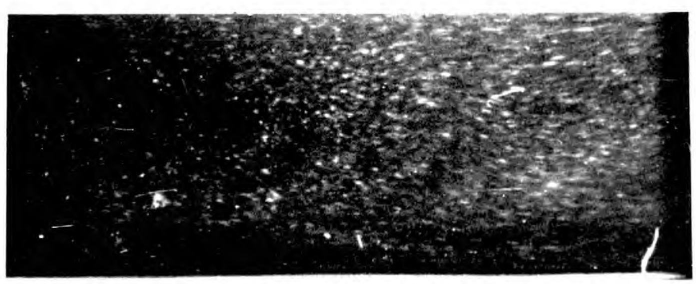

III 2000

SECONDARY CURRENTS AT $\theta = 150°$

flow depth = 7.5 cm

PLATE (V_8)

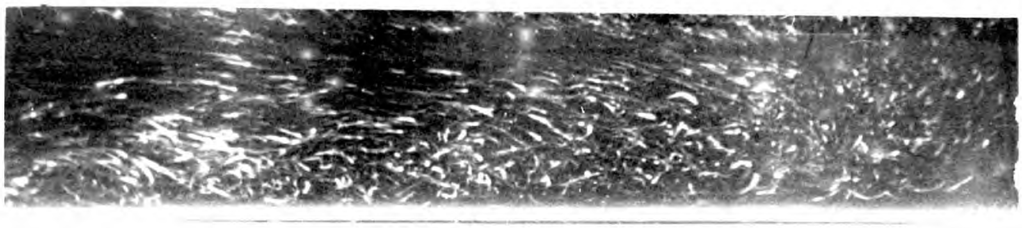

Re =6160

6690

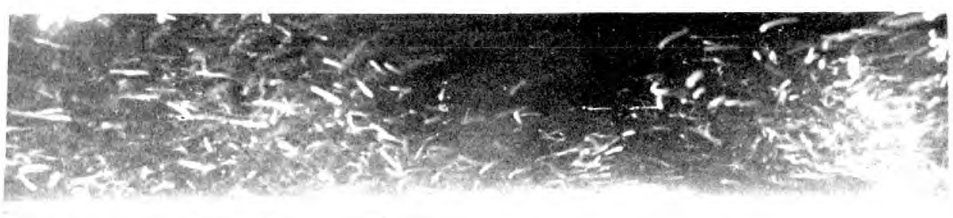

7500

SECONDARY CURRENTS AT θ =150°

(channel I) flow depth= 7.5 cm

PLATE (V_ 9)

On the plates opposite, the right-hand side is the outer side of the bend.

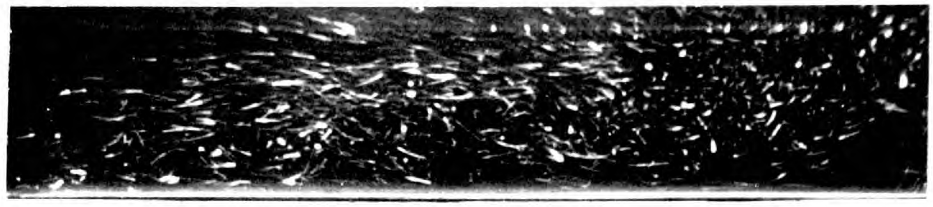

Re=6160

6690

7500

SECONDARY CURRENTS AT θ=150°

(channel I) flow depth = 7.5 cm

PLATE (V-10)

On the plates opposite, the
right-hand side is the outer
side of the bend.

Re =6500

7050

7910

SECONDARY CURRENTS AT $\theta = 150°$

(channel I) flow depth = 3. 75 cm

PLATE (V_11)

flow is also revealed. When the depth is small (h = 3.75 cm., b/h = 13.8), the helical motion is further complicated by a rather random system of vortices. Better photographs could probably be obtained by trying altered widths of the illuminated slit and exposure time.

It may be concluded broadly that, in rivers or natural streams of wide cross-sections, the helical motion consists of several cells at any cross-section, though a main cell predominates. Changes in density of the flow, due to changes in the concentration of suspended sediments across the river bend, together with irregularities of the river boundaries, further contribute to the complexities of spiral motion around river bends.

CHAPTER VI

BED SHEAR STRESS DISTRIBUTION AROUND A BEND

The acceleration and deceleration of flow due to the redistribution of velocities around the bend is likely to affect the distribution of bed shear stress. As is mentioned in Chapter IV, the momentum exchange due to secondary currents causes high velocity region, and so steep velocity gradients, to occur near the outer side and below the water surface in the downstream half of the bend.

Moreover, unlike straight open channel flows, the velocity and the resultant shear stress very near the bed are generally directed towards the inner side of the channel, making an angle α_o with the circumferential direction. For this reason, both the longitudinal and the radial components of bed shear stress can be recognized and need to be known, in order to assess how considerable is the effect of secondary flow on the distribution of bed shear stress.

The experimental procedure

A simple method of measuring the two components of bed shear around the bend was applied: the shear stress components were deduced by measuring the speed and direction of pre-calibrated small glass spheres (2 mm. diameter) rolling on the channel bed. These glass spheres were first calibrated in a smooth rectangular straight channel (56 cm. wide, 12 m. long) in the laboratory. Uniform flow in each run was established in the straight channel by means of an adjustable tail gate. The speed of the rolling spheres on the bed of the straight channel was averaged over a section 1.8 m. long at the mid-length of the channel. The corresponding value of the average shear stress in each run was calculated from

$$\tau_o = \gamma h s,$$

in which h is the depth of flow, s is the slope of the channel bed. Readings of the speeds at each run were repeated five times, and the mean values of these were plotted against τ_o for different runs, as shown in Fig. (IV-1-1)

The assumptions made in adopting this method of measurement were :

1) The velocity distribution of the flow near the bed is not affected by the moving grain.

2) The circulation around the rolling sphere is negligible.

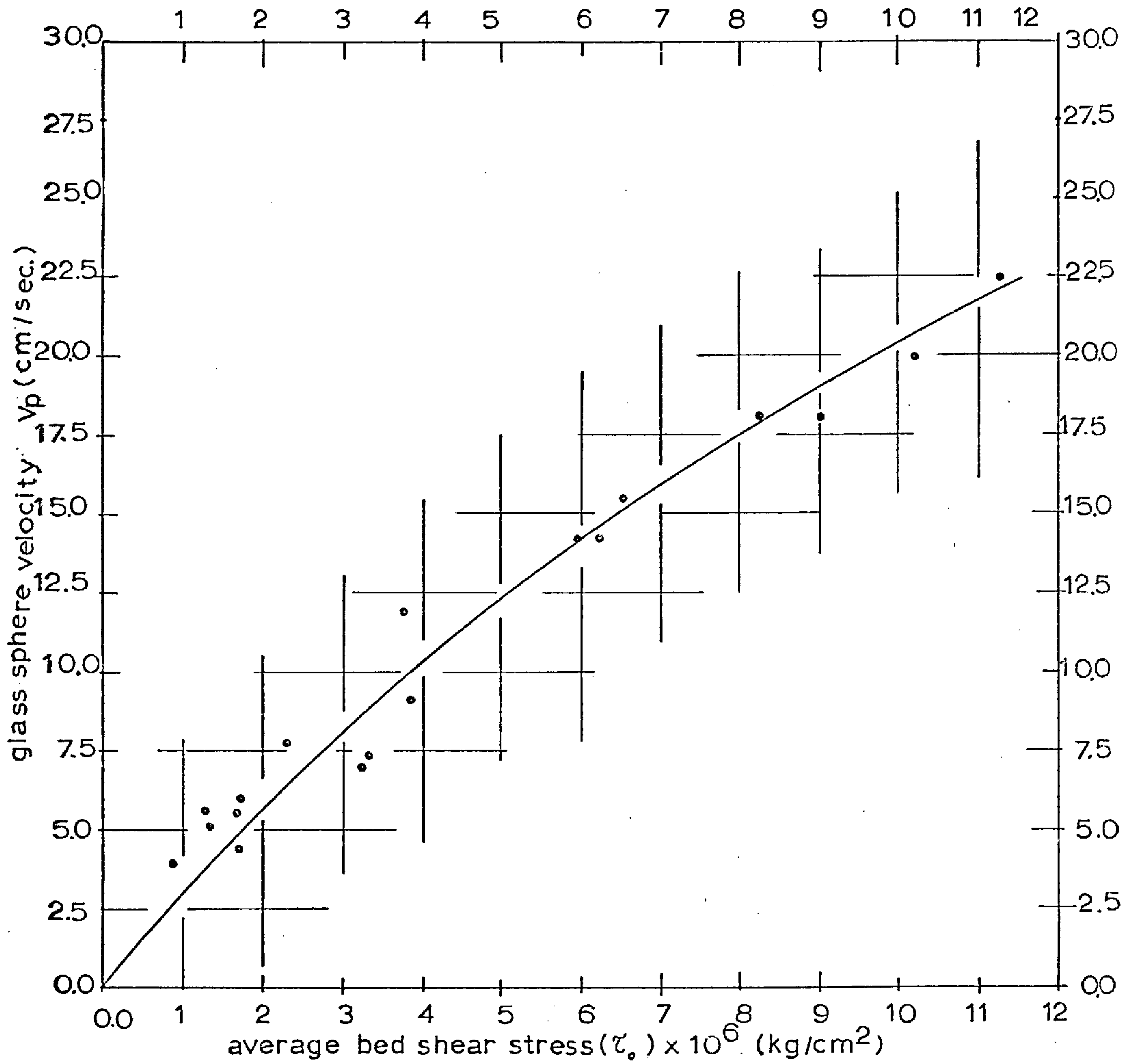

τ_o VS. GRAIN VELOCITY V_p IN STRAIGHT UNIFORM FLOW

FIG ~~III-1~~ IV-1-1

3) The sphere trajectory is the same as that of the flow it replaces.

4) The size and shape of all the rolling spheres are the same.

The resulting calibration curve was used in evaluating the shear stress in the two curved channels I and III (Channel I: $r_c/b=3$; Channel III: $r_c/b=7.9$). Measurements in these two channels were carried out at the following cross-sections: 1.4 m. and 0.28 m. upstream of the bend entrance, 0°, 30°, 60°, 90°, 120°, 150°, 180°, 0.28 m. and 1.4 m. downstream of the bend exit. At each cross-section, shear stress was measured at six points, 10 cm. apart, in Channel I, and at four points, 5 cm. apart, in Channel III, Fig.(VI-1).

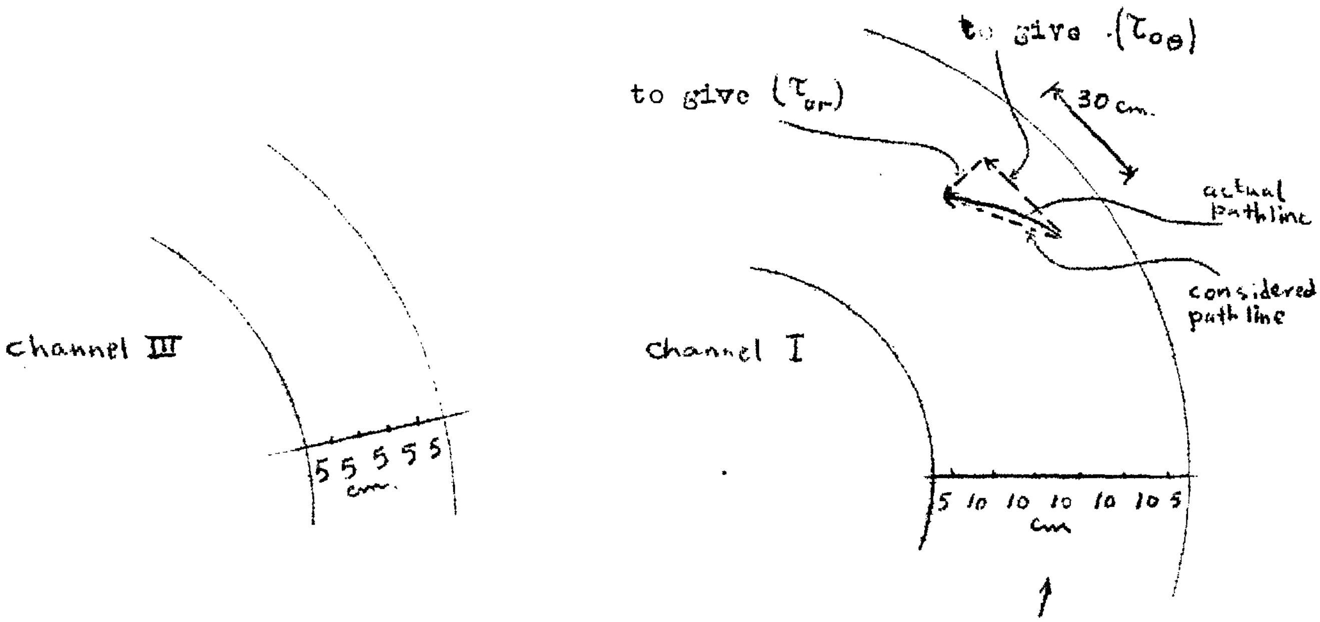

FIG VI-1

The speeds of the rolling grains in both channels were averaged over 0.30 m. distance, except at $\theta = 0^{o}$, the bend entrance, where the averaging was over 0.15 m. distance. Readings at each point were repeated five times, and the mean values were considered.

In experiments on the curved channels, water was running for one hour before the measurements were taken. In the straight channel, the length of time was half-an-hour before each run.

The experimental conditions in the two curved channels were :

	$Q(m^3/sec)$	d_4(1.4m.u/s the bend)m.	$\bar{V}_4$(m/sec)	m(m)	$T(C^o)$	$Re = \frac{\bar{V}m}{\nu}$
Channel I	0.0040	0.038	0.173	0.033	18.3	5500
Channel III	0.0025	0.041	0.236	0.030	17.2	6680

The pathlines of the rolling spheres on the bed were resolved into longitudinal (tangential) and transversal (radial) components. In doing this, the pathlines of the spheres were assumed to be straight over the 0.30 m. distance at each point; the difference between the assumed and the actual pathline was negligible, Fig.(VI-1).

Contour lines of both components of shear stress around the bend, Figs.(VI-2) to (VI-5), were then constructed for the two curved channels (I and III) in terms of the dimensionless ratio of local shear at each point in the bend to the mean value over cross-section 1 (1.4 m. u/s the bend entrance) :

$$\tau_{o\theta\theta i}/\overline{\tau}_{o1} \qquad ; \qquad \tau_{or\theta i}/\overline{\tau}_{o1}$$

in which $\tau_{o\theta\theta i}$ is the longitudinal component $\tau_{o\theta}$ of shear at cross-section θ and at a point i (Σ i = 6 in Channel I and 4 in Channel III), $\tau_{or\theta i}$ is the radial component τ_{or} of shear at the same point i and cross-section θ , and $\overline{\tau}_{o1}$ is the average of τ_{o1i} values at cross-section 1.

Also plotted, in Figs.(VI-6) and (VI-7), are the transversal profiles of bed shear at several cross-sections around the bend.

<u>The experimental findings</u>

i) <u>Longitudinal shear stresses</u>. It is seen from Fig. (VI-2), corresponding to Channel I, $r_c/b = 3$, that high intensity of longitudinal shear occurs near the inner side between $\theta = 30^{\circ}$ and $\theta = 120^{\circ}$, after which it gradually shifts to predominate near the outer side with increasing intensity; it attains a maximum value at the outer side very near the bend exit and continues along this side for a distance nearly twice the channel width downstream of the bend exit. On the other hand, in Channel III, $r_c/b = 7.9$, which is of less relative curvature b/r_c, the maximum longitudinal shear

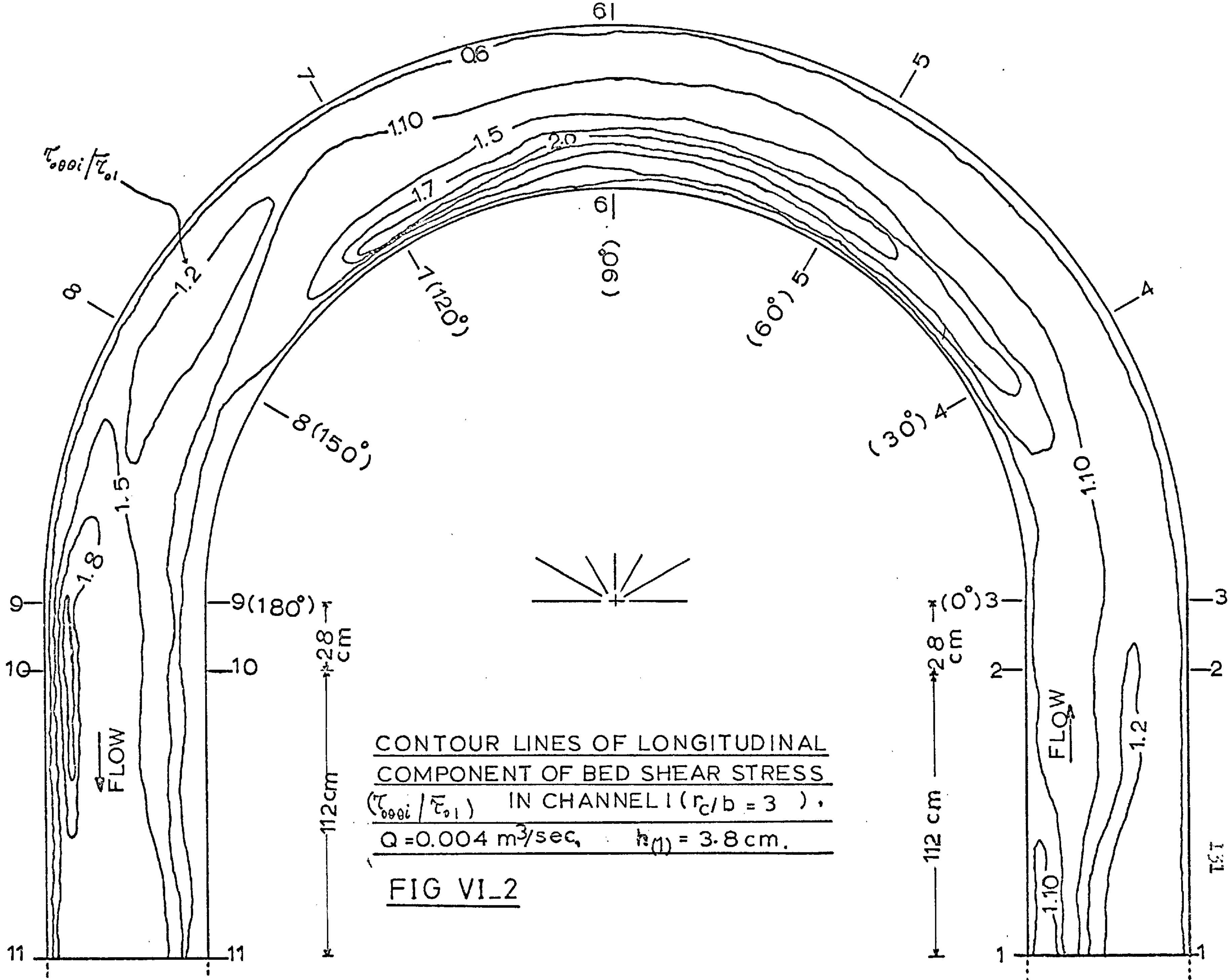

CONTOUR LINES OF LONGITUDINAL COMPONENT OF BED SHEAR STRESS ($\tau_{o\theta\theta i}/\tau_{o1}$) IN CHANNEL I ($r_c/b = 3$), $Q = 0.004\ m^3/sec$, $h_{(1)} = 3.8$ cm.

FIG VI_2

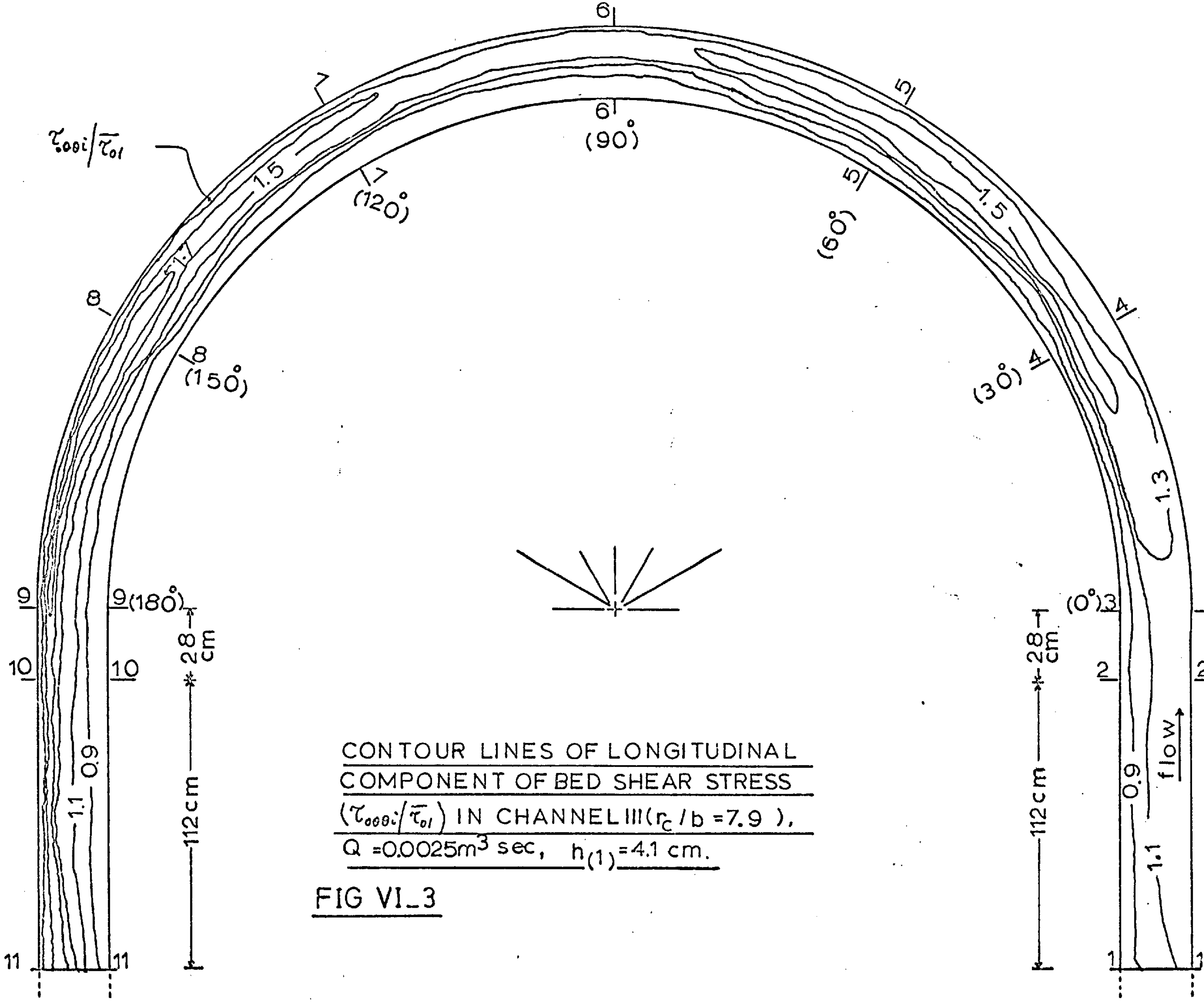

CONTOUR LINES OF LONGITUDINAL COMPONENT OF BED SHEAR STRESS $(\tau_{000i}/\overline{\tau}_{01})$ IN CHANNEL III (r_c/b = 7.9), Q = 0.0025 m^3 sec, $h_{(1)}$ = 4.1 cm.

FIG VI_3

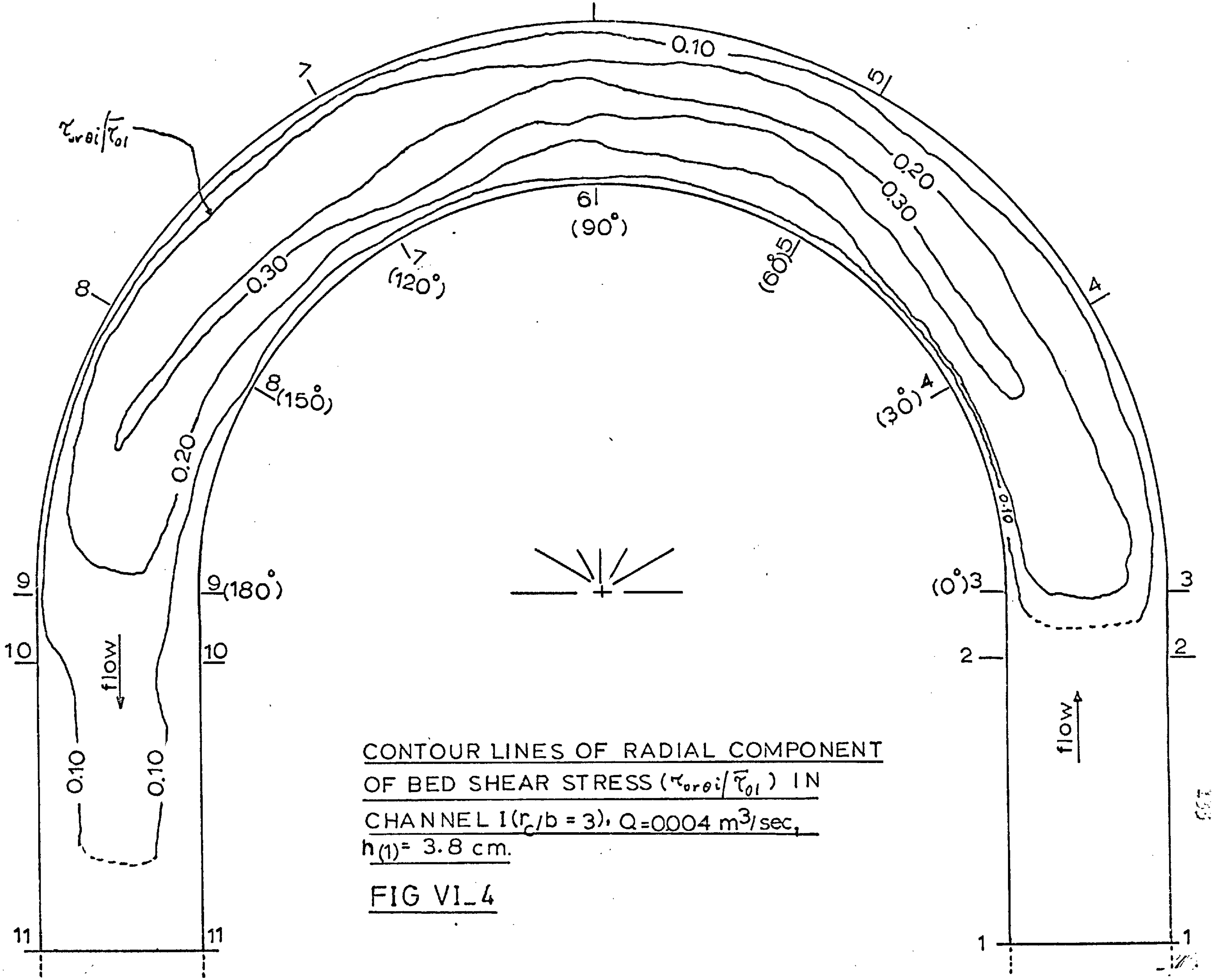

CONTOUR LINES OF RADIAL COMPONENT OF BED SHEAR STRESS ($\tau_{or\theta i}/\bar{\tau}_{01}$) IN CHANNEL I ($r_c/b = 3$), $Q = 0.004\ m^3/sec$, $h_{(1)} = 3.8$ cm.

FIG VI_4

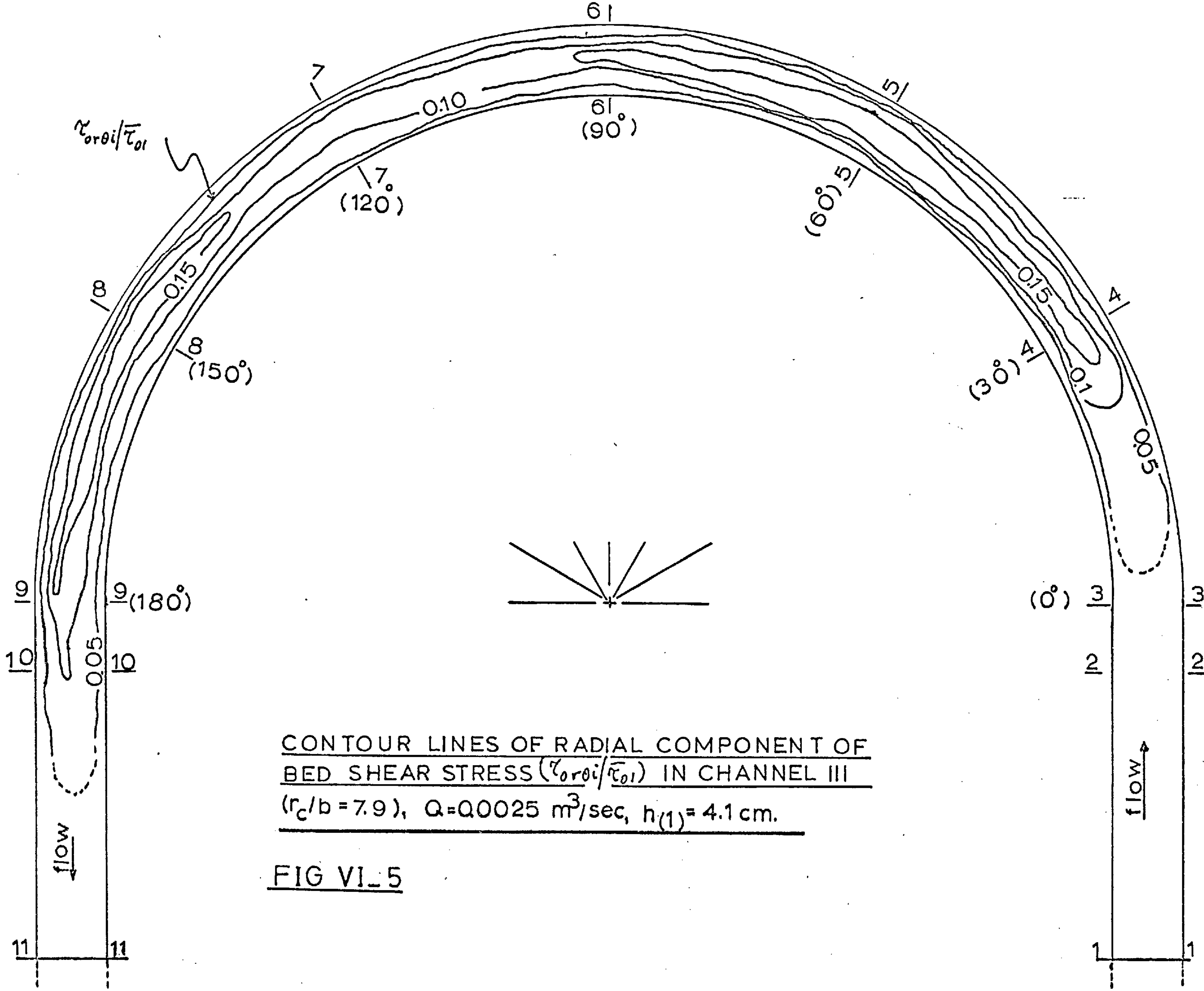

CONTOUR LINES OF RADIAL COMPONENT OF BED SHEAR STRESS ($\tau_{or\theta i}/\overline{\tau_{01}}$) IN CHANNEL III ($r_c/b = 7.9$), $Q = 0.0025\ m^3/sec$, $h_{(1)} = 4.1$ cm.

FIG VI-5

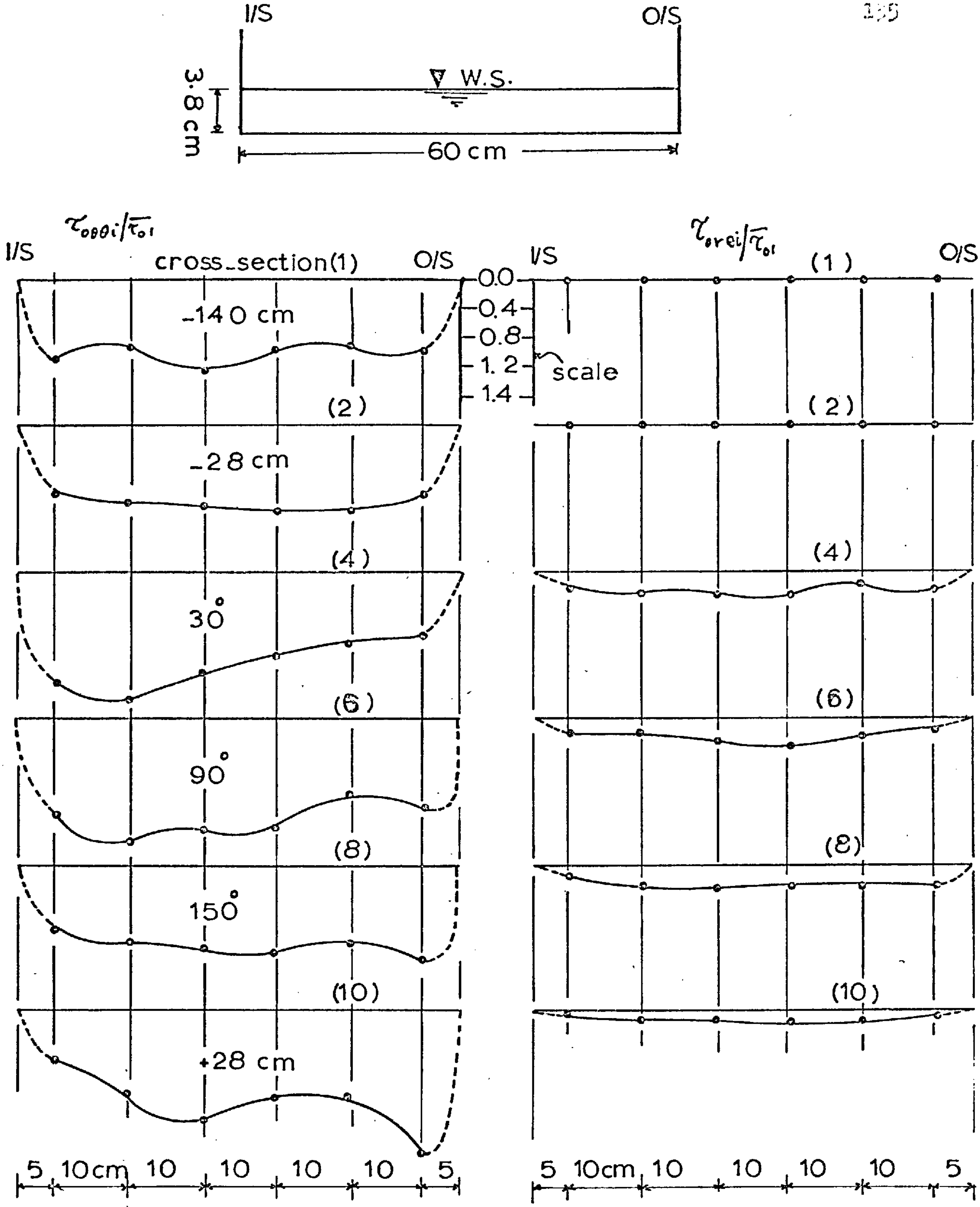

DISTRIBUTION OF BED SHEAR STRESS AT SEVERAL CROSS-SECTIONS IN CHANNEL I ($r_c/b = 3$), $Q = 0.004\ m^3/sec$, $h_{(1)} = 3.8$ cm.

FIG VI_6

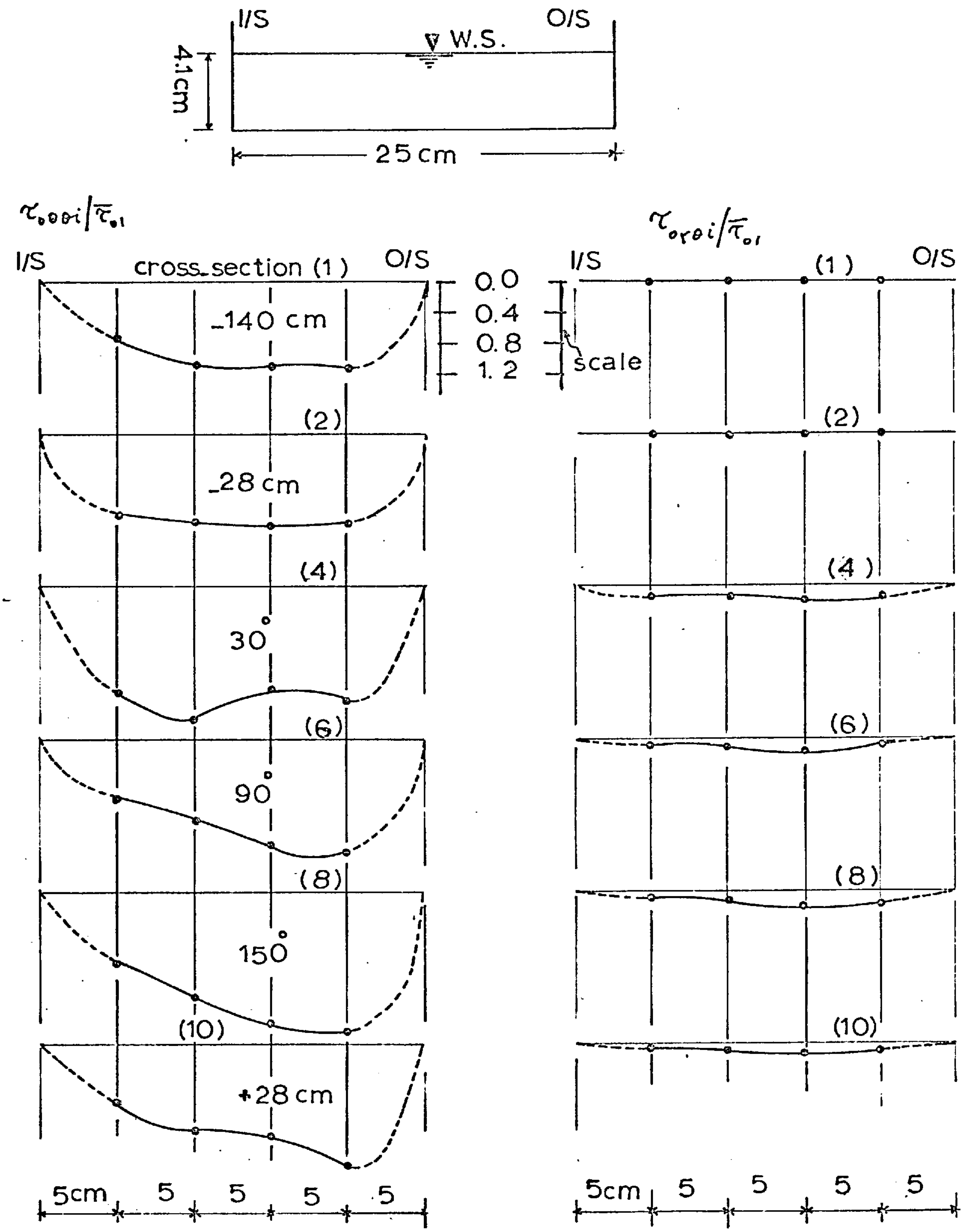

DISTRIBUTION OF BED SHEAR STRESS AT SEVERAL CROSS-SECTIONS IN CHANNEL III ($r_c/b = 7.9$),
$Q = 0.0025 m^3/sec$, $h_{(1)} = 4.1$ cm.

FIG VI-7

near the outer side, Fig.(VI-3), starts about θ = 120°.

At some points in the two channels, the local values of longitudinal shear stresses are seen to exceed the mean shear stress in the approach channels by as much as 100% :

In Channel I, $r_c/b = 3$:

at θ = 60° and at 15 cm. from i/s : $\tau_{o\theta} / \overline{\tau}_{o1} = 2.09$

at θ =180° and at 5 cm. from o/s : $\tau_{o\theta} / \overline{\tau}_{o1} = 1.96$

In Channel III, $r_c/b = 7.9$:

at θ = 30° and at 10 cm. from i/s : $\tau_{o\theta} / \overline{\tau}_{o1} = 1.75$

at θ =150° → 180° and at 5 cm. from o/s :

$$\tau_{o\theta} / \overline{\tau}_{o1} = 1.86$$

Ippen et al (1960), using a Preston tube for measuring the longitudinal components only of bed shear stress around a 60° curved trapezoidal channel of 60 cm. bottom width and 1.52 m. central radius of curvature (a relatively short bend θ = 60°), found that the maximum relative shear was 2.4, occurring near the outside downstream of the bend exit.

ii) Radial shear stress. From Figs.(VI-4) and (VI-5), it may be seen that the maximum intensity of radial shear at any cross-section occurs near the middle of its width. The local values of this component, relative to the mean longitudinal value at cross-section 1 ($\tau_{or\theta i} / \overline{\tau}_{o1}$), increases with increasing curvature.

In Channel I, $r_c/b = 3$
at $\theta = 90^\circ$ and at 36 cm. i/s : $\tau_{or}/\bar{\tau}_{o1} = 0.40$
In Channel III, $r_c/b = 0.19$
at $\theta = 60^\circ$ and at 15 cm. i/s : $\tau_{or}/\bar{\tau}_{o1} = 0.19$

Discussion and conclusions

From the present experiments, it can be seen that in channels of lower curvature, Channel III relative to Channel I, the regions of maximum relative longitudinal shear move in the upstream direction, and the magnitude of maximum relative shear decreases with decreasing curvature. The same effect is also revealed in the case of radial component of shear. On the other hand, by comparing Channel I, b/r_c=0.33, θ=180°, with that of Ippen et al (1960), which was of very close value of relative curvature (b/r_c=0.39) but of shorter curve (θ=60°), it can also be seen that for shorter bends of the same curvature, the maximum relative shear near the outside moves downstream of the bend exit.

It can be concluded from the present study that :

1) Shorter bends (small θ) of higher curvatures (big b/r_c) increase the difference between the maximum longitudinal component of shear in the bend or downstream of its exit, and the mean value of shear in the straight approach channel; these bends cause the former component to move downstream of the bend. They also increase the difference between local values in the

same cross-section. The maximum local value of shear stress in the bend may be double the mean value in the straight channel. Sharper bends also cause the increase of magnitude of the maximum relative radial shear component in the bend, occurring at the mid-width, and cause it to move ~~upstream~~ downstream.

2) The locations of high longitudinal shear stress are associated with the course of the filament of high velocity (Chapter IV).

CHAPTER VII

FLOW AROUND CURVED CHANNELS WITH ERODIBLE BEDS

The movement of bed load in channels and rivers is governed by many factors, the relative effects of which differ in every case. The geometry of river boundaries and the bed load movement at a bend and downstream of it, as distinct from straight flow, are dependent on the secondary currents due to stream curvature. In some regions, the bed configuration is much influenced by these secondary rather than the main currents of the stream, and in some extreme cases the irrigation or navigation purposes of the river may be seriously affected.

The following study is mainly directed to finding the effects of secondary currents in the bend on the configuration of the loose bed, and to locating the regions of high scour and deposition.

The experimental procedure

Due to the relatively small discharges in the experiments, an artificial plastic sand (Bakelite) of specific gravity about (1.3) was used. This sand was soaked in water before being spread over the channel bed.

Experiments were carried out in Channel I ($r_c/b = 3$, $b = 0.61$ m.), and in Channel III ($r_c/b = 7.9$, $b = 0.255$ m.) The average thickness of the sand layers over the bed of Channel I was about 3.85 cm., and that of Channel III was about 5 cm. The sand layers in both channels were levelled to an accuracy of about 2.5 mm. (this was checked by drawing contour lines of the sand layer before the commencement of the experiments). These layers extended from about 0.6 m. upstream of the bend entrance to 1.80 m. downstream of the bend exit. A smooth entry and exit for the sand layers was maintained by fitting a wooden piece, shaped to a quadrant of an ellipse, at each end, and the regions in the immediate vicinity to these were filled with natural sand in order to reduce scour due to possible local disturbances. It was found that the omission of these precautions at both ends caused great scour of the sand layer, particularly at the downstream end; this scour proceeded upstream and seriously affected the bed form throughout the bend in a very short time.

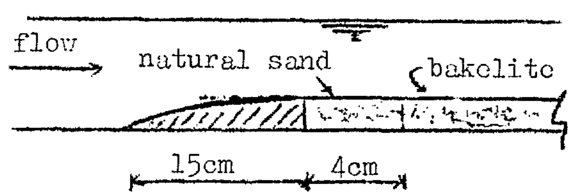

To reduce sudden scour over the sand layers due to any sudden acceleration of the flow at its commencement, the two end tanks were filled with water before the runs were started, and the flow was then gradually increased to the experimental value.

To establish the recurrence of the bed configuration under the same flow conditions, the experiment was repeated once in Channel I and three times in Channel III. Photographs were taken of the regions where considerable changes in bed form developed, and contour lines were constructed after one experiment in Channel I.

The experimental conditions of the runs in the two channels were as follows :-

<u>Channel I</u>

$Q = 4.63 \times 10^{-3}\ m^3/sec.$

depth of water over the sand layer at $\theta = 30^\circ$: $h = \cancel{2.75}\ 4.60$ cm.

corresponding mean velocity at $\theta = 30^\circ$: $\bar{v}_\theta = 0.166$ m/sec

corresponding hydraulic radius (m) : m = 3.95 cm.

average temperature : $T = 18.6^\circ$ C.

Reynolds number at cross-section $\theta = 30^\circ$ $Re = \dfrac{\bar{v}\,.\,m}{\nu} = 6280$

sand thickness : 3.85 cm.

time for experiments : 2 hr. 40 min.

<u>Channel III</u>

$Q = 3.05 \times 10^{-3}\ m^3/sec.$

depth of water over the sand layer at $\theta = 30^\circ$: $h = 3.65$ cm.

corresponding mean velocity at $\theta = 30^{\circ}$: $\bar{v}_{\theta} = 0.33$ m/sec

corresponding hydraulic radius (m) : m = 0.10

average temperature : T = 17.8° C

Reynolds number at cross-section $\theta = 30^{\circ}$ $Re = \dfrac{\bar{v}\ .m}{\nu} = 7830$

sand thickness : ~~2 in.~~ 5 cm.

time for experiments : 2 hr.

The experimental findings

Despite minor differences, the bed forms of repeated experiments have the following common features :-

i) Channel I :- See Figs.(VII-1-i),(VII-1),(VII-2) and Plates (VII-1) and (VII-3)

1. A classical type of rippled bed, as usually found

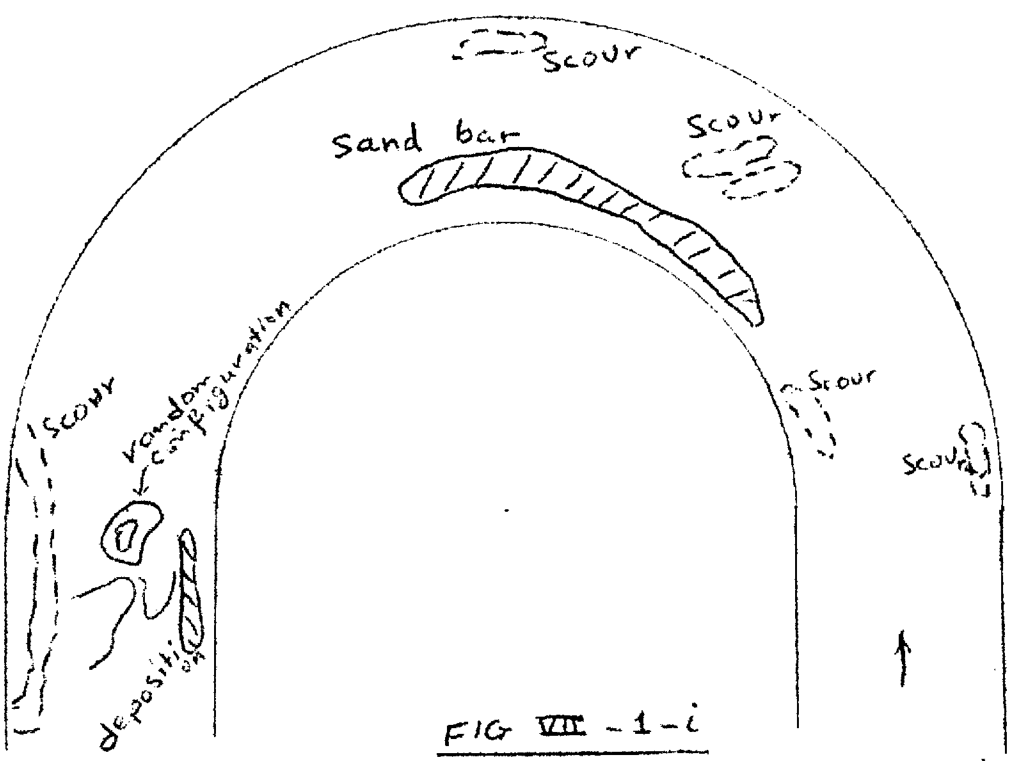

FIG VII - 1 - i

Channel I

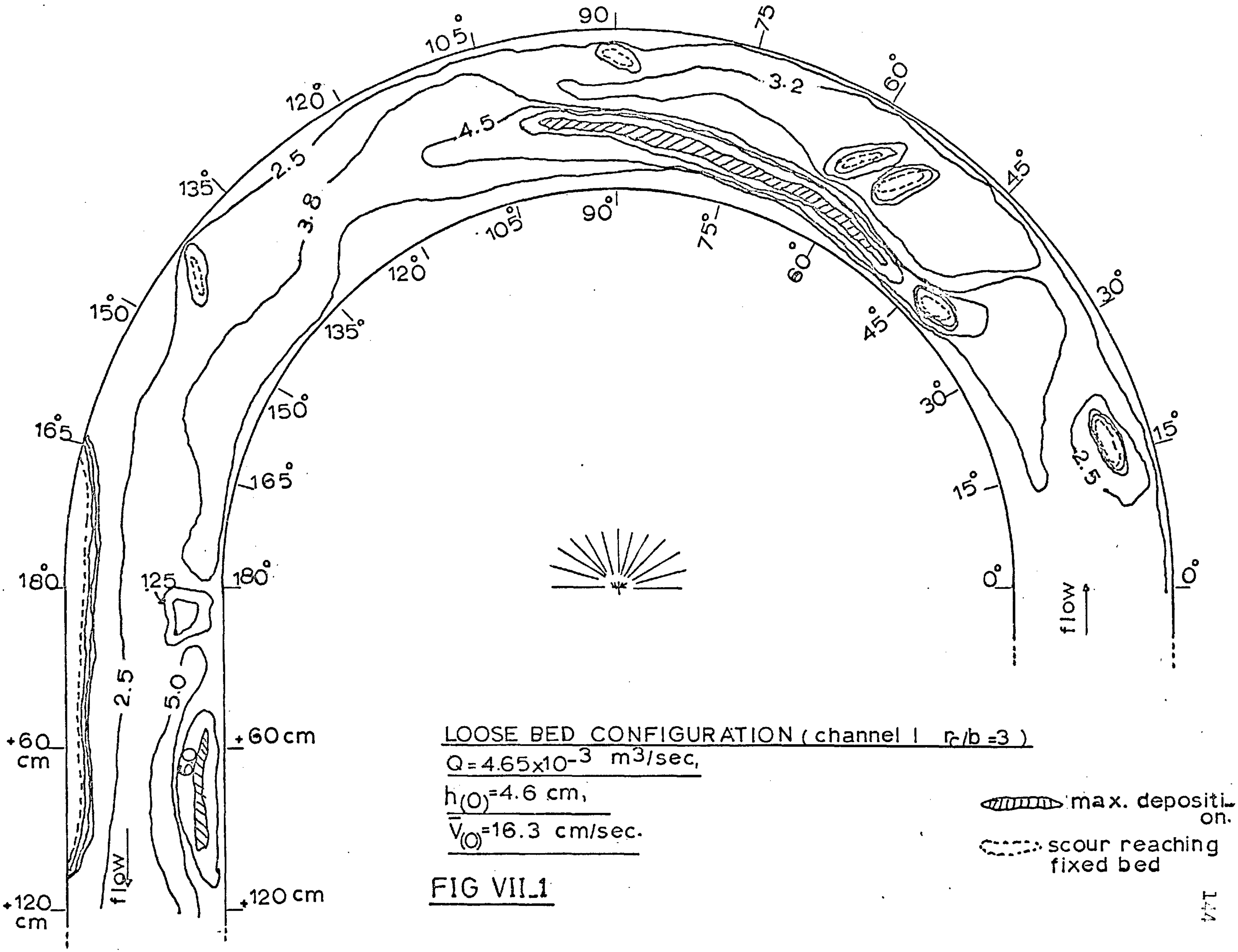

LOOSE BED CONFIGURATION (channel I $r_c/b = 3$)

$Q = 4.65 \times 10^{-3}$ m^3/sec,

$h_{(0)} = 4.6$ cm,

$\bar{V}_{(0)} = 16.3$ cm/sec.

FIG VII_1

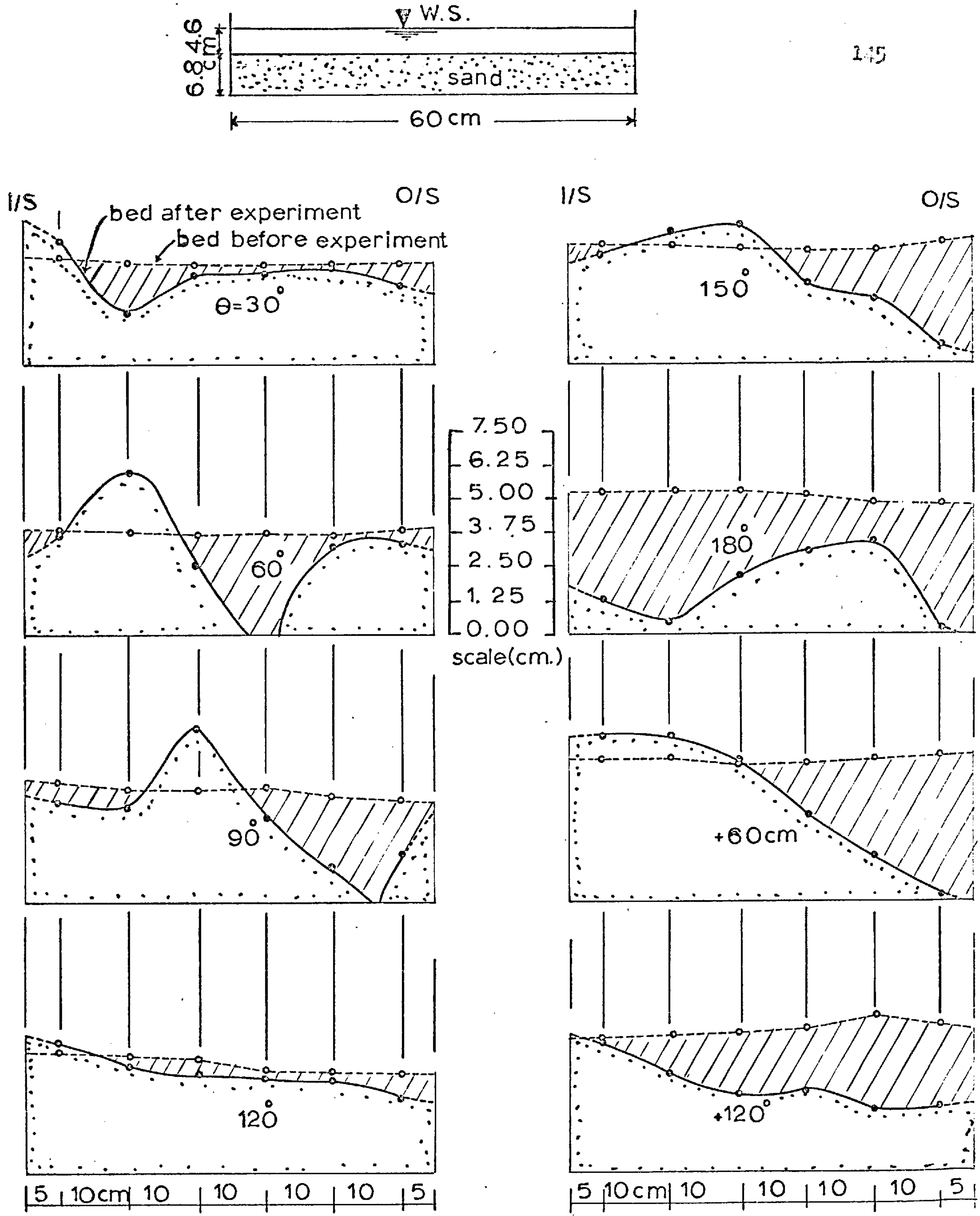

FIG VII_2 TRANSVERSE BED PROFILES (channel I $r_c/b=3$)

$Q = 4.65 \times 10^{-3}$ m³/sec; $h_{(0)} = 4.6$ cm; $\bar{V}_{(0)} = 16.3$ cm/sec.

PLATE (VII-1)

Loose bed configuration channel I ($r_c/b=3$)

Q 465 x 10^{-3} m^3/sec,
h_o=4.6 cm; v_o=16.3 cm/sec

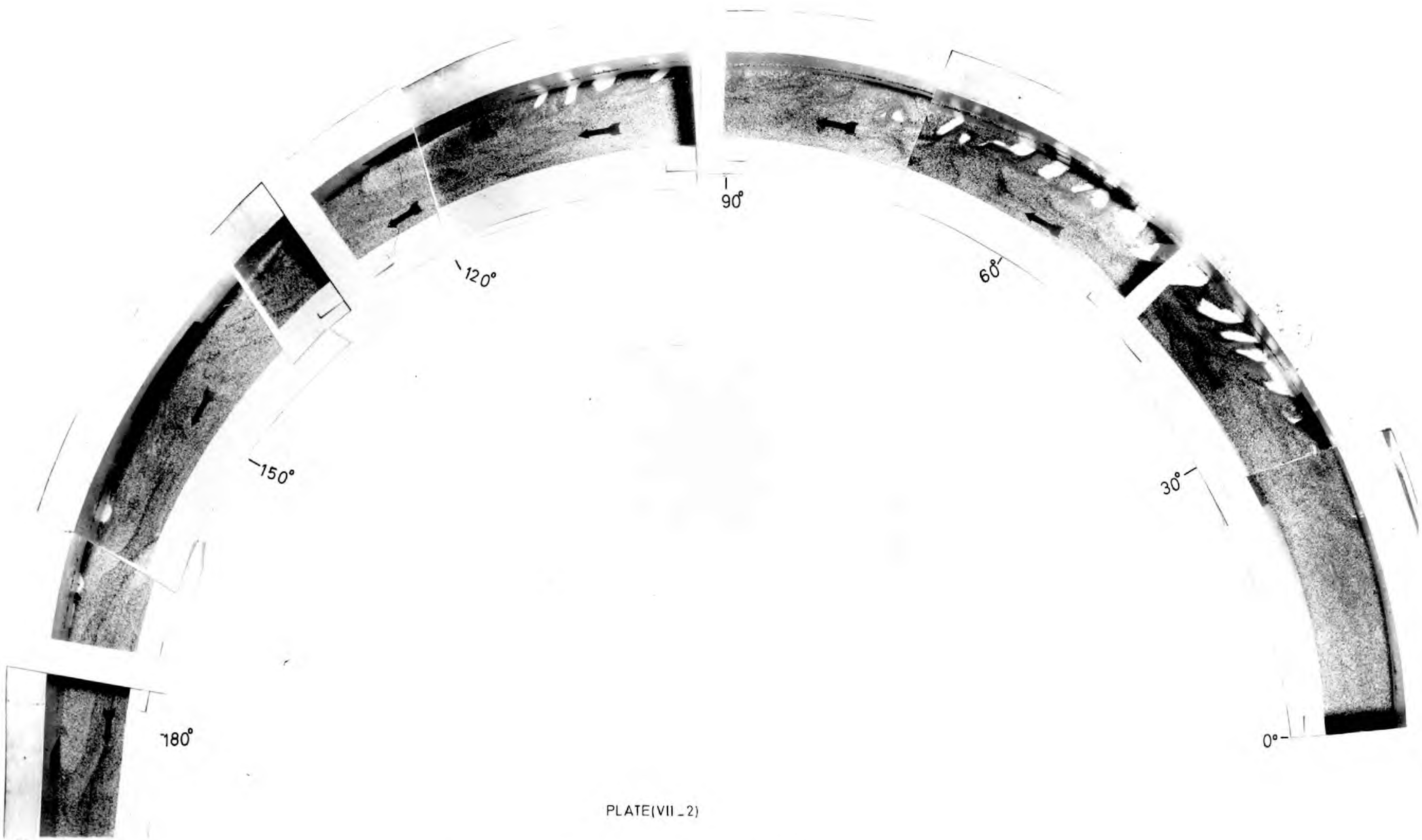

PLATE(VII_2)

LOOSE BED CONFIGURATION (channel III $r_c/b=7.9$)

$Q=2.9\times10^{-3}$ $m^3/sec.$ $d_0=3.82$ cm. $v_0=31.6$ cm/sec.

in straight broad channel flow, occured in the region $\theta = 0^\circ$ and $\theta = 45^\circ$. In addition to this, however, a deep hollow was observed near the inner-side at $\theta = 30^\circ$.

2. Deep isolated hollows, reaching down to the fixed bed and directed inward at an angle from the circumferential direction, were observed at the centreline of cross-section $\theta = 60^\circ$.

3. A high sand bar near the inner-side, starting from $\theta = 45^\circ$ and continuing downstream to about $\theta = 105^\circ$.

4. Random distinct local scour and deposition over the region $\theta = 135^\circ \rightarrow 150^\circ$.

5. A long ditch reaching down to the fixed bed very near the outer-side, starting from the bend exit and continuing downstream over a distance of about double the channel width.

6. Random scour and deposition, as in 4, but more intense, covering the region downstream of the bend exit.

ii) Channel III :- See Plate (VII-2)

1. Scour down to the fixed bed appeared near the outside, starting from $\theta = 45^\circ$ and continuing to about double the channel width downstream of the bend exit.

2. A high sand bar developed near the inner-side between $\theta = 30^\circ$ and $\theta = 180^\circ$.

3. Small irregularities downstream of the bend exit.

θ = 45° → 65°

170° → +1.5 ft. (46 cm)

150° → 180°

180° → +2.5 ft (75 cm)

LOOSEBED CONFIGURATION (channel I $r_c/b = 3$)

$Q = 4.65 \times 10^{-3}$ m³/sec. $d_0 = 4.6$ cm. $v_0 = 16.3$ cm/sec.

PLATE (VII_3)

Discussion and conclusions

The experimental observations can be analysed in the following :-

A. In the transitional region from straight to curved flow $\theta = 0^\circ \rightarrow 20^\circ$, the main (tangential) flow has the predominant effect, and the bed form is similar to that in straight channel flow.

B. The intense longitudinal scour near the outer-side occurs at regions of high gradients of longitudinal velocities. These regions move in the upstream direction for longer bends or bends of milder curvature (starting at $\theta = 180^\circ$ in Channel I, $\theta = 45^\circ$ in Channel III).

C. The sand bar near the inner-side, being a result of deposition of sediments coming from upstream under the effect of helical motion, occurs at regions of low gradients of longitudinal velocities. These regions also move upstream for longer bends of milder curvature (starting at $\theta = \cancel{45^\circ}\ 30^\circ$ in Channel III and $\theta = \cancel{50^\circ}\ 45^\circ$ in Channel I).

D. The deep individual hollows near the middle of the channel width are the results of high intensity of radial shear stress in the bend, (Chapter VI).

E. The random bed form at the bend exit is due to the alteration in flow pattern in this transitional region, where currents change again from curved to straight channel flow.

From the above discussion, the following conclusions can be drawn :-

(1) The region under the most serious effect of stream curvature is that near the outer-side of the bend, where intense scour exists.

(2) In bends of high curvature (Channel I, $b/r_c = 0.33$), the region mentioned in (1) lies in the straight section of the channel downstream of the bend and starts just at the bend exit; it moves upstream into the bend when the curvature decreases (Channel III, $b/r_c = 0.126$).

(3) The development of a sand bar near the inner-side of a channel bend is the result of deposition in this region of low velocities of sediments carried from upstream under the effect of helical motion.

(4) The bed configuration, as found by experiments, can be analysed on the basis of velocity or shear distribution around the bend (Chapters IV and VI).

CONCLUSIONS AND SUGGESTIONS FOR FURTHER RESEARCH

1) In a stream curved in plan, the maximum tangential velocity in any cross-section does not occur at the water surface. In the downstream half of a bend, the maximum tangential velocity occurs far below the water surface. This is attributable to the effect of secondary currents and is confirmed in both laminar and turbulent flow states.

2) The maximum tangential velocity of any cross-section and for any depth in a curved turbulent flow occurs near the inner side at the early region of the bend, and gradually shifts towards the outer side (crossing the centreline at locations depending on the channel curvature) as a result of momentum exchange. In the range of channel curvature studied ($0.127 \leqslant b/r_c \leqslant 0.333$), the maximum forward (tangential) velocity was found to be very close to the outer side at the bend exit and persisted at such maximum value (which even increases with higher curvature) for a distance between 1 - 3 times the channel width downstream from the bend exit, depending on the curvature of the bend.

In the laminar flow state, however, the shift of high forward velocity towards the outer side occurs even in the very early region of the bend ($\theta = 30^{\circ}$). This is attributable to the stronger relative secondary currents ($\frac{v_{rz}}{v_\theta}$) compared with those in turbulent flow. Following around the bend, this maximum velocity keeps near the outer side, becoming steadily larger.

3) Flow around channel bends, although of a three-dimensional nature, is amenable to an approximate numerical solution by a method of finite differences. The effect of the approximations and simplifying assumptions on the accuracy of the results, as compared with the measured values, depends primarily on the degree of channel curvature b/r_c and on the aspect ratio b/h of the flow. When $r_c/b \gg b/h \gg 1$, a good deal of accuracy of numerical solution based on a two-dimensional flow analysis can be obtained. In the regions of the side walls of a wide stream, however, this method fails to give satisfactory results, and greater accuracy can be obtained only if the size of the grid network is decreased in these regions.

4) Radial profiles of water surface around the bend have a rather peculiar shape when the flow velocity is very low, and do not conform to any simple formula of velocity distribution across the channel width; a depression of the water surface at the centreline in these cases was consistently observed and can be attributed to the existence of maximum velocity at the middle of the cross-

section.

5) Longitudinal water surface profiles exhibit a consistent rise of water surface before the bend entry. As all the flow conditions studied were in the sub-critical state ($F = \frac{v}{\sqrt{gd}} \ll 1$), (i.e., slow flow), it is expected that the existence of the bend inflicts a back-water effect on the flow in the straight approach channel upstream of the bend. Increasing the flow velocity decreases this rise in water surface.

6) The bed angles α_o (representing the strength of secondary flow) were found to increase with increasing curvature b/r_c, or when the aspect ratio b/h decreases. Observations in Channel I (a wide channel) showed a reversed deviation of α_o (i.e., outward) in the region near the inner side. A possible cause of this could be changes in flow temperature (and so, density) across this wide channel. Photographs of the secondary currents in two cross-sections ($\theta = 30^o$ and 150^o) in both Channels I and III showed complicated patterns of spiral motions. It is reasonable, therefore, to expect a multi-cell spiral motion around bends of wide rivers and natural streams; in these cases, differences in concentrations of suspended sediments across the river, and irregularities in its boundaries, contribute to the breakdown of a theoretical single spiral over the

cross-section.

7) Flow angles in the remainder of the stream showed similar trends as those of α_o as regards the effect of channel curvature and aspect ratios. The existence of a small reversed vortex at the top corner near the outer side (as originally revealed by Einstein and Harder) was also detected.

Future extensive measurements of flow angles over many points in the cross-section may help towards a better understanding of the nature of the spiral motion.

Photographs taken of the same flows and locations but at different times showed some difference in the distribution of spirals over the cross-section. Although the number of photographs taken at the same place was limited to two, this recalls the suggestion that spiral motion around bends is never steady but changes slightly with time. Further study in this field seems desirable.

8) Longitudinal components of bed shear stress ($\tau_{o\theta}$) around the bend conformed with the distribution of forward velocity, and radial components of bed shear stress (τ_{or}) conformed with the distribution of bed angles, out of which the radial velocity component can be measured. $(\tau_{o\theta})_{max}$ was always found near the outer side at the bend exit. In higher curvatures it even moves downstream

of the bend exit. $(\tau_{or})_{max}$ was always found near the centreline of the channel in the region $\theta = 30^\circ \rightarrow 120^\circ$. In ~~higher~~ milder curvatures, the region of $(\tau_{or})_{max}$ concentrates in a shorter region, starting from $\theta = 30^\circ$.

9) Studies on flows over loose beds in Channels I and III confirmed the results obtained from bed shear and velocity measurements. In all the cases investigated, the region under the maximum longitudinal scour was found near the outer side at the bend exit. In addition to this, Channel III, which had a smaller curvature, scoured near the outer side in the upstream half of the bend. This also conformed to velocity measurements in this channel.

Radial scour was detected in Channel I at the centreline of the region $\theta = 45^\circ \rightarrow 60^\circ$, and this was ascribed to the effect of radial shear stress, which has maximum intensity in this region.

The development of a sand bar near the inner side of the two channels (I and III) was also detected. Its cause is ascribed to the helical motion which carries bed sediments from upstream towards the inner side of the bend. After a long period of time, this sand bar of deposited sediments emerges above the water surface, and this is possibly the cause of river braiding and the development of river islands.

APPENDIX A

RESISTANCE TO FLOW IN CURVED CHANNELS

In curved channels it is usually found that there are additional energy losses above those in straight channel flows. The following phenomena might be concerned in developing these additional losses :-

1) Distortion in velocity distribution in all three dimensions of the flow and the resulting alteration in shear stress distribution;

2) Secondary currents in the bend, causing an increased momentum exchange;

3) Possible separation of the flow from the curved walls and consequent development of eddy zones.

The proportional contribution of each of these causes depends upon the flow conditions and channel geometry.

However, in a bend situated between two long straight approaches, the additional energy loss due to the local deceleration and acceleration of the curved flow probably extends over a relatively short stretch of the channel, including the bend and parts of the straight approaches, beyond which the energy line has its otherwise uniform slope. In other words, the local additional energy losses inherent to curved flow are always accompanied by fewer energy losses upstream or downstream of the bend; thus the average energy loss over the whole stretch is the same as that in a straight part of the channel.

In all flow states, the curved section of the channel acts as an obstacle (Chow, 1959), causing the flow first to decelerate and then to accelerate. In subcritical flow $(h > h_c)$, the deceleration imposes a backwater effect similar to that of a dam (M1 curve), on the upstream side (this has been measured and discussed in Chapter V); the rise of water surface towards the bend entrance requires, from the specific energy curve Fig.(A-1), a corresponding rise in the specific energy line. It is this rise in the specific

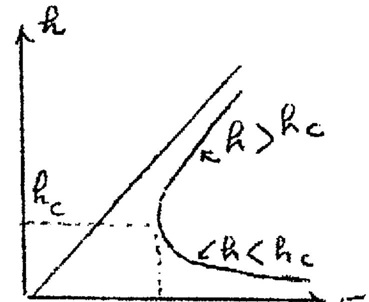

FIG(A-1)

content at the bend entrance which is dissipated in the bend and at some distance downstream of it, through acceleration of the flow, thereby bringing the flow depth to its uniform value and the energy gradient back to its uniform slope. In super-critical flow $(d < d_c)$ the decelerated water due to the bend can only be found downstream of the bend entrance, i.e., within the bend; from Fig.(A-1), a rise in water surface requires, in this case, a corresponding drop in energy line after which the flow is accelerated back, bringing the energy gradient to its uniform slope. If the decelerating flow should cause the water surface to rise up higher than the critical depth, a hydraulic jump will occur, after which the flow will behave as in the first case (subcritical flow).

Friction coefficient for curved open channel flow

It is not only because curved open channel flow is principally non-uniform, but also owing to the existing secondary currents, that the friction factor C_f in bends (defined in the same way as in flow over a flat plate, i.e., $C_f = \tau_o / \rho \frac{\bar{v}^2}{2}$ or alternatively as $C_f = \frac{2g\ ms}{\bar{v}^2}$) is a function of several additional parameters. In addition to those in uniform straight channels, where $C_f = \phi(Re, k/\ell, \ell/b)$, one can add, in the 180° semicircular bend, r_c/b and $\frac{\theta}{180}$, so that :

$$C_{f(bend)} = \phi_1(Re,\ k/\ell,\ \ell/b,\ r_c/b,\ \theta/180) \qquad (A-1)$$

in which ϕ_1 is a function to be determined, $Re = \frac{\bar{v}.m}{\nu}$ is Reynolds number, k/ℓ is relative roughness, ℓ/b is the inverse of aspect ratio of the cross-section, r_c/b is the inverse of degree of curvature, and $\frac{\theta}{180}$ describes the cross-section concerned in the bend.

Experiments have, therefore, been carried out in the three channel bends (Channels I,II and III) to define the function given in Eq.(A-1). The middle section of the bend, $\theta = 90°$, was considered in this investigation. The depth of water was kept very close to 2.5 cm. in the three curved channels so that a relation between C_f and R_e (for small ℓ/b in the three channels) was of the form

$$C_f = \phi_2(R_e\ ,\ r_c/b) \qquad (A-2)$$

A comparison was made between the obtained results of $C_f - R_e$ (using a digital computer with a programme shown in Appendix B) with r_c/b as a parameter, and those obtained in a long straight smooth channel 30 cm. wide and about 10 m. long by Memon (1967). To detect the effect of the parameter ℓ/b, some of the results obtained by Allen and Ullah (1967), in a very deep channel ℓ = 10 cm. and b = 2.5 cm., are also quoted. To calculate the slope of the energy line at $\theta = 90^\circ$, the heads at two sections $\theta = 60^\circ$ and $\theta = 120^\circ$ were measured, so that S is very approximately given by

$$S = \frac{H_{60^\circ} - H_{120^\circ}}{\ell\,(60^\circ - 120^\circ)}$$

All depth measurements were read through the static pressure tapping points at the bed and referred to a still water level (see Chapter III), and the difference in bed level (equal to 0.25 mm.), between sections $\theta = 60^\circ$ and $\theta = 120^\circ$, was also taken into consideration. The energy gradient in the straight channel (Memon, 1967) was taken as the slope of the channel bed, as uniform flow was established there.

In laminar flow in straight broad rectangular channels, C_f is a function only of R_e. Its value was derived by Allen and Ullah (1967), as :

$$C_f = 6/R_e \qquad \text{(A-3)}$$

This equation, together with the experimental results for the bends, was plotted in Fig.(A-2), and the following conclusions can be drawn :-

1) It is certain that C_f in curved laminar flow is higher than that in straight flow, whatever the aspect ratio of the flow.

2) The transition from laminar to turbulent flow is less marked in curved than in straight flow. This was also observed by Eustic (1911) for flow in curved pipes.

3) No conclusive results can as yet be drawn in regard to the turbulent flow region due to the limited number of measurements, with maximum experimented Re about 3000.

The total head loss (ΔH) over the whole length of the curve was calculated for different Reynolds numbers from measurements at the bend entrance and exit in Channel II (r_c/b = 6.5). This result was compared with that in straight channels (Memon, 1967) of the same length and width. The only difference between the two cases was that the depth of the straight channel was much less than that of the curved channel: in the straight channel ℓ/b was between 0.016 and 0.151, whereas in the curved one it was very close to 0.100.

The results are plotted in Fig.(A-3) as (head loss x ℓ/b) vs. R_e. Also plotted in Fig.(A-3), the ratio of head loss

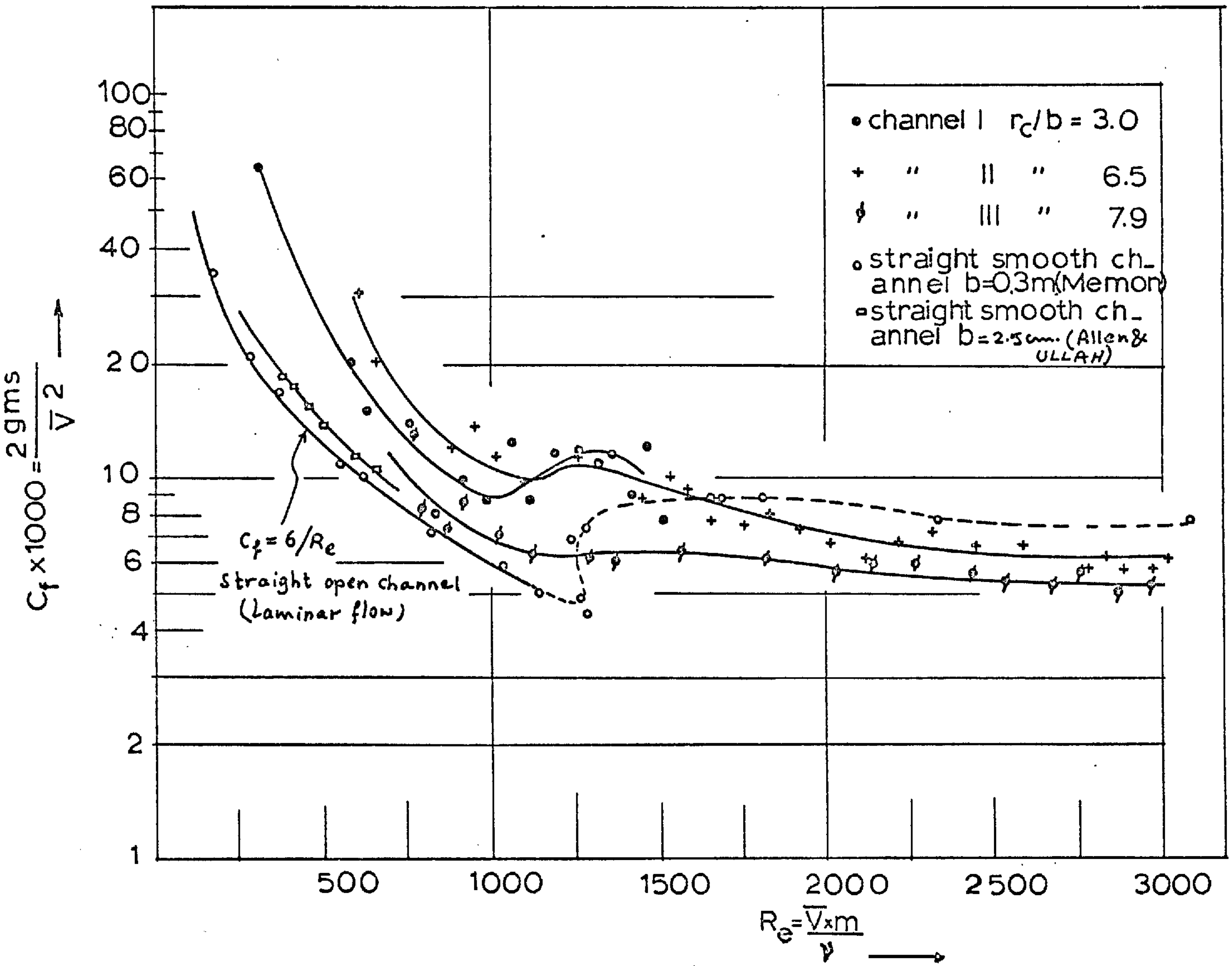

FIG A_2 FRICTION FACTOR IN CURVED OPEN CHANNEL FLOW

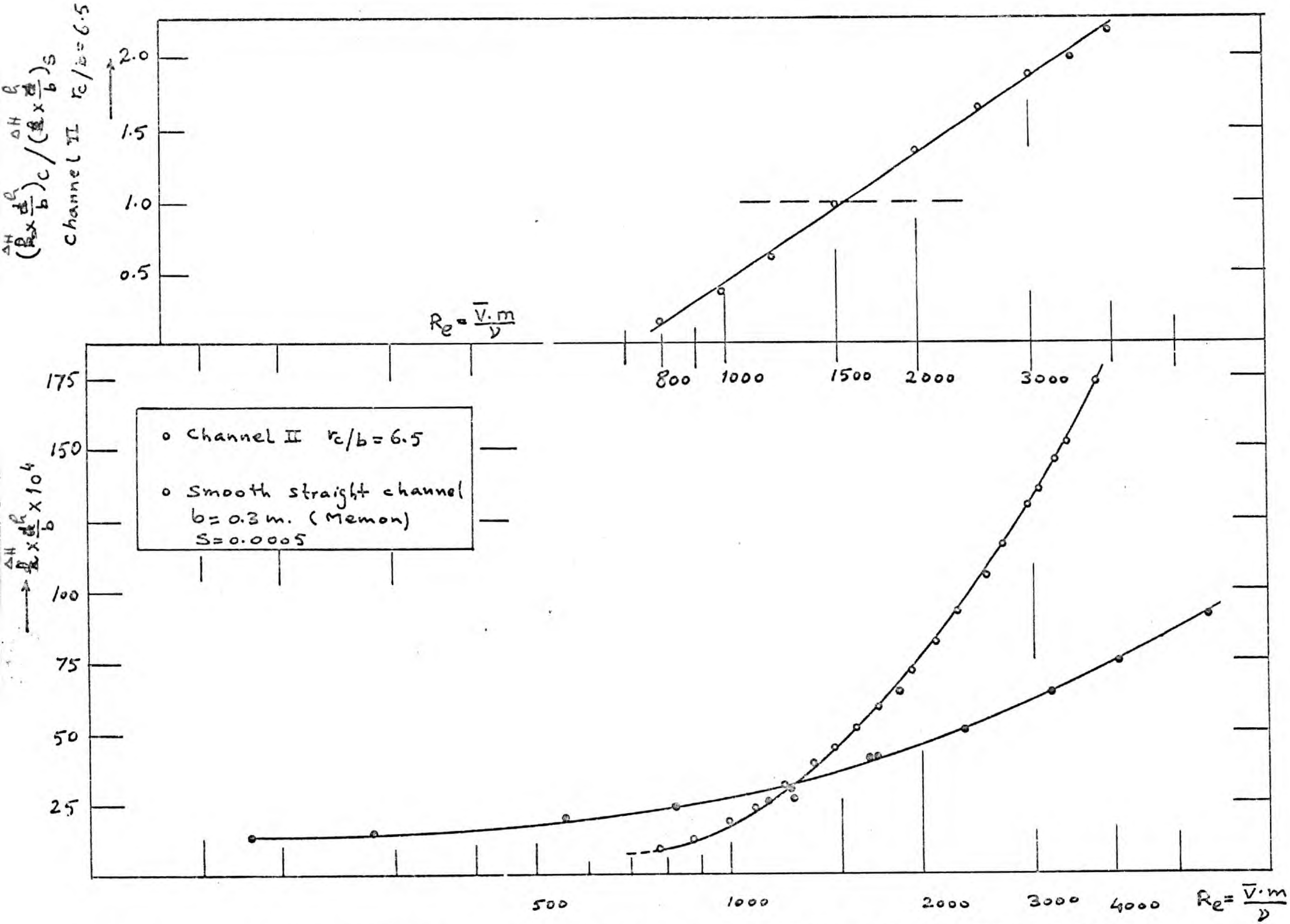

FIG A_3 COMPARISON BETWEEN HEAD LOSSES IN CURVED AND STRAIGHT CHANNELS OF EQUAL LENGTHS along a curved channel to that in a straight channel vs. R_e.

It can be concluded, from the last figure, that the aspect ratio has considerable effect on the total loss in low speed flows of shallow depths; also that the ratio of bend to straight flow losses increases almost linearly with Reynolds number.

APPENDIX B

COMPUTER PROGRAMMES

Notations used in the programmes *
(v_θ distribution)

Experimental notations		Computer notations
Z, r, θ	....	K, I, M
v_θ	....	C
r	....	R
v_r	....	CR
v_z	....	CZ
$v_{\theta m}$	....	F/5
v_{r2}	....	CRG
v_{r1}	....	CRF
v_{z2}	....	CZU
v_{z1}	....	CZD
v_{z1}	....	$\frac{CZU + CZD}{2}$
$\frac{\Delta v_\theta}{\Delta r}$	....	$\frac{CX}{B}$
$\frac{\Delta v_\theta}{\Delta z}$	....	$\frac{CY}{H}$
$\frac{\Delta v_\theta}{r \Delta \theta}$	....	$\frac{CV}{r\Delta\theta}$

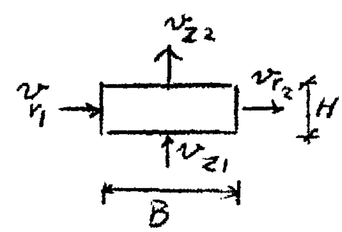

* when solving for Channel III, I = 7

```
      PROGRAM TO FIND VELOCITY DISTRIBUTION IN CURVED CHANNEL FLOW
      DIMENSION C(7,15,13),R(15),CR(7,15,13),CZ(7,15,13),B(16),F(15),CRA
     1,F(15),CRA(7,15,13),CZA(7,15,13),CX(7,15,13),CY(7,15,13),H(6),CRF(
     37,15,13),CRG(7,15,13),CZU(7,15,13),CZD(7,15,13)
RF(   DO 3 K=2,6
      READ (5,2) (C(K,I,1),I=2,14)
    2 FORMAT (13F5.2)
    3 CONTINUE
      READ (5,4) (R(I),I=2,14)
    4 FORMAT (13F5.1)
      DO 5 K=2,6
      DO 6 I=2,14
      CR(K,I,1)=0.0
      CZ(K,I,1)=0.0
    6 CONTINUE
    5 CONTINUE
      DO 50 I=3,13
      B(I)=2.0
   50 CONTINUE
      DO 28 K=3,5
      H(K)=0.5
   28 CONTINUE
      H(2)=0.75
      H(6)=0.75
      B(2)=1.0
      B(14)=1.0
      DO 80 M=2,13
      DO 10 I=2,14
      F(I)=C(2,I,M-1)
      DO 11 K=3,6
      F(I)=F(I)+C(K,I,M-1)
   11 CONTINUE
   10 CONTINUE
      DO 31 I=2,14
      CR(2,I,M)=12.0*(-0.191*F(I)/R(I)+20.5*F(I)/R(I)**3)
      IF(I.EQ.2.OR.I.EQ.14)CR(2,I,M)=0.33*CR(2,I,M)
      IF(I.EQ.3.OR.I.EQ.13)CR(2,I,M)=0.66*CR(2,I,M)
      CR(3,I,M)=12.0*(-0.080*F(I)/R(I)-43.2*F(I)/R(I)**3)
      IF(I.EQ.2.OR.I.EQ.14)CR(3,I,M)=0.33*CR(3,I,M)
      IF(I.EQ.3.OR.I.EQ.13)CR(3,I,M)=0.66*CR(3,I,M)
      CR(4,I,M)=0*(0.016*F(I)/R(I)-64.8*F(I)/R(I)**3)
      IF(I.EQ2.OR.I.EQ.14)CR(4,I,M)=o.33*CR(4,I,M)
      IF(I,EQ.3.OR.I.EQ.13)CR(4,I,M)=0.66*CR(4,I,M)
      CR(5,I,M)=12.0*(0.094*F(I)/R(I)-50.4*F(I)/R(I)**3)
      IF(I.EQ.2.OR.I.EQ.14)CR(5,I,M)=0.33*CR(5,I,M)
      IF(I.EQ.3.OR.I.EQ.13)CR(5,I,M)=0.66*CR(5,I,M)
      CR(6,I,M)=12.0*(0.173*F(I)/R(I)+14.4*F(I)/R**3)
      IF(I.EQ)2.OR.I.EQ.14)CR(6,I,M)=0.33*CR(6,I,M)
      IF(I.EQ.3.OR.I.EQ.13)CR(6,I,M)=0.66*CR(6,I,M)
```

```
      IF(I.EQ.3.OR.I.EQ.13)CR(6,I,M)=0.66*CR(6,I,M)
   31 CONTINUE
      DO 34 I=2,14
      CZ(1,I,M)=0.0
      CZ(7,I,M)=0.0
   34 CONTINUE
      DO 19,K=2,6
      CR(K,1,M)=0.0
      CR(K,15,MO=0.0
   19 CONTINUE
      DO 39 I=2,14
      DO 59 K=2,6
      CRF(K,I,M)=(CR(K,I,M)+CR(K,I-1,M))/2.0
      CRG(K,I,M)=(CR(K,I,M)+CR(K,I+1,M))/2.0
      IF(I.EQ.14)CRG(K,14,M)=0.0
      CRA(K,I,M)=CRG(K,I,M)-CRF(K,I,M)
      CZA(K,I,M)= -CRA(K,I,M)*H(K)/B(I)
   59 CONTINUE
   39 CONTINUE
      DO 48 I=2,14
      CZD(2,I,M)=0.0
      CZU(2,I,M)=CZD(2,I,M)+CZA(2,I,M)
      CZD(3,I,M)=CZU(2,I,M)
      CZU(3,I,M)=CZD(3,I,M)+CZA(3,I,M)
      CZD(4,I,M)=CZU(3,I,M)     CZU(4,I,M)=CZD(4,I,M)+CZA(4,I,M)
      CZD(5,I,M)=CZU(4,I,M)
      CZU(5,I,M)=CZD(5,I,M)+CZA(5,I,M)
      CZD(6,I,M)=CZU(5,I,M)
      CZU(6,I,M)=CZD(6,I,M)+CZA(6,I,M)
      CZU(6,I,M)=0.0
   48 CONTINUE
      DO 96 I=2,14
      DO 97 K=2,6
      CZ(K,I,M)=(CZD(K,I,M)+CZU(K,I,M))/2.0
   97 CONTINUE
   96 CONTINUE
      CX(K,I,M)=C(K,I+1,M-1)-C(K,I,M-1)
      CY(K,I,M)=C(K+1,I,M-1)-C(K,I,M)
      DO 44 I=2,14
      DO 45 K=2,6
      IF(I.EQ.14)CX(K,14,M)=CX(K,13,M)
      IF(K.EQ.6) CY(6,I,M)=CY(5,I,M)
      CV(K,I,M)= -R(I)*0.262/C(K,I,M-1)*(CR(K,I,M)*CX(K,I,M)/B(I)+CZ(K,I,
     1 I,M)*CY(K,I,M)/H(K)+CR(K,I,M)*C(K,I,M-1)/R(I))
      C(K,I,M)=(C(K,I,M-1)+CV(K,I,M))*2.54
   45 CONTINUE
   44 CONTINUE
      WRITE (6,100) ((I,K,M,CR(K,I,M),CZ(K,I,M),C(K,I,M),CV(K,I,M),I=2,1
```

```
     14),K=2,6)
 100 FORMAT (1X,3I5,F7.3,3X,F.7.4,3X,F6.2,3X,3X,F7.3,3X
  80 CONTINUE
     STOP
     END

$DATA
$EOF
```

Programme to solve for the distribution of $v_{\theta m}$

Experimental notations	Computer notations
r, θ	I, M
vθ	CM
r	R
$v_{\theta m}$	CMA

When solving for Channel III , I=7

```
      Dimension C(7,15,13),R(15),B(15),CM(15,13),CMA(15,13),CB(15,13),C
     1A(15,13);CMF(15,13)
      DO 3 k=2,6
      READ (5,2) (C(K,I,1),I=2,14)
    2 format (13F5.2)
    3 CONTINUE
      READ (5,4) (R(I),I=2,14)
    4 FORMAT (13F5.1)
      B(2)=1.0
      B(14)=1.0
      DO 10 I=3,13
      B(I)=R(I+1)-R(I)
   10 CONTINUE
      DO 15 I=2,14
      CM(I,1)=C(2,I,1)
      DO 11 K=3,6
      CM(I,1)=CM(I,1)+C(K,I,1)
   11 CONTINUE
      CMA(I,1)=CM(I,1)/5.0
   15 CONTINUE
      DO 80 M=2;13
      DO 30 I=2,13
      CB(I,M)=CMA(I+1,M-1)-CMA(I,M-1)
   30 CONTINUE
      DO 61 I=2,14
      CA(I,M)=-0.262*(0;067*CB(I;M)/B(I)+0.00006*CMA(I,M-1)**3/R(I))
      IF(I.EQ.14) CA(14,m)=CA(13,M)
      CMA(I,M)=CMA(I,M-1)+12.0*CA(I,M)
      CMF(I,M)=CMA(I,M)/3.71
   61 CONTINUE
      WRITE (6,100) (I,M,CA(I,M),CMA(I,M),CMF(I,M),I=2,14)
  100 FORMAT (1X,2I5,F9.5,3X,F9.2,3X,F9.2)
   80 CONTINUE
      STOP
      END
$DATA
$EOF
```

Programme to find the friction factor

Experimental notations	Computer notations
Run number	J
b	B
Q	Q
$h_{\theta=60}$	D1
$h_{\theta=120}$	D2
s	H1
T(c)	T
$x10^6$	F
c_f	C

```
      DIMENSION J(50),B(50),D1(50),D2(50),H1(50),T(50),F(50),H(50)
     1,R(50),C(50)
      DO 10 I=1,40
      READ (5,100) J(I),B(I),Q(I),D1(I),D2(I),H1(I);T(I);F(I)
 100  FORMAT (I2,1X,F4.2,1X,F6.4,1X,F5.3,1X,F5.3,1X,F6.5,1X,F4.1,1X,F5.3
     1)
      IF(I.GT.20) GO TO 55
      H(I)=(D1(I)/12.0+(Q(I)**2/(64.4*(0.83*D1(I)/12.0)**2)))-(0.034/12.
     10+D2(I)/12.0+(Q(I)**2/(64.4*(0.83*D2(I)/12.0)**2000
      GO TO 56
  55  H(I)=(D1(I)/12.0+(Q(I)**23964.4*(0.83*D1(I)/12.0)**2)))-(0.029/12.
     10+D2(I)/12.0+(Q(I)**2/(64.4*(0.83*D2(I)/12.0)**2)))
  56  R(I)=(12.0*Q(I)*10.0**5)/(F(I)*(12.0*B(I)+D1(I)+D2(I)))
      C(I)=((B(I)*(D1(I)+D2(I))324.00000)**3*(64.4*H1(I)+(12.0*Q(I)/(D1(
     1I)*B(I)))**2-(Q(I)*12.0/(B(I)*D2(I)))**2))/(Q(I)**2+(F(I)+D1(I)/12
     2.0+D2(I)/12.0)*T(I))
      WRITE (6,200) J(I),R(I),C(I),H(I)
 200  FORMAT (1X,I2,2X,F7.1,2X,F6.4,2X,F6.4)
  10  CONTINUE
      STOP
      END
$DATA
$EOF
```

APPENDIX C

EXPERIMENTAL DATA

Table 1. v_θ (in cm/sec) vs z (in cm) Laminar flow. $Q = 0.19 \times 10^{-3}$ m^3/sec., Re = 246, h = 7.5 cm.

z = depth above bed, v_θ cm/sec. θ = 30

	5 cm from o/s		15 cm		25 cm		35 cm		45 cm		55 cm	
	z	v_θ	z	v_θ	z	v_θ	z	v_θ	z	v_θ	z	v_θ
$\theta = 30^\circ$	1.09	0.53	0.63	0.33	0.69	0.28	0.58	0.23	7.28	0.50	1.02	0.25
	1.24	0.51	1.09	0.63	0.76	0.25	0.73	0.28	6.85	0.48	1.49	0.35
	3.58	1.02	1.32	0.73	1.19	0.38	1.12	0.41	6.23	0.48	1.77	0.35
	1.62	0.69	1.42	0.84	1.77	0.51	1.32	0.48	5.55	0.48	2.23	0.33
	1.34	0.84	2.00	0.79	1.90	0.48	1.72	0.46	5.01	0.48	2.54	0.43
	1.14	0.53	1.57	1.02	2.63	0.41	2.32	0.48	4.30	0.53	3.08	0.43
	2.61	1.02	2.03	1.04	2.92	0.38	2.71	0.58	3.42	0.48	3.63	0.48
	3.12	0.92	2.51	1.09	7.26	0.56	2.89	0.58	2.98	0.48	4.26	0.53
	0.99	0.38	2.98	0.94	4.36	0.61	3.47	0.50	2.51	0.48	5.11	0.53
	6.50	0.73	2.92	1.09	6.39	0.76	4.20	0.58	1.32	0.27	6.10	0.53
	4.65	0.73	2.58	1.34	6.75	0.68	5.03	0.63	0.99	0.15	7.18	0.48
	5.50	0.63	3.81	1.09	6.92	0.68	5.37	0.61				
			4.16	1.09	7.26	0.48	5.81	0.58				
			4.95	1.09	7.04	0.38	6.23	0.56				
			5.35	1.14	6.28	0.43	6.57	0.53				
			5.75	1.17			6.80	0.53				
			6.05	1.12			6.26	0.48				
			6.92	1.01			7.15	0.48				
$\theta = 150^\circ$	0.84	0.66	0.41	0.13	1.09	0.35	0.96	0.31	0.33	0.18	1.21	0.25
	1.58	0.73	0.88	0.23	1.65	0.39	1.90	0.45	0.58	0.28	1.62	0.43
	2.43	0.61	1.04	0.25	3.16	0.47	2.23	0.45	0.98	0.38	7.50	0.30
	2.54	0.61	1.39	0.35	6.45	0.60	4.76	0.60	1.39	0.49	3.92	0.47
	5.88	0.71	1.72	0.39	4.68	0.58	2.57	0.47	2.48	0.61	4.80	0.43
	3.01	0.56	2.03	0.43	6.57	0.45	6.22	0.69	4.45	0.71	5.81	0.45
	4.48	0.63	2.62	0.43			3.70	0.47	7.45	0.47		
	2.64	0.63	2.73	0.41			5.61	0.62	5.86	0.66		
	7.55	0.71	2.78	0.54								
			3.90	0.54								
			4.82	0.56								
			5.68	0.58								
			7.12	0.50								

Table 2. v_θ (in cm/sec) vs z (in cm) Laminar flow.

$Q = 0.33 \times 10^{-3}$ m^3/sec.
Re = 422
h = 7.5 cm.
θ = 30

	5 cm from o/s		15 cm		25 cm		35 cm		45 cm		55 cm	
	z	v_θ	z	v_θ	z	v_θ	z	v_θ	z	v_θ	z	v_θ
$\theta = 30^\circ$	0.59	0.43	0.21	0.19	0.86	0.38	0.76	0.36	1.14	0.44	1.60	0.21
	0.63	0.47	0.32	0.23	1.07	0.42	0.99	0.36	1.80	0.63	2.13	0.30
	0.84	0.61	0.59	0.49	1.80	0.61	1.82	0.65	2.43	0.74	2.61	0.34
	1.47	0.71	0.82	0.63	4.80	0.88	2.27	0.76	2.59	0.74	3.46	0.38
	2.25	0.76	1.04	0.61	3.34	0.72	2.59	0.84	4.96	0.76	3.88	0.49
	2.92	0.84	2.63	0.91	7.10	0.63	3.16	0.84	5.40	0.78	4.38	0.45
	3.43	0.74	3.64	0.91	7.30	0.44	3.36	0.88	4.78	0.63	5.93	0.61
	3.72	0.76	4.80	0.86			5.59	0.91			6.23	0.49
	4.23	0.76	5.55	0.84			6.20	0.88			7.15	0.74
	5.80	0.78	6.22	0.80			6.90	0.82			7.93	0.59
	6.18	0.80	7.25	0.39			4.55	0.82				
	7.85	0.43										
$\theta = 150^\circ$	0.69	0.33	0.56	0.53	1.22	0.99	1.88	0.74	7.30	0.72	3.72	0.63
	2.79	0.91	0.89	0.76	1.78	0.99	3.95	0.89	7.05	0.74	4.32	0.59
	0.79	0.46	1.47	1.04	3.93	1.02	4.83	0.84	6.87	0.74	7.10	0.53
	1.02	0.50	1.65	0.94	7.28	0.84	5.16	0.91	5.36	0.76	5.90	0.76
	1.96	0.79	1.96	1.02	6.90	0.89	2.54	0.70	4.06	0.74	2.98	0.70
	3.82	0.96	2.05	1.06	3.29	1.12	6.80	0.79	1.20	0.46	5.83	0.78
	0.50	0.25	2.21	1.08	4.22	1.14	7.13	0.68	1.90	0.70	4.26	0.53
	2.85	1.06	2.82	1.11	5.55	0.68	1.32	0.63	2.54	0.63	2.84	0.63
	4.90	1.02	3.33	0.94	1.14	0.53	2.47	0.70			1.93	0.48
	5.86	0.84	3.43	0.94			6.55	0.70				
	7.14	1.02	3.80	0.94								
	7.29	1.02	3.93	0.91								
			4.26	0.91								
			4.90	0.86								
			5.30	0.86								
			5.91	0.91								
			6.42	0.89								
			6.92	0.91								

Table 3. v_θ (in cm/sec) vs z (in cm) Laminar flow.

$Q = 0.43 \times 10^{-3}\ m^3/sec.$
Re = 545 $h = 7.5$
$\theta = 30$

	5 cm from o/s		15 cm		25 cm		35 cm		45 cm		55 cm	
	z	v_θ	z	v_θ	z	v_θ	z	v_θ	z	v_θ	z	v_θ
$\theta = 30^\circ$	0.38	0.49	1.01	0.78	0.78	0.63	0.40	0.43	0.47	0.80	1.98	0.86
	0.65	0.65	1.29	0.88	0.88	0.88	0.58	0.63	1.15	0.99	2.33	0.86
	0.84	0.84	1.34	0.92	1.59	1.03	1.31	0.92	1.36	1.05	3.19	0.82
	1.58	1.11	2.07	1.01	2.60	1.05	1.70	1.03	2.43	1.19	4.30	0.80
	4.00	1.37	3.65	1.05	3.69	1.09	2.13	1.16	4.30	1.15	6.98	0.47
	5.28	0.96	5.60	1.09	4.25	1.16	3.52	1.34	5.30	1.01	1.21	0.78
	7.30	0.63	6.50	1.01	6.80	1.03	4.60	1.29	6.33	0.88		
					5.46	1.03	4.93	1.29				
							5.91	1.16				
							6.65	1.05				
$\theta = 150^\circ$	2.28	1.47	0.69	0.56	0.18	0.25	1.02	0.96	0.54	0.33	1.60	0.71
	2.51	1.49	1.24	1.01	0.36	0.54	0.96	0.71	1.19	0.61	2.34	0.76
	3.16	1.45	1.49	1.12	0.71	0.78	1.83	0.94	0.89	0.48	2.84	0.84
	5.62	1.60	1.88	1.14	1.45	1.21	2.62	0.89	1.50	0.71	4.14	0.82
	6.59	1.67	2.08	1.35	2.33	1.19	5.25	1.03	1.78	0.76	5.01	0.71
	3.67	1.52	2.56	1.50	3.04	1.14	6.13	0.96	2.03	0.69	5.52	0.82
	5.80	1.58	2.66	1.35	5.25	1.03	6.38	0.89	2.38	0.69	6.00	0.84
	5.58	1.47	2.96	1.27	6.25	1.17	2.18	0.87	2.90	0.84	6.30	0.86
	1.70	1.16	3.19	1.39	6.85	1.05	4.04	0.91	3.09	0.88	6.85	0.82
	4.56	1.58	3.42	1.41	2.79	1.05	4.21	0.99	5.30	0.94	7.15	0.84
			4.06	1.33			0.76	0.69	5.95	0.82		
			4.18	1.39					6.75	0.86		
			4.68	1.37					7.30	0.82		
			4.88	1.37								
			5.08	1.35								
			6.55	1.27								
			6.64	1.24								
			7.00	1.35								

Table 4. $\frac{v_{\theta m}}{\bar{v}_o}$ around the bend. Channel I (turbulent flow)

$\bar{v}_o$ = 9.45 cm/sec. top values measured
bottom values calculated

Θ	5 cm from i/s	15 cm	25 cm	35 cm	45 cm	55 cm
15°	1.05 0.90	0.98 0.90	1.02 0.97	0.88 0.87	0.87 0.88	0.74 0.75
30°	0.90 0.90	0.83 0.89	0.83 0.97	0.73 0.87	0.68 0.88	0.51 0.78
45°	0.79 0.89	0.89 0.88	0.90 0.97	0.81 0.88	0.77 0.88	0.61 0.80
60°	0.66 0.88	0.84 0.87	0.83 0.98	0.83 0.89	0.77 0.88	0.66 0.83
75°	0.70 0.87	0.85 0.86	0.89 0.98	0.87 0.90	0.85 0.87	0.70 0.86
90°	0.74 0.86	0.84 0.85	0.92 0.98	0.93 0.91	0.96 0.87	0.92 0.89
105°	0.79 0.85	0.90 0.84	0.97 0.98	1.02 0.93	1.03 0.86	0.94 0.91
120°	0.81 0.83	0.90 0.82	0.98 0.98	1.02 0.95	1.04 0.85	0.96 0.94
135°	0.78 0.81	0.90 0.81	0.96 0.98	1.01 0.97	1.04 0.84	0.99 0.97
150°	0.82 0.79	0.90 0.79	0.97 0.99	1.01 1.00	1.06 0.83	0.99 1.00
165°	0.79 0.76	0.92 0.78	0.96 0.99	1.02 1.03	1.08 0.82	1.03 1.02
180°	0.73 0.72	0.91 0.76	0.95 0.99	1.00 1.06	1.10 0.81	1.11 1.05

Table 5. $\frac{v_{\theta m}}{\bar{v}_o}$ around the bend. Channel III (turbulent flow)

$\bar{v}_o = 14.5$ cm/sec. top values measured
bottom values calculated

θ	5 cm from i/s	10 cm	15 cm	20 cm
15°	1.04 0.97	1.10 1.06	1.01 0.99	1.06 1.07
30°	1.01 0.96	1.06 1.07	1.06 0.98	1.06 1.08
45°	0.92 0.95	1.06 1.08	1.10 0.97	1.06 1.09
60°	0.93 0.94	1.04 1.09	1.11 0.96	1.08 1.11
75°	0.93 0.92	1.02 1.10	1.10 0.94	1.10 1.12
90°	0.88 0.90	0.98 1.12	1.09 0.93	1.09 1.13
105°	0.90 0.88	1.00 1.14	1.10 0.91	1.11 1.14
120°	0.88 0.85	0.99 1.16	1.08 0.88	1.11 1.15
135°	0.85 0.82	1.01 1.19	1.09 0.85	1.15 1.17
150°	0.86 0.78	1.02 1.22	1.11 0.82	1.15 1.18
165°	0.89 0.74	1.03 1.27	1.11 0.78	1.16 1.19
180°	0.85 0.68	1.00 1.32	1.11 0.74	1.18 1.20

Table 6. Bed angles in turbulent flow across the width for different flow depths at $\theta = 60^{\circ}$ and $\theta = 120^{\circ}$.

Channel I : $Q = 4.3 \times 10^{-3}$ m^3/sec.

θ	h	5 cm from o/s		15 cm		25 cm		35 cm		45 cm		55 cm	
		α_o	$\tan\alpha_o$	α_o	$\tan\alpha_o$	α_o	$\tan\alpha_o$	α_o	$\tan\alpha_o$	α_o	$\tan\alpha_o$	α_o	$\tan\alpha_o$
60°	3.59	12	0.21	13	0.23	15	0.27	15.5	0.28	12	0.21	8.5	0.15
	4.93	15	0.27	19.5	0.35	19	0.34	19	0.34	19	0.34	14	0.25
	6.13	15.5	0.28	20.5	0.37	23.5	0.43	22	0.40	22	0.40	17	0.31
	7.57	19	0.34	25	0.47	28.5	0.54	26.5	0.50	23.5	0.43	20	0.36
	8.92	21	0.38	28	0.53	30	0.58	29.5	0.57	27	0.51	21	0.38
	10.01	21.5	0.39	28	0.53	33.5	0.66	32	0.62	28.5	0.54	22	0.40
	11.41	22.5	0.41	27.5	0.52	34.5	0.69	35	0.70	33	0.65	23.5	0.43
120°	3.40	13.5	0.24	14	0.25	13.5	0.24	14	0.25	16	0.29	14	0.25
	5.20	16.5	0.30	20.5	0.37	20	0.36	18	0.32	18	0.32	16	0.29
	6.08	17.5	0.32	20.5	0.37	20.5	0.37	21	0.38	20	0.36	18.5	0.33
	7.5	20.5	0.37	20.5	0.37	22	0.40	23	0.42	20.5	0.37	19	0.34
	9.08	22	0.40	24	0.44	27.5	0.52	26.5	0.50	22.5	0.41	19.5	0.35
	10.22	23	0.42	28	0.47	28.5	0.54	27.5	0.52	22.5	0.41	21.5	0.39
	11.42	23.5	0.43	25.5	0.48	29.5	0.57	30	0.58	24.5	0.46	21.5	0.39

Table 7. Bed angles at the centreline around the bend vs. Reynolds numbers (Three channels)

depth measured at 1.4 m. u/s the bend entry

h(cm)	Re	-0.6m	-0.08m	30	60	90	120°	150°	180	+0.6m	+1.2m
					Channel I						
5	445	2	20	33	30	31	28	26	18	7	0
5.1	860	2	12	29	27	26.5	24	24	18	9	3
3.42	5880	0.5	7.5	14	12.5	13.5	11.5	11	5	3.5	3
					Channel II						
5	494	1	6	24	21	24	24	22	17	7	3
5	1080	2	6	21	20	24	22	20	16	6	2
5	6700	0	1	18	15	18.5	18	18	10	6	2
					Channel III						
5	470	1	3	23	20	21	20	22	18.5	6	2.5
5	1025	1.5	2	19	19.5	18.5	18	20	15	5	4
5	6500	0	2	15	10	11	15	13	10	3	1

Table 8.

$\tan\alpha_o$ vs. ℓ/r_c and $\tan\alpha_o$ vs. $(\ell/r_c)^{\frac{1}{2}}\ (Re)^{-\frac{1}{4}}$

$\theta = 60^o$ and $\theta = 120^o$ at centreline (Three channels)

θ	ℓ/r_c			$\tan\alpha_o$			Re			$(\ell/r_c)^{\frac{1}{2}}(Re)^{-\frac{1}{4}}$		
	I	II	III	I	II	III	I	II	III	I	II	III
60^o	0.020	0.050	0.060	0.28	0.37	0.43	6500	7100	7270	0.015	0.025	0.027
	0.027	0.044	0.053	0.34	0.33	0.37	6370	7300	7520	0.018	0.023	0.025
	0.034	0.038	0.046	0.40	0.27	0.34	6230	7650	7790	0.021	0.021	0.023
	0.041	0.032	0.037	0.50	0.23	0.30	6100	7920	8180	0.023	0.019	0.020
	0.049	0.025	0.031	0.57	0.21	0.27	6000	8250	8410	0.025	0.017	0.019
	0.056	0.020	0.025	0.62	0.18	0.21	5900	8600	8790	0.027	0.015	0.016
	0.062	0.019	0.023	0.70	0.17	0.19	5800	8620	8880	0.029	0.014	0.016
120^o	0.019	0.050	0.060	0.25	0.33	0.35	6520	7100	7270	0.015	0.025	0.027
	0.029	0.044	0.052	0.32	0.27	0.31	6350	7370	7590	0.019	0.023	0.024
	0.033	0.038	0.045	0.38	0.25	0.29	6250	7620	7790	0.021	0.021	0.023
	0.041	0.032	0.036	0.42	0.21	0.27	6050	7920	8180	0.023	0.019	0.020
	0.049	0.025	0.031	0.50	0.19	0.25	6000	8250	8410	0.25	0.017	0.019
	0.054	0.020	0.024	0.52	0.18	0.21	5880	8600	8790	0.027	0.015	0.016
	0.063	0.019	0.022	0.58	0.14	0.18	5800	8700	8880	0.029	0.014	0.015

Table 9. Flow angles along the depth in the three channels

top reading at 5 cm o/s — h at 1.4 u/s the bend = 7.6 cm
middle " " centreline — Q (I) = 4.3×10^{-3} m^3/sec
bottom " " 5 cm i/s — Q (II & III) = 3.1×10^{-3} m^3/sec

Station	height above channel bed (cm)												
	0.15			0.75	1.25		2.50			3.8			...
	I	II	III	I	II	III	I	II	III	I	II	III	
	1	0	0	0	0	0	0	0	0	-0.5	0	0	
-0.5m	3	0	0	0	-1	0	-1	0	0	0	0.5	0	...
	0	0	0	0	-1	0	-1	0	0	-1	0.5	0	
0°(I)	5	0	0	2	0	0	0.5	0	0	0	0	0	
-0.10m	9	1	0	2.5	1	0	-2.5	0	0	-1	0	0	...
(II)&(III)	3	0	1	1.5	-1	0	1.5	0	0	-1.5	0	0	
	10	9	3.5	3	1	2	1	-1	1.5	-1	-2.5	0	
15°	12	9	2	3	2	0.5	1.5	-0.5	0	-0.5	-2.5	0	...
	7	7.5	1	5	2	1	1	-1.5	0.5	0	-2.5	0.5	
	12	8	7	3	-0.5	3	1	-1	1	-1	-1	-0.5	
30°	15	16	7	6	6	3	1	1	1	-2	-2.5	-0.5	...
	10	12	7	4	7	5	-2	0.5	2	-3	-2	-1	
	20	9	8	7	6	5	-1	-2	-0.5	0	-2.5	-0.5	
45°	27	18	12	18.5	5.5	8	5	2	0	2.5	-1.5	-1	...
	24	18	11	12.5	8	7	3.5	2	1.5	0	-0.5	-1.5	
	10	9.5	9	5	4	4	2	-3	0	-1	-3.5	-2	
60°	23	14	10	13	4	6	5	1	1.5	1	-3	-1	...
	16	11	6.5	10	4	4	3	0.5	-0.5	1	-3	-2	
	12	7.5	7.5	5	4	3	2	-3	-2	-2	0	-2	
75°	22	10	10	15	3	4	8	0	0	4	-2.5	-2	...
	11.5	10	9	9	3	4	5	0	0.5	2	-1	0	
	14	7	6.5	4	3	2	-2	-1.5	-2	0	-1.5	-3	
90°	22	10	8.5	15	1.5	3	5	-1.5	-1	2	-1.5	-1.5	...
	14	12	6.5	9	2	2	3	0	-1	0	-1.5	-2.5	
	10	9	7	4	-0.5	2.5	-1	-2	-1	-2	-1	-2	
105°	18.5	9	8	11	3	4	4	-1	0	1.5	-1	-1	...
	11	8.5	7.5	7	3	3	1	-1	1.5	-1	-1	-0.5	
	8	8.5	6.5	5	4	2	-1	-1	-2	-1	-1	-3.5	
120°	18	10	7	13	2	2	5	-1	-1	4	-1	-2	...
	12	10	5.5	8	2	2	2	-1	-0.5	1	-1	-2	
	11	10	5	7	3	2.5	-1	0	-2.5	-2	-0.5	-3	
135°	13.5	13	7	9	5	4	3	2	1	0	1	-1	...
	9	10	7	7.5	5	3.5	1	2	0.5	-1	1.5	-0.5	
	9	12	7	4	4.5	3.5	0	-1	0	-1	-1	-2	
150°	12	14	10	9	7.5	6	2	2.5	1.5	0	-1	0	...
	11	12	10	6	7	6	0	1	0	-2	1	-1.5	
	8.5	12	8	5	5	3	-1	-1	-1	-3	-3	-2.5	
165°	11	13	8	9	6	6	3	2	2.5	-1	0	-1	...
	10	11.5	8.5	6	6	5	2.5	0	1.5	-2	0	0	
	7	7	4.5	4	-2	1	-1	-1	-2.5	-3	0	-3.5	
180°	10	8	6	8.5	1.5	1.5	0	-0.5	-1.5	-3	-2	-1.5	...
	8	7	4.5	4	3	2	0	0	-2	-2	-2.5	-3	
	2	2	1	1	0	0.5	1	-1	-0.5	0	-1	-0.5	
+0.5m	5.5	4	3	6	2.5	2.5	1	0	1	0	-1	0	...
	2	5	3	2	2.5	2.5	1	0	1	0	-1	0	

Table 9. (Continued)

Station	height above channel bed (cm)								
	5.0			6.5			7.1		
	I	II	III	I	II	III	I	II	III
	0	0	0	0	-0.5	0	0	0	0
-0.5m	0	0	0	0	-0.5	0	+2	0	0
	0	0	0.5	0	0	-1	+2	-0.5	-1.5
0°(I)	-1.5	0	0	-1.5	0	0	-2	0	0
-0.10m	-1	-1	0	-2.5	-1	0	-2.5	-1	0
(II)&(III)	-1.5	0	0	-0.5	0	0	-1.5	-2	0
	-1	-3	0	1	0	0	1	2	-2
15°	0	-3	0	0	-3	0	-5	-5	0
	-1	-3	0.5	0	-3	0	-0.5	-2	-1
	1	-1	-2	3	1	-2	3	4	-2
30°	-1	-4	-1	-3	-3	-1	-1	-2	-2
	-4	-4.5	-1	-2	-1	-2	-2	-2	-3
	1	-2.5	-0.5	4	1	-0.5	5	3	-1
45°	-3	-2	-3	-4	-5	-4	-6	-7	-4.5
	-1	-2	-2	-3	-4	-2.5	-5	-4	-5
	0	-1	-2.5	2	2	-2	4	5	-2
60°	-2	-4	-2	-5	-4	-2.5	-7	-5	-4
	-1	-4	-2	-1	-4	-3	-2	-5	-4
	0	0	0	5	2	1	6	4	1
75°	-2	-2	-2.5	-6	-2	-2.5	-9	-2	0
	-1	-2	-1	-2	-2	-1.5	-5	-4	-2
	1	1	-1	2	3.5	1	4	4	3
90°	-3	-0.5	-1	-6	-1	-1	-10	-1.5	-1
	-1	-2	-2.5	-2	0	-2.5	-4	-2	-3
	0	-1	-2	3	2	2	6	2.5	3
105°	-3	-1	-1	-5	0	-1	-9	-0.5	0
	-2	-0.5	-1	-4	-1.5	-1	-5	-2	-1.5
	0.5	-1	-2.5	1	1	0	2	4	3
120°	0	-1	-2	-2	-1	-2	-4	-1	-2
	0	-1	-2	0	-1	-2.5	-1	-1	-3.5
	-2	-0.5	-2	4	3.5	1	5.5	5.5	3
135°	-3	0	-1.5	-3.5	0	-1.5	-4.5	1	-1.5
	-2	0	-1.5	-2	0	-2	-1.5	-1	-2
	-2	0	-2	+2	4	1	3.5	6	4
150°	-3	-1	-1.5	-5	-1.5	-1.5	-6	-1	-2
	-3	1	-1.5	-5	-1	-2.5	-5	-1	-2
	0	0	-1	3	3	2	3	5	4
165°	0	0	-1	-4	-1	-1	-3	0	-1
	-1	0	0	-3	-1	0	-1.5	-1	-1
	0	1.5	-3.5	2	3	0	3.5	3.5	2
180°	-3	-2.5	-2	3.5	-3	-2	-4.5	-1	-3
	-3	-3	-3	-2	-3	-3	-5	-1	-2
	1	-1	-0.5	1	-1	1.5	4	0.5	-1.5
+0.5m	0	-1	-1.5	-1	-1	-1.5	-2	-2	-1.5
	0	-2	-1	0	-3	-2	-3	-2	-1.5

Table 10. Bed shear stress distribution around the bend (Channels I & III)
top value : $\tau_{o\theta}/\bar{\tau}_{o1}$ bottom value : $\tau_{or}/\bar{\tau}_{o1}$

Q(I) = 4 x 10^{-3} m^3/sec, h (~~I~~) (1) = 3.8 cm; Q(III) = 2.5 x 10^{-3} m^3/sec, h (~~III~~) (1) = 4.1 cm

$\theta°$	5 cm from o/s		10 cm	15 cm		20 cm	25cm	35 cm	45 cm	55 cm
	I	III	III	I	III	III	I	I	I	I
-1.4m	0.98 0	1.10 0	1.08 0	0.91 0	1.08 0	0.74 0	0.97 0	1.27 0	0.91 0	1.10 0
-0.28m	0.93 0	1.15 0	1.17 0	1.18 0	1.15 0	1.02 0	1.18 0	1.10 0	1.05 0	0.95 0
0	0.68 0	1.02 0	1.15 0.02	0.70 0	1.11 0	1.04 0.02	0.78 0	0.91 0	0.91 0	0.91 0
30	0.94 0.21	1.45 0.10	1.34 0.18	0.98 0.17	1.75 0.11	1.36 0.11	1.14 0.32	1.35 0.31	1.77 0.31	1.48 0.23
60	1.08 0.30	1.68 0.10	1.53 0.19	1.08 0.23	1.42 0.18	1.10 0.13	1.24 0.34	1.62 0.22	2.09 0.22	1.57 0.13
90	1.23 0.15	1.46 0.04	1.38 0.17	1.05 0.23	1.02 0.07	0.75 0.06	1.48 0.40	1.48 0.31	1.70 0.19	1.31 0.19
120	1.24 0.23	1.58 0.11	1.46 0.12	1.14 0.26	1.34 0.07	0.80 0.07	1.29 0.19	1.16 0.19	1.75 0.41	1.05 0.15
150	0.87 0.12	1.86 0.15	1.73 0.20	1.10 0.26	1.36 0.11	0.94 0.07	1.16 0.27	1.22 0.27	1.05 0.27	1.31 0.26
180	1.96 0.11	1.86 0.15	1.25 0.12	1.50 0.15	1.07 0.12	0.75 0.07	1.51 0.01	1.52 0.09	1.22 0.19	0.80 0.09
+0.28m	1.96 0.01	1.60 0.06	1.16 0.11	1.19 0.10	1.11 0.07	0.75 0.05	1.19 0.12	1.51 0.12	1.10 0.10	0.65 0.01
+1.4m	1.65 8	1.65 0	1.34 0	1.35 0	1.08 0	0.09 0	1.29 0	1.39 0	1.52 0	0.72 0

Table 11. Friction factor (C_f) in curved open channel flow

	Run	b(m)	$Q \times 10^3 m^3/sec$	$h_{\theta\pi}$=60(cm)	$h_{\theta\pi}$=120(cm)	T^o(C)	$Re = \frac{\bar{v} \cdot m}{\nu}$	$C_f = \frac{2gms}{\bar{v}^2}$
	1	0.61	0.19	2.430	2.410	20.6	303	0.0645
	2	"	0.37	2.390	2.355	"	577	0.0205
	3	"	0.40	2.445	2.395	"	624	0.0150
	4	"	0.49	2.380	2.355	"	760	0.0143
	5	"	0.54	2.445	2.410	"	841	0.0084
	6	"	0.59	2.420	2.370	"	920	0.0101
	7	"	0.64	2.420	2.390	"	993	0.0087
	8	"	0.68	2.410	2.360	"	1059	0.0124
I	9	"	0.72	2.420	2.390	"	1123	0.0089
	10	"	0.76	2.395	2.345	"	1185	0.0116
	11	"	0.80	2.380	2.340	"	1251	0.0120
	12	"	0.84	2.385	2.345	"	1312	0.0110
	13	"	0.88	2.295	2.350	"	1368	0.0116
	14	"	0.91	2.375	2.325	"	1421	0.0091
	15	"	0.94	2.390	2.330	"	1473	0.0123
	16	"	0.97	2.375	2.320	"	1521	0.0078
	1	0.25	0.19	2.730	2.645	16.8	609	0.0312
	2	"	0.21	2.735	2.650	"	651	0.0201
	3	"	0.24	2.745	2.660	"	743	0.0111
	4	"	0.26	2.760	2.690	"	801	0.0100
	5	"	0.29	2.760	2.680	"	886	0.0121
	6	"	0.31	2.760	2.680	"	954	0.0139
	7	"	0.33	2.710	2.610	"	1017	0.0115
	8	"	0.36	2.690	2.610	"	1103	0.0098
	9	"	0.39	2.710	2.645	"	1185	0.0108
	10	"	0.41	2.740	2.660	"	1268	0.0115
	11	"	0.47	2.745	2.645	"	1463	0.0088
	12	"	0.50	2.710	2.640	"	1548	0.0102
	13	"	0.52	2.690	2.610	"	1594	0.0094
II	14	"	0.55	2.690	2.615	"	1670	0.0077
	15	"	0.55	2.695	2.605	"	1713	0.0064
	16	"	0.58	2.700	2.620	"	1763	0.0078
	17	"	0.61	2.715	2.635	"	1838	0.0081
	18	"	0.63	2.695	2.615	"	1916	0.0075
	19	"	0.66	2.670	2.595	"	2012	0.0068
	20	"	0.69	2.680	2.610	"	2130	0.0061
	21	"	0.72	2.685	2.610	"	2205	0.0069
	22	"	0.75	2.710	2.640	"	2304	0.0074
	23	"	0.80	2.720	2.645	"	2438	0.0068
	24	"	0.86	2.735	2.665	"	2637	0.0068
	25	"	0.91	2.735	2.660	"	2763	0.0059
	26	"	0.94	2.740	2.655	"	2831	0.0063
	27	"	0.94	2.760	2.695	"	2895	0.0058
	28	"	0.97	2.735	2.690	"	2981	0.0058
	29	"	0.99	2.735	2.700	"	3026	0.0062

Table 11. (Continued)

	Run	b(m)	$Q \times 10^3 m^3/sec$	ℓ_θ=60(cm)	ℓ_θ=120(cm)	$T^o(C)$	$Re=\frac{\bar{v}.m}{\nu}$	$CR=\frac{2gms}{\bar{v}^2}$
	1	0.25	0.26	2.845	2.735	16.2	761	0.0132
	2	"	0.27	2.860	2.770	"	801	0.0084
	3	"	0.29	2.870	2.800	"	866	0.0074
	4	"	0.31	2.800	2.720	"	921	0.0089
	5	"	0.35	2.802	2.720	"	1036	0.0072
	6	"	0.37	2.830	2.745	"	1118	0.0064
	7	"	0.41	2.770	2.700	"	1221	0.0098
	8	"	0.43	2.815	2.730	"	1292	0.0063
	9	"	0.46	2.690	2.620	"	1378	0.0062
III	10	"	0.52	2.565	2.505	"	2429	0.0059
	11	"	0.60	2.540	2.480	"	1574	0.0067
	12	"	0.67	2.545	2.505	"	1813	0.0063
	13	"	0.71	2.560	2.525	"	2037	0.0059
	14	"	0.75	2.610	2.540	"	2145	0.0062
	15	"	0.81	2.640	2.585	"	2265	0.0062
	16	"	0.84	2.670	2.615	"	2532	0.0056
	17	"	0.89	2.710	2.665	"	2667	0.0053
	18	"	0.92	2.745	2.705	"	2760	0.0059
	19	"	0.95	2.745	2.695	"	2861	0.0051
	20	"	0.99	2.770	2.730	"	2962	0.0054

REFERENCES

1. Ali, K. (1964) Flow dynamics in trapezoidal open channel bends. Colorado State University, Ph.D. Thesis.

2. Allen, J. and Shahwan, A. (1954) The resistance to flow of water along a tortuous stretch of the River Irwell (Lancashire) - an investigation with the aid of scale-model experiments. Proc.,Inst.C.E.,Vol.3, Part III, 1954.

2A. ALLEN, J. and ULLAH (1967) Proc. I.C.E Feb. Paper No 6946

3. Ananyan, A.K. (1957) Fluid flow in bends of conduits. Published by A.S.(USSR),Erevan-1957

4. Chow, V.T. (1959) Open-channel hydraulics. McGraw-Hill.

5. Einstein, H.A. and Harder, J.A. (1954) Velocity distribution and the boundary layers at channel bends. Trans. Am.Geoph.Union, Vol. 35, 1964.

6. Fox, J.A. and Ball, D.J. (1968) The analysis of secondary flow in bends of open channels. Proc.Inst.C.E., Vol. 39, March 1968.

7. Hawthorne, W.R. (1951) Secondary circulation in fluid flow. Proc.Roy.Soc. Vol.206

8. Hawthorne, W.R. (1954) The secondary flow about struts and airfoils. J.Aero.Sci. Vol.21, 1954

9. Ippen, A.T. et al (1960) The distribution of boundary shear stresses in curved trapezoidal channels. M.I.T. Hydrodynamics Lab. T.R. 43, Oct.1960

10. Ippen, A.T. et al (1962) Stream dynamics and boundary shear distribution for curved trapezoidal channels. M.I.T.Hydrodynamics Lab. T.R.47, Jan.1962.

11. Leopold, L.B. et al (1960) Flow resistance in sinuous or irregular channels. U.S.Geol.Survey. Prof.paper 282-D.

12. Memon, H.M. (1967) Resistance to flow in open channels. Imperial College, London. Ph.D.Thesis.

13. Malouf, K.M. (1950) The movement of detritus around models of river and channel bends. Imperial College, London. Ph.D.Thesis.

14. Prus-Chacinski, T.M. and Francis, J.R.D. (1952) Discussion to paper "On the origin of river meanders", by P.W. Werner. Trans. Am.Geoph. Union. Vol.33, 1952

15. Prus-Chacinski, T.M. (1955) The secondary flow in a meandering channel. Imperial College, London. D.I.C.Dissertation

16. Prus-Chacinski, T.M. (1967) Secondary motions applied to storm sewage overflows. Proc.Inst.C.E. Vol.37 , May 1967.

17. Raju, S.P. (1937) Experiments on the resistance to flow in curved open channels. Munich Hydraulic Institute. Ph.D.Thesis.

18. Rozovskii, I.L. (1957) Flow of water in bends of open channels. Published by A.S.(USSR),Kiev-1957

19. Schlichting, H. (1968) Boundary layer theory. McGraw-Hill.

20. Shukry, A. (1950) Flow around bends in an open flume. Trans.A.S.C.E. Vol.115. Paper no.2411

21. Thomson, J. (1876) On the origin of winding in rivers in alluvial plains, with remarks on the flow of water around bends in pipes. Proc. Roy.Soc. Vol.25.

22. Vanoni, V. (1946) Transportation of suspended sediment by water. Trans. A.S.C.E., Vol. 111. Paper no. 2267

23. Wadekar, G.T. (1956) Secondary flow in curved channels. Imperial College, London. Ph.D.Thesis.

24. White, C.M. (1929) Streamline flow through curved pipes. Proc.Roy.Soc. Vol. 123 A

25. Yen, Ben-Chie (1965) Characteristics of subcritical flow in a meandering channel. Inst.Hydraulic Research, University of Iowa.